5-2009

The synthesis and systematic evaluation of modified polymeric foams and electrically conductive polyimide/carbon/metal films

John Macharia Kinyanjui
University of Nevada, Las Vegas

THE SYNTHESIS AND SYSTEMATIC EVALUATION OF MODIFIED POLYMERIC FOAMS AND ELECTRICALLY CONDUCTIVE POLYIMIDE/CARBON/METAL FILMS

by

John Macharia Kinyanjui

Bachelor of Science
Geneva College, Beaver Falls, PA
1999

Master of Science
University of Nevada, Las Vegas
2003

A dissertation submitted in partial fulfillment
of the requirements for the

Doctor of Philosophy Degree in Chemistry
Department of Chemistry
College of Sciences

Graduate College
University of Nevada, Las Vegas
May 2009

UNLV
UNIVERSITY OF NEVADA LAS VEGAS

Dissertation Approval

The Graduate College
University of Nevada, Las Vegas

April 28, 2009

The Dissertation prepared by

John Macharia Kinyanjui

Entitled

The Synthesis and Systematic Evaluation of Modified Polymeric Foams and Electrically Conductive Polyimide/Carbon/Metal Films

is approved in partial fulfillment of the requirements for the degree of

Doctor of Philosophy in Chemistry

[redacted]
Examination Committee Chair

[redacted]
Dean of the Graduate College

[redacted]
Examination Committee Member

[redacted]
Examination Committee Member

[redacted]
Graduate College Faculty Representative

ABSTRACT

The Synthesis and Systematic Evaluation of Modified Polymeric Foams and Electrically Conductive Polyimide/Carbon/Metal Films

by

John Macharia Kinyanjui

Dr. David W. Hatchett, Examination Chair
Assistant Professor of Chemistry
University of Nevada, Las Vegas

Thermally processed PU foams are examined as a function of processing temperatures (25, 45, 65, and 85°C) at the side, middle, and center of a simple cylindrical mold. The PU foams show both chemical and morphological differences as a function of the processing temperature and radial position within the mold. Thermal degradation of uretoneimine structures, the emergence of carbodiimide structures, and extent of reaction of isocyanate groups are measured using photoacoustic FTIR spectroscopy. Chemical gradients and morphology differences between the side, middle, and center of the molded foam are observed for all processing temperatures. The data indicate that thermal activation at the center of the mold is important for samples regardless of processing temperature. Furthermore, in spite of thermal processing at temperatures well above the decomposition of uretoneimine structures (40°C), chemical gradients remain within the simple molded foams.

Thermally treated epoxy foams were found to undergo both chemical and structural changes associated with the degradation of Diels-Alder bonds and changing structural

packing of siloxane units in the foam network. FTIR results show that these changes are not reversible and occur immediately after thermal exposure. The combination of changing chemistry, structure, and thermal expansion lower the overall density of the foam by approximately 41% relative to the pristine foam. The change in density also influences the modulus of the material which is reduced by 68% after ten thermal cycles. The results indicate that thermal exposure reduces the rigidity of the material through chemical and structural changes that cause the foam to expand, lowering the density and modulus in the process.

A composite material was successfully prepared by incorporating carbon black in PI. Platinum metal was successfully deposited on the resulting PI/Carbon film using cyclic voltammetry. Results obtained from four-point probe conductivity measurements show that increased carbon loading or platinum loading enhances the electrical conductivity of the composite. However, beyond 10% carbon loading, the mechanical integrity of the film is compromised. TGA and DSC results show that the thermal stability of PI is maintained with carbon incorporation and platinum deposition. PI/carbon/Pt was found be thermally stable up to 561°C as determined by DSC and 559°C as determined by TGA. SEM imaging suggests that carbon is well dispersed in PI while XPS results show that the platinum deposited Carbon/PI is metallic. The deposition of gold on carbon/PI was found to enhance its sensitivity to the ferricyanide redox couple. However, slower electron transfer is observed at both PI/Carbon/Pt and PI/Carbon/Au films as compared to Pt and Au planar electrodes.

TABLE OF CONTENTS

LIST OF FIGURES

LIST OF SCHEMES

LIST OF TABLES

ACKNOWLEDGEMENTS

I would like to take this opportunity to thank my academic advisor Dr. David Hatchett under whose indelible help, encouragement and direction that I have been able to achieve many a milestone during my stay at UNLV, this being one of them. We did it once again! My deepest and sincerest appreciation goes to him and his wonderful family for their kindness and friendship to me.

Secondly, I wish to thank my examination committee members; Dr. Clemens Heske, Dr. Spencer Steinberg and Dr. Brendan O'Toole. They have also been actively involved in my dissertation project in one way or the other and I will always be grateful for their invaluable advice on the course and focus of my research.

A special thanks to Dr. Jim Aubert at Sandia National Laboratories for providing epoxy foam samples analyzed in this project. I would also like to thank Dr. Anthony Smith who assisted me with installing equipment for electrical conductivity measurements presented herein. Thanks to Dr. Lothar Weinhardt (currently at University of. Würzburg), Timo Hoffmann and Kyle George who as part of Dr. Heske's group helped in obtaining and interpreting x-ray photoelectron spectroscopy (XPS) data. I would also like to thank, Dr. Dong-Chan Lee whose door was always open for any questions. Thanks to Dr. Robert Mohan and Julio Malpica, from Dr. O'Toole's group, who we collaborated in the preparation and mechanical testing of polyurethane foam samples. Their help is greatly appreciated.

I must also thank members of our research group especially Dr. Asanga Ranasinghe who has always provided immense advice and help to me in the course of writing this dissertation. His friendship is greatly appreciated. Special thanks to my fellow graduate students Jade Morgan, Nicole Millick, Sandra Elkouz and Pauline Serrano for all their assistance. To the best group of undergraduates Gina Castruita, Brad Walling, Grace Park, Thuy Tran, Wally Atterberry who have tirelessly assisted me in carrying out my research, I could not have done it without your help.

Special thanks for funding and salary support from the Department Of Energy through the High Pressure Science Center (HIPSEC), Center for Energy Research (CER) and the Hydrogen Fuel Cells and Storage Technology (FCAST) project. I would also like to express my gratitude to the Department of Chemistry for support through the course of my study here at UNLV. Specifically, let me thank Mark Miyamoto and Deborah Masters at the department office who have assisted me tremendously in every facet of my graduate student life. Their warmth, kindness and readiness to assist me will always be cherished.

Finally and most importantly let me also thank my family and friends to whom I dedicate this dissertation. To my beautiful fiancée Ms. Gladwell Gacuga, I love you so much and am so glad that I met you. Thank you for your moral support and being such a wonderful listener. To my father the Venerable Canon David Kinyanjui and my mother Rosemary Kinyanjui who have always supported me in all my endeavors and pursuits, I say thank you from the bottom of my heart. You have always believed in me and pushed me to pursue excellence but most of all learn to trust in God. To my two beautiful sisters Mrs. Beatrice Kinyanjui Mpinga and Dr. Sarah Kinyanjui, I wish to say thank you for

always being there for me. Special thanks to Mr. & Mrs. J. Robert Manuel III, who have always been my parents away from home. To all my friends, please accept my thank you for always being there when I needed you.

CHAPTER 1

GENERAL INTRODUCTION

1.1 Introduction

The chemical modification, functionalization and combination of different chemical species can be used to develop new materials with unique chemical, physical or mechanical properties when compared to the starting materials. New or enhanced chemical, physical or mechanical properties may be realized in the process, which allows new applications to be envisioned and developed. Prior to realizing new applications for these materials, however, a clear understanding of their new or enhanced properties is essential. Furthermore, more complex properties of the functionalized or modified materials as compared to their parent materials require a systematic evaluation. Analytical tools and methods have been developed to study, correlate and expand our knowledge of the complex chemical, physical, and mechanical properties of these materials.

The first part of this project investigates changes in the chemical composition and mechanical stability of thermally treated modified polyurethane (PU) foam and Diels-Alder epoxy based foams. These foams are candidates for replacing aging polyurethane foam currently used for shock mitigation and encapsulation of electrical components in our national nuclear stockpile. Moreover, these foams have complex chemistry that influences the physical and mechanical properties of the materials. The modified

polyurethane foam contains uretoneimine crosslinks that provide enhanced structural rigidity over traditional polyurethane foam currently used in other applications. The polyurethane foams require harsh removal methods (i.e. sand blasting or use of caustic chemicals) which can damage any encapsulated electronic or mechanical components. In contrast, epoxy based foams incorporate Diels-Alder chemistry which allows the foam to be removed from encapsulated devices without damaging the potted components. Although these two foam systems have been proposed as encapsulants for nuclear warheads, the complex chemistry associated with each material will influence the final physical and chemical properties and determine their applicability. The foams must have high chemical and mechanical stability when exposed to thermal gradients to be useful. Evaluating the influence of thermal exposure on the chemical, physical and mechanical properties of foam systems is a daunting task requiring a large suite of experimental techniques. The first part of this study will focus on the development of experimental tools for the evaluation of the chemical, physical and mechanical properties of foam systems with complex chemistry that vary as a function of thermal exposure. The goal is to correlate any chemical changes in the foam systems with changes in their physical or mechanical properties. More importantly, the suite of characterization tools developed will allow the chemical, physical and mechanical properties of other complex materials to be systematically evaluated.

Polyimide is widely used in electrical insulation because of its excellent chemical and thermal stability, high tensile strength, good adhesion properties and low electrical conductivity. These unique characteristics make polyimide especially attractive for high temperature applications beyond the range where other common polymeric materials can

be used. One envisioned use of this polymer is as a flexible metallized back-end electrode material for solar devices or as an electron donor layer material for organic photovoltaic solar cells. However, the electrical insulating properties of polyimide do not allow the polymer to be used in applications that require electron transport. The polymer must be modified to provide an electrically conducting material, while still maintaining the overall thermal and chemical stability and mechanical strength of polyimide. The second part examines the modification of electrical properties of polyimide, through the incorporation of graphite to form a composite material. The incorporation of graphite into polyimide changes the electronic properties of the polymer while maintaining its mechanical properties. The conductive composite is further modified by electrochemical deposition of a transition metal onto the polymer surface for catalytic applications. The new physical properties of the polyimide/carbon/metal composites when combined with the inherent thermal stability of the polymer allow applications to be explored that were not previously possible. For example, the suitability of the composites as working electrodes in electrochemical reactions is explored. This is only possible because the composite has enhanced electrical conductivity in comparison to the pristine polyimide. Additionally, other applications can be envisioned using these materials for solid state applications such as photovoltaic devices and field effect transistors (FET). The chemical, physical, and mechanical properties of these materials are complex and must be evaluated for applications to be realized. Therefore, the synthesis, optimization of chemical constituents, and complete characterization of the composite properties is critical.

FTIR spectroscopy is used to evaluate changes in the chemical composition of both

polyurethane and epoxy-based foams during thermal treatment. The thermal stability of materials is investigated using differential scanning calorimetry (DSC), thermal gravimetric analysis (TGA) and thermo-mechanical analysis (TMA). Additionally, mechanical analysis techniques are used to determine the compressive strength of the materials studied. Imaging techniques, such as light microscopy and scanning electron microscopy (SEM), are also employed to investigate the morphological characteristics of the materials. Electrochemical techniques, specifically cyclic voltammetry, are utilized for the deposition of metal onto polyimide/carbon composites in addition to probing electrochemical reactions supported by the polyimide/carbon/metal composites.

1.2 Polyurethane Foam Study

1.2.1 Background

Polyurethane foams have found a wide array of applications in thermal insulation because of their extremely low thermal conductivity. Polyurethane foams belong to a larger family of cellular solids. The unique physical structure of a cellular solid is comprised of an inner "cell" structure and a surrounding "strut" structure. Cellular solids with perforated cells or broken struts that allow air to fill all the void space in the solid are referred to as open cell solids and are typically flexible and exhibit lower elastic moduli. Cellular solids whose cells are not perforated and are gas-filled are referred to as closed cell solids. Closed cell solids are structurally rigid with higher elastic moduli as compared to open cell solids. In addition to high elastic moduli, very low thermal conductivities are also exhibited by closed cell solids making them highly insulating. Gas-filled closed cells serve as heat sequestering regions in the solid which prevent heat

from diffusing through the solid.

Rigid closed cell polyurethane foams are currently prevalent in our national stockpile as shock absorbing materials and as encapsulants for electronic parts in nuclear warheads. Scheme 1.1 presents the general reaction for the formation of the urethane linkage, the repeating unit of polyurethane, from a diisocyanate and a diol. This reaction is referred to as the gel reaction. The functional group, R_1, of the diisocynante can be varied depending on the desired structural characteristics of the resulting polyurethane foam. For example, the use of aromatic rings leads higher structural rigidity as compared to the use of straight chain alkyl groups which leads to a more flexible polymeric material. However, flexibility or rigidity of the polyurethane is not solely dependent on the R_1 functional group of the diisocyanate. Because of the high reactivity of the diisoyanate group, secondary reactions accompany the polymerization reaction, leading to a more complex three-dimensional foam structure network.

The foaming reaction (also referred to as the gel reaction) occurs simultaneously with the polymerization of the diisocyanate to form urethane linkages. A blowing agent is required to facilitate the formation of a closed cell cellular structure leading to the formation of gas bubbles that are trapped in the cell. The most common blowing agents used in the manufacture of PU foams include water and hydrocarbons gases.[1-4] The gel reaction using water as the blowing agent is also presented in Scheme 1.1. In this reaction water reacts with diisocyanate to form a carbamic acid intermediate which subsequently decomposes to form a primary amine in addition to releasing carbon dioxide which is trapped in the cell structure of the foam. The primary amine formed can further react with the diisocyanate to form urea linkages. The urea linkage is one of the

components that contributes to the complex 3-dimensional network of the foam microstructure.

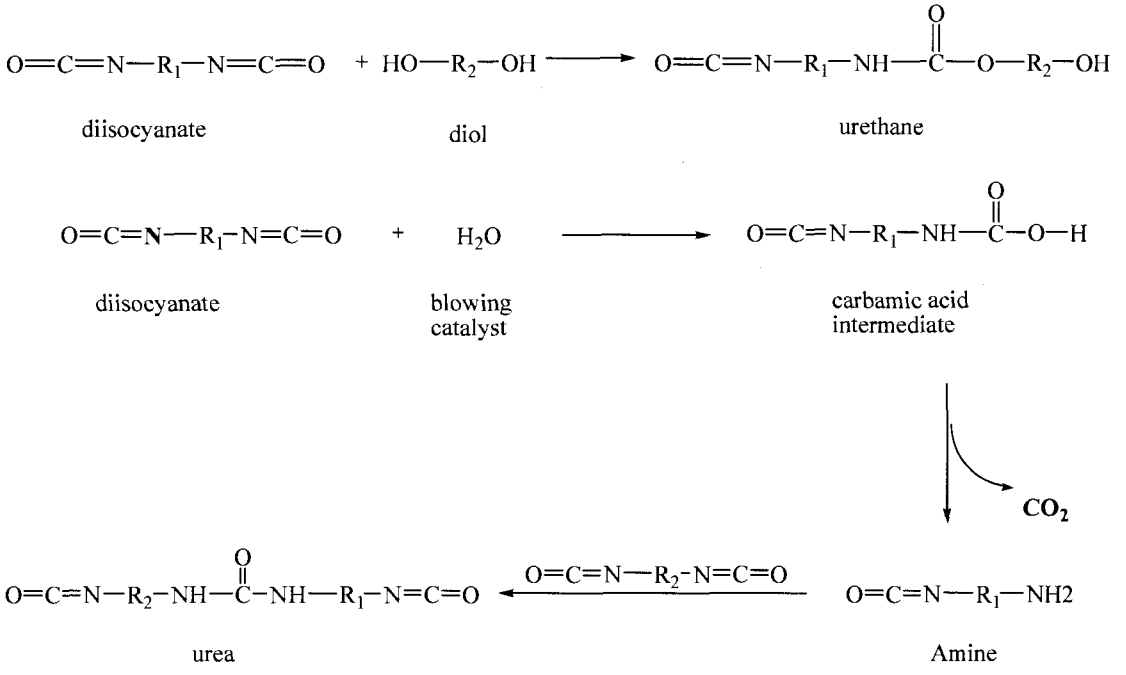

Scheme 1.1: General reaction for the foam reaction using water as the blowing catalyst leading to the formation of the urethane linkage, CO_2, a primary amine and urea

Other secondary reactions are also known to occur, leading to the formation of secondary products (such as allophonate and buiret moieties) that result from the reaction of urethane with isocyanate (allophonate) and urea with isocyanate (buiret) respectively. However allophonates and buiret are not chemically stable at the polyurethane formulation temperatures. As a result, these compounds degrade to their original parent compounds. The formation of diisocynate dimers (uretidinenedione) and trimers (isocyanurates) is also possible. Unlike allophonates and buiret, isocyanurates are

chemically stable at the foam formulation temperatures and will not degrade during the formulation process. As a result, isocyanurates remain as a chemical component of the foam.

Rigid foams currently used in national defense applications were primarily prepared from the polymerization of toluene diisocyanate (TDI). Two of the most common toluene diisocyanates used in the manufacture of polyurethane are 2,4- toluene diisocyanate and 2,6- toluene diisocyanate. The main drawback of using TDI based polyurethane foams are the health hazards posed by TDI. For example, human exposure even to low amounts of TDI is known to cause respiratory complications such as asthma.[5-7] As an alternative to using TDI-based polyurethane foams, researchers at Sandia National Laboratories have investigated the use of 4,4-methylene diisocyanate (MDI) to formulate polyurethane foams aimed at replacing the current aging TDI-based foam. The main advantage derived from preparing PU foam from the polymerization of MDI is that there are fewer health hazards posed by MDI as compared to those posed by TDI. Scheme 1.2 presents the chemical structures of TDI and MDI. In addition to lower toxicity of MDI as compared to that of TDI, the formation of uretoneimine crosslinks resulting from a side reaction involving the urethane linkage and MDI offers an added advantage of improved structural rigidity of MDI over TDI.

1.2.2 MDI Foam Chemistry

The rigid polyurethane foam investigated in this project is prepared from a commercially supplied MDI under the trade name Rubinate 1680 (Huntsman Corporation). Rubinate 1680 is a liquid at room temperature with a melting point below 20°C. Rubinate 1680 is a partially polymerized variant of 4,4-methylene diisocyanate

containing the carbodiimide repeating unit in addition to 4,4-methylene diisocyanate as presented in Scheme 1.3. The carbodiimide repeating unit can further react with another MDI molecule in a condensation reaction to form the uretoneimine linkage as shown in Scheme 1.3.

The formation of uretoneimine linkages in MDI-based polyurethane foams creates a network of crosslinks that enhances the foam's structural rigidity. However, the degradation of these linkages is thermally activated at relatively low temperatures. [8] The degradation of uretoneimine to carbodiimide and isocyanate proceeds at 40°C and above.

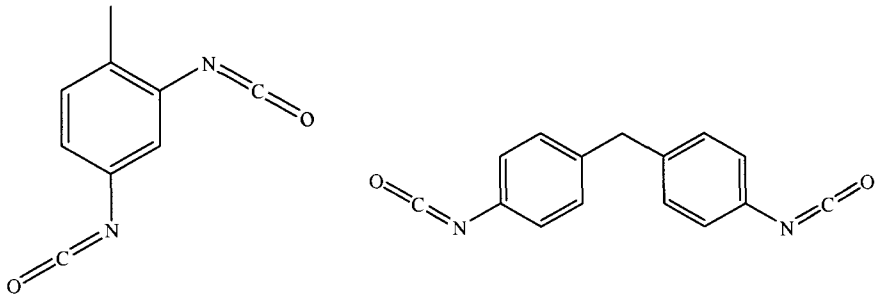

2,4 Toluene Diisocyanate (TDI) 4,4 Methylene Diisocyanate (MDI)

Scheme 1.2: Chemical Structures of 2,4-Toluene Diisocyanate (TDI) and 4,4-Methylene Diisocyanate, two common diisocyanates used in manufacturing polyurethane foams

1.2.3 Polyurethane Foam Study – Focus

ReCrete foam was developed by scientists at Sandia National Laboratories as a candidate foam for the replacement of the aging TDI-based polyurethane foam currently used in the US nuclear arsenal. ReCrete is water blown and is formulated from Rubinate 1680 and Voranol 490, a high functionality commercial polyol (Dow Chemical

Company) specifically formulated for rigid foam applications.

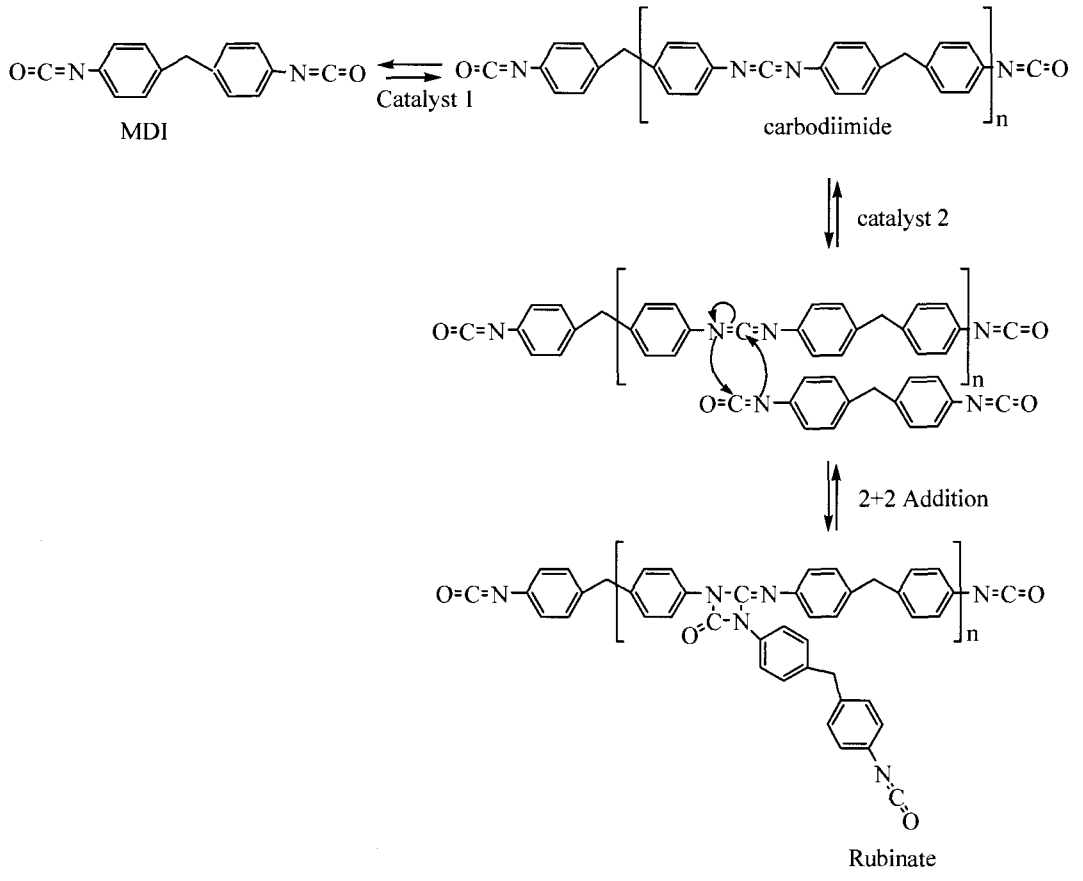

Scheme 1.3: Polymerization reaction in the formation of carbodiimide, the repeating unit in Rubinate 1680. The carbodiimide can further react with diisocynate to form the uretoneimine linkages that constitute Rubinate 1680

Previous studies in our laboratory have shown that the post-cure temperature at which ReCrete foam is processed has an effect on the chemical and mechanical properties of the foam. [8] Specifically, the processing (post-cure) temperature was found to influence the amount of unreacted isocyanate and the concentration of uretoneimine linkages. An increase in the processing temperature leads to a more chemically homogeneous foam

since the chemical reactivity of the isocyanate group increases with the processing temperature and therefore decreases the amount of unreacted isocyanate in the foam. However, an increase in the processing temperature leads to decreased structural rigidity of the foam. This is attributed to the degradation of the uretoneimine linkages with increased processing temperature leading to less cross-linking within the foam microstructure. Inversely, as the uretoneimine linkages are degraded with higher processing temperatures, the concentration of the carbodiimide increases.

The variations that occur in the chemical compositions of the uretoneimine linkage, carbodiimide and isocyanate in the radial geometry of ReCrete foam as a function of the post-cure processing temperature is the focus of this study. Fourier Transform Infrared (FTIR) spectroscopy is employed to investigate the changes in the intensities of functional groups specific to the uretoneimine, carbodiimide and isocyanate groups. The complex microstructure of PU foams created from polymerization of the diisocyanate and other secondary reactions requires highly methodical evaluation of the FTIR spectra. To quantify the concentration of each functional group at each radial position as a function of temperature, a methodology has been developed to measure and quantify FTIR spectra in addition to identifying a sensitive FTIR technique to perform sample measurements. FTIR photoacoustic spectroscopy is selected to measure the FTIR spectra of the polyurethane foam. Optical imaging aids in investigating changes in the cell structure across the radial geometry of the foam caused by increasing the post cure processing temperature.

1.3 Diels-Alder Epoxy Based Foam Chemistry

1.3.1 Background

One major drawback of using polyurethane foam as an encapsulation material is the difficulty of removing the foam from the encapsulated device due to polyurethane's propensity to adhere strongly to surfaces. Removal of the foam could be necessitated in situations where the encapsulated device needs to be accessed for repair or replacement. The integrity of the encapsulated device cannot be assured during the removal process since such removal methods as sandblasting are required to remove the foam.

Removable epoxy-based foams **(REFs)** that employ Diels-Alder chemistry were developed by scientists at Sandia National Laboratories and are another set of candidate foams (in addition to MDI-based foam) for replacing aging TDI-based polyurethane foam.[9, 10] These foams are based on removable Diels-Alder epoxy based resin analogs.[11, 12] The inclusion of Diels-Alder chemistry in the resin backbone gives the removable functionality to the epoxy based foams.

1.3.2 Epoxy Resin Chemistry

Since their advent in 1936, epoxy-based materials have found a wide range of applications, making the production of such materials a multibillion-dollar industry. Some of the common applications for epoxy-based materials include use as adhesives, coatings, hardeners, paints and coatings. Epoxy-based resins are commonly used as adhesives for household applications because of their good adhesion properties on a wide range of surfaces.

The epoxy ring, the active functional group in epoxy resins, is a carbon ring connected by an ether bond. The chemical structure of the epoxy ring is presented in

Scheme 1.4. Other commonly used names for the epoxy ring included epoxide ring or oxirane ring.

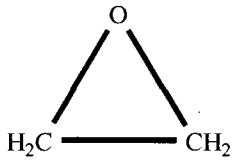

Scheme 1.4: The chemical structure of the epoxy ring

The adhesion properties of epoxy-based resins are derived from the high reactivity of the epoxide group towards many nucleophilic groups leading to the formation of crosslinks between these groups. One of the most commonly used epoxy-based resins is the diglycidyl ether of bisphenol A (DGEBA) resins prepared from reacting bisphenol-A and 1-chloro-2,3-epoxy-propane (also referred to as epichlorohdrin). Scheme 1.5 presents the chemical structure of DGEBA. DGEBA is one among the three epoxy-based resins used in the formulation of the **REF** studied in this project.

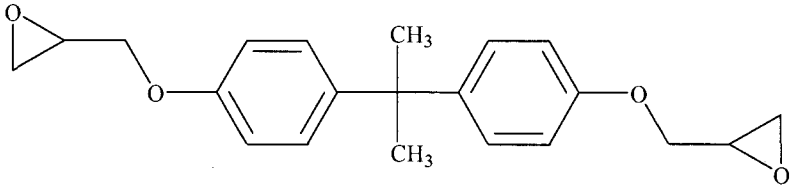

Scheme 1.5: Chemical structure of Diglycidyl ether of bisphenol A (DGEBA)

The two epoxy rings at each end of DGEBA provide two reactive sites which can react to initialize polymerization. In the polymerization reaction the epoxy groups in epoxy resin can either be reacted with other epoxy groups (chain polymerization) or a

curative such as a polyamine (step-growth polymerization) leading to the formation of crosslinks. The resulting product comprises of a polymer crosslink network that provides the strong adhesion properties of the resin. This polymerization reaction in which the epoxy group is reacted with another epoxy group or with a curative is also commonly referred to as the "curing" reaction.

Polyamines are some of the most commonly used curatives in the curing of DGEBA. The general reaction between an epoxy group and a primary amine is presented in Scheme 1.6. Using a diamine curative provides two primary amine groups that can react with the two epoxy groups in the terminal ends of DGEBA, therefore ensuring chain propagation as the curing reaction proceed. Specifically, in this project, Ancamine® 2049 and Ancamine® 2205 diamine (Air Products and Chemicals Inc.) curatives are used in the amine curing of epoxy resins used to formulate the **REFs** studied.

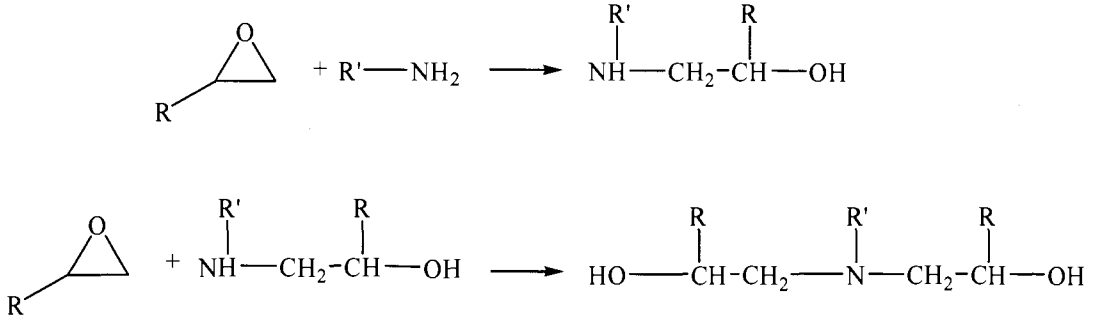

Scheme 1.6: Epoxide group reaction with a primary amine

In addition to DGEBA, two other tailor made epoxy based resins that incorporate two Diels-Alder adducts on both ends are also used in formulating the **REFs** studied in this project, namely removable epoxy resin 1 **(RER1)** and removable epoxy resin 2 **(RER2).**

The chemical structures for **RER1** and **RER2** are presented in Scheme 1.7.

a.

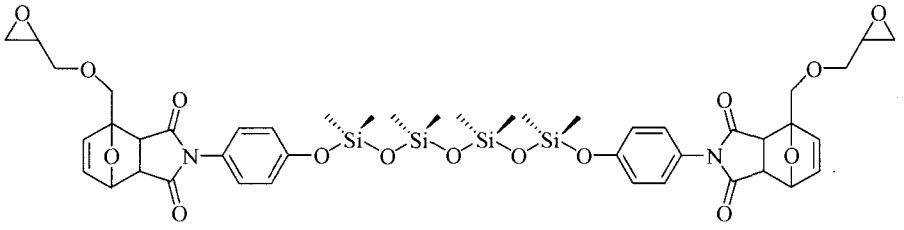

b.

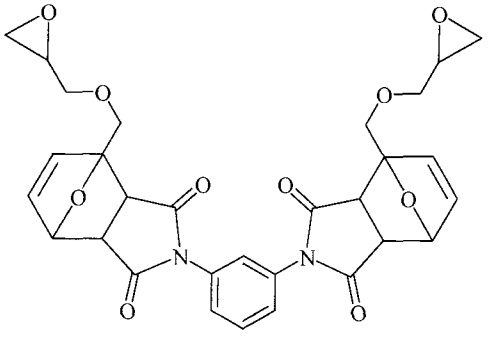

Scheme 1.7: Removable epoxy resins (RER) used in formulating REF's investigated in this project a. RER1 resin b. RER2 resin

For the **RER1** resin siloxane linkages are used as a backbone connecting the two Diels-Alder adducts. These unique modifications to the epoxy resin lead to changes in the chemical and physical properties of the resins and the **REFs** prepared from these resins. Specifically, introducing the Diels-Alder chemistry leads to a removable resin or foam while introducing the siloxane linkages to **RER1** leads to a low viscosity liquid that can easily be mixed with the diamine curative at ambient conditions.

1.3.3 Diels-Alder Chemistry

Diels-Alder chemistry integrated into epoxy resins that are used to formulate the **REFs** investigated in this project provides the capability to remove **REFs** and to access encapsulated materials by utilizing the reversible Diels-Alder reaction. This reaction, first reported by Otto Paul Hermann Diels and Kurt Alder in 1928 (for whom the reaction is named) involves the cycloaddition reaction between a conjugated diene of an alkene or alkyne with a dienophile. The general Diels-Alder reaction between a simple diene and a dienophile to form a cyclohexene is presented in Scheme 1.8.[13]

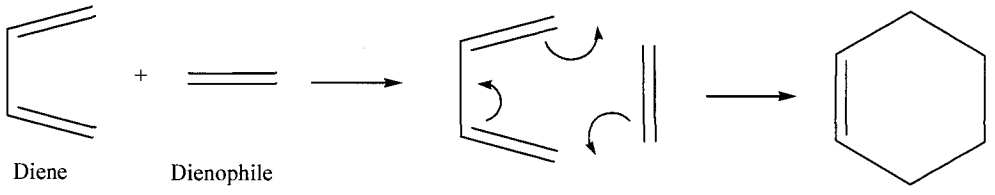

Scheme 1.8: General Diels-alder reaction between a simple diene and a dienophile

The diene can be an alkene or an alkyne possessing two double bonds (in the case of an alkene) or two triple bonds (in the case of an alkyne). The dienophile is normally an alkene possessing a single double bond. Specifically, the reversible reaction between a furan (diene) and a maleimide (dienophile) to form a Diels-Alder adduct is utilized in the preparation of the **REFs** used in this project and is presented in Scheme 1.9. The presence of electron withdrawing groups conjugated to the dienophile lowers the activation energy for the reaction. In the case of maleimide, two carbonyl groups act as the electron withdrawing groups. Conversely, the presence of an electron donating group

in the diene leads to faster reaction kinetics. In the case of furan, an alkyl group substituent acts as the electron donor.

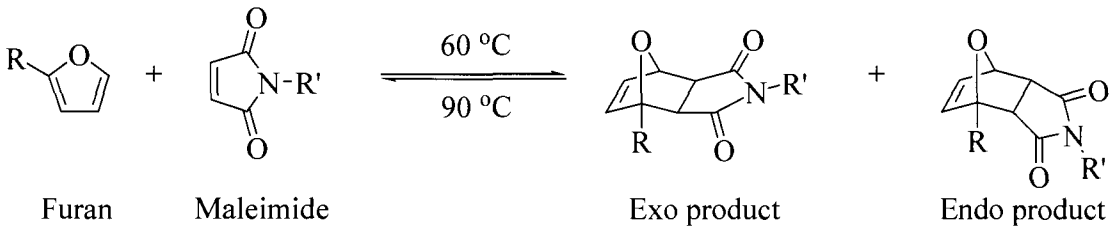

Scheme 1.9: Reversible Diels-Alder Reaction between a Furan and Maleimide

The forward Diels-Alder reaction between furan and maleimide proceeds at 60°C while the reverse (retro) reaction occurs at 90°C and above. In the reaction, two stereoisometrically distinct products are possible namely the endo and exo products. The endo product results when the furan and maleimide react in a staggered orientation in relation to each other while the exo products results when these reactants react when aligned on top of each other. The exo product is the more stable and dominant product.

1.3.4 Role of Siloxane Linkages in Diels-Alder Epoxy Based Foams

Siloxane tethers are employed in the **RER1** epoxy resin as a means to control the viscosity of the resin. [9] The generic structure of siloxane is given as R_2Si-O-Si whereby the R group could either represent hydrogen or an alkyl group. The tetrasiloxane tether incorporated into the **RER1** resin is presented in Scheme 1.10. Introducing siloxane linkages in the resin backbone leads to a liquid with a low viscosity that can be easily combined with the diamine curative during the formulation of the foam. In addition to controlling the viscosity of the resin, siloxane tethers have been shown to enhance the

thermal stability of the DGEBA resin.[14-16] Siloxane is prepared from the condensation of silanols as shown in Scheme 1.11

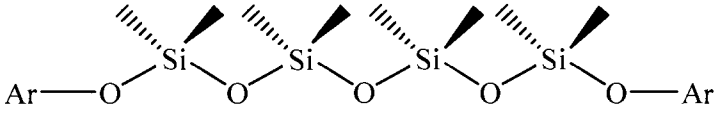

Scheme 1.10: Tetrasiloxane tether used to anchor the Diels-Alder pair found in **RER1** resin.

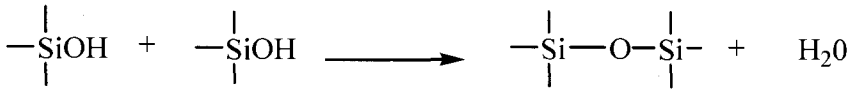

Scheme 1.11: Preparation of siloxane from the condensation of silanols

Polar and non-polar inter-chain interactions between the siloxane tethers are possible and provide additional structural interactions in the foam. The oxygen of the siloxane is a possible interaction site for polar interactions while non-polar interactions between the dimethyl groups attached to the Si atom are also possible. Polar interactions could include Van-der-Waals interactions or hydrogen bonding. Hydrogen bonding is also possible between hydrogen atoms of the OH groups formed during the amine curing reaction with oxygen of the siloxane group and nitrogen atoms of the tertiary amine formed during this reaction. Such interactions have been reported for siloxane-based polymers or polysiloxanes.[17] Taking advantage of their polar characteristics, polysiloxanes are widely used as packing material in chromatography columns.

The effect of thermal cycling on the chemical and physical interactions in the **REF** network is investigated in this project. It is possible that these interactions are influenced

or disrupted during thermal cycling of the foam. Any changes in the chemical properties could lead to changes in the physical properties, weakening the foam structure.

1.3.5 Diels-Alder Epoxy Based Foams – Focus

Although the formulation process and the chemical and mechanical properties of Diels-Alder epoxy foams are well documented, the variations in these properties as a function of thermal exposure or thermal cycling have not been investigated in detail. [11, 12] The influence of thermal exposure and cycling is of critical importance since any foam must be able to withstand large temperature fluctuations to be useful in defense applications. The foams have to withstand low temperatures at high altitudes in addition to high temperatures due to thermal radiation released from components in direct contact with the foam.

This project investigates changes in the physical, chemical, and mechanical properties of the foam resulting from repeated heating and cooling are evaluated. For example, the presence of Diels-Alder adducts in the foam network presents a possible point of weakness in the mechanical structure of the foam. Although the Diels-Alder reaction is reversible, the formation and reformation of the Diels-Alder adduct in a complex **REF** network may be affected by the presence of other linkages such as crosslinks formed by the reaction between the diamine curative and epoxide groups of the resins. Furthermore, the complex foam network is comprised of other products that result from side reactions which occur during the foaming reaction. One such reaction is a Michael addition reaction between pentaerythritol tetraacrylate (PETA) and the diamine curative. PETA is used as a stabilizing agent through the formation of micelles that enhance the dispersion of reactants during the foaming reaction.[18, 19] This reaction involves the unsaturation

of amine groups leading to the formation of chemical crosslinks that contribute to the complex polymer network and chemistry of the removable foam.

In addition to changes in the chemical composition of the foam, other aspects of the **REF** are studied. The mechanical properties of the foam are interrelated to its chemical properties by measuring the structural rigidity of the foam. The breakage of chemical linkages or physical interactions within the foam network can lead to the overall structural weakening of the foam. We have previously shown in studies performed by our group that the breakage of linkages in a ReCrete PU foam network leads to the decreased structural rigidity. [8] Specifically for the ReCrete foam, the drop in the structural rigidity of foam is attributed to the degradation of uretoneimine linkages found in polyurethane foam.

Thermal expansion of the epoxy foam is examined as a function of thermal exposure. Expansion in the foam could signify irreversible change in the chemistry of the system due to the breakage of chemical crosslinks and the loss of physical interactions within the foam network. The structural rigidity of the foam material is highly dependent on its density. Therefore, expansion and contraction of the foam can lead to changes in its density which translate to changes in the foam's structural rigidity [20]

1.4 Conductive Polyimide/Carbon/Metal Composites

1.4.1 Background

The initial goal of these studies was to develop thin, flexible, light-weight substrates to replace the often bulky, heavy and fragile glass substrates used in the conventional fabrication of solar cells. The flexible light weight substrates are especially suitable for

space or terrestrial applications where the weight of the solar device must be minimized and the solar device must be folded to fit into compact areas for deployment. We envisioned the development of a free-standing flexible polymeric electrode material as a starting point with the following defined characteristics:

1. A target electrical conductivity of 1 ohm-cm.
2. High thermal stability between 200-300°C.
3. Resistance to harsh acidic or basic mediums.
4. Incorporation of catalytic metals such as gold, platinum, silver or transition metals as photocatalysts into the topmost layers or on the surface.

Polyimides have found a wide range of applications because of their attractive thermal, chemical and mechanical properties. Kapton® tape, Kapton® film and other competing products are used widely in high temperature electrical insulation applications due to their high thermal stability, low electrical conductivity and high tensile strength. For example, Kapton® HN film is highly stable at operating temperatures of -269°C to 400°C and has a tensile modulus of 2.5GPa and electrical resistivity of about 10^{17} Ω-cm. [21] Numerous studies have been carried out to investigate the suitability of polyimide as a substrate for solar cells because of the polymer's thermal stability and mechanical flexibility.[22-26] In some cases substrates are prepared using commercially available polyimide films, such as DuPont Kapton® or UBE Upilex® films, while in some studies polyimide substrates are prepared from a polyimide precursor, a polyamic acid (PAA) solution which offers more flexibility in the fabrication and processability of the substrates.

Polyimide (PI) requires the incorporation of a conductive material onto its surface

or into its matrix for the polymer to become electrically conductive. The incorporation of conductive carbon particles into polyimide films is explored. The resulting conductive polyimide/carbon composite can be used for a variety of applications. In addition to functioning as back-end electrodes in solar cell devices, the deposition of transition metals which can include gold, platinum and palladium onto the film surface is possible, making the composite suitable for electrocatalytic applications. The electrocatalytic oxidation of primary alcohols for fuel cell applications is envisioned for the polyimide/carbon/metal composites.

The direct electrochemical deposition of gold, platinum and palladium metals on the surface of polyimide/carbon composites to form polyimide/carbon/metal composites is explored. The suitability of these polyimide/carbon/metal composites as working electrodes used to probe electrochemical reactions is also investigated

1.4.2 Polyimide Chemistry

The chemical structure of polyimide is comprised of an imide functional group repeating unit as presented in Scheme 1.12. Functional groups (R_1, R_2 and R_3) incorporated into the polyimide backbone can be varied with by either introducing linear chains or aromatic rings into the polymer's repeating unit. Polyimides containing aromatic groups in their repeating unit belong to the classification group of aromatic polyimides. Adjusting the functional groups can be used to design polyimides with certain desired physical and mechanical characteristics. For example, introducing aromatic groups into the polyimide backbone leads to enhanced thermal stability while the introduction of polar groups as poly(ethlyene glycol) improves its solubility [27-29] In addition to varying the R groups, two heterocyclic imide groups fused by an aromatic

ring can be incorporated into the repeating units of polyimide leading to enhanced thermal stability.

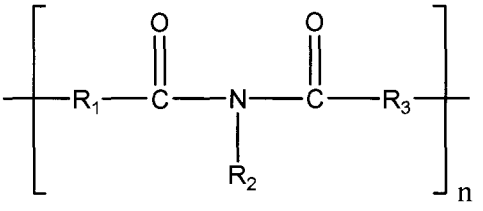

Scheme 1.12: General repeating structure of a polyimide

Scheme 1.13 presents the chemical structure for poly(pyromellitic dianhydride-4,4'-oxydianiline)imide also known as PMDA-ODA polyimide. PMDA-ODA is the aromatic polyimide constituting Kapton® HN film which is also the polyimide investigated in this project. The repeating structure of PMDA-ODA polyimide constitutes two heterocyclic imide rings fused together by a benzene ring with an aromatic ether group (Ar-O-Ar) connected to the nitrogen of one of the imide rings. The name of an aromatic polyimide is derived from the names of the starting reactants used in its preparation. For example, poly(pyromellitic dianhydride-4,4'-oxydianiline)imide polyimide gets its name from pyromellitic dianhydride and 4,4'-oxydianiline, the starting reactants in the formation the imide.

1.4.2.1 Preparation of Polyimides

PMDA-ODA polyimide belongs to a group of aromatic polyimides referred to as condensation polyimides. This is because the reaction to form these polyimides involves the removal of water, alcohol or ammonia prior to the formation of the polyimide.[28]

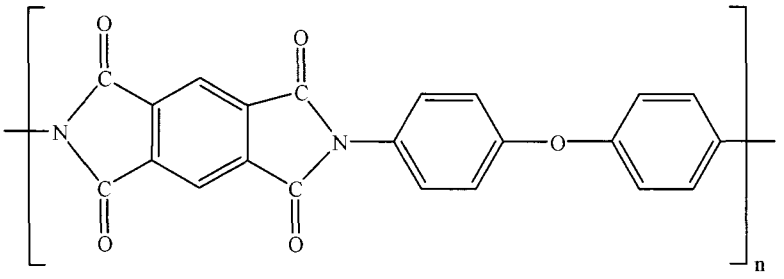

Scheme 1.13: Chemical structure for Poly(pyromellitic dianhydride-4,4'-oxydianiline)imide

The two-step reaction for the formation of PMDA-ODA polyimide is presented in Scheme 1.14. The first reaction involves the nucleophilic attack of one of the carbonyl carbon groups of the pyromellitic dianhydride by the NH_2 group leading to ring opening and formation of a poly(pyromellitic dianhydride-4,4'-oxydianiline)amic acid. Pyromellitic dianhydride is a good electron acceptor (electrophile), reacting readily with the electron rich amino group (nucleophile). The second step in PMDA-ODA polyimide preparation is referred to as the imidization step. The imidization step is an intramolecular condensation reaction involving the loss of a water molecule from the poly(pyromellitic dianhydride-4,4'-oxydianiline)amic acid. The reaction can be considered an intramolecular dehydration reaction since this reaction leads to the loss of water. The imidization reaction can be achieved through chemical agents (chemical imidization) or through heating (thermal imidization). In most applications, especially the preparation of polyimide films, thermal imidization is preferred over chemical imidization. One of the drawbacks of chemical imidization is that suitable solvent systems must be found to ensure that both the precursor and the polyimide stay in solution during the imidization process.

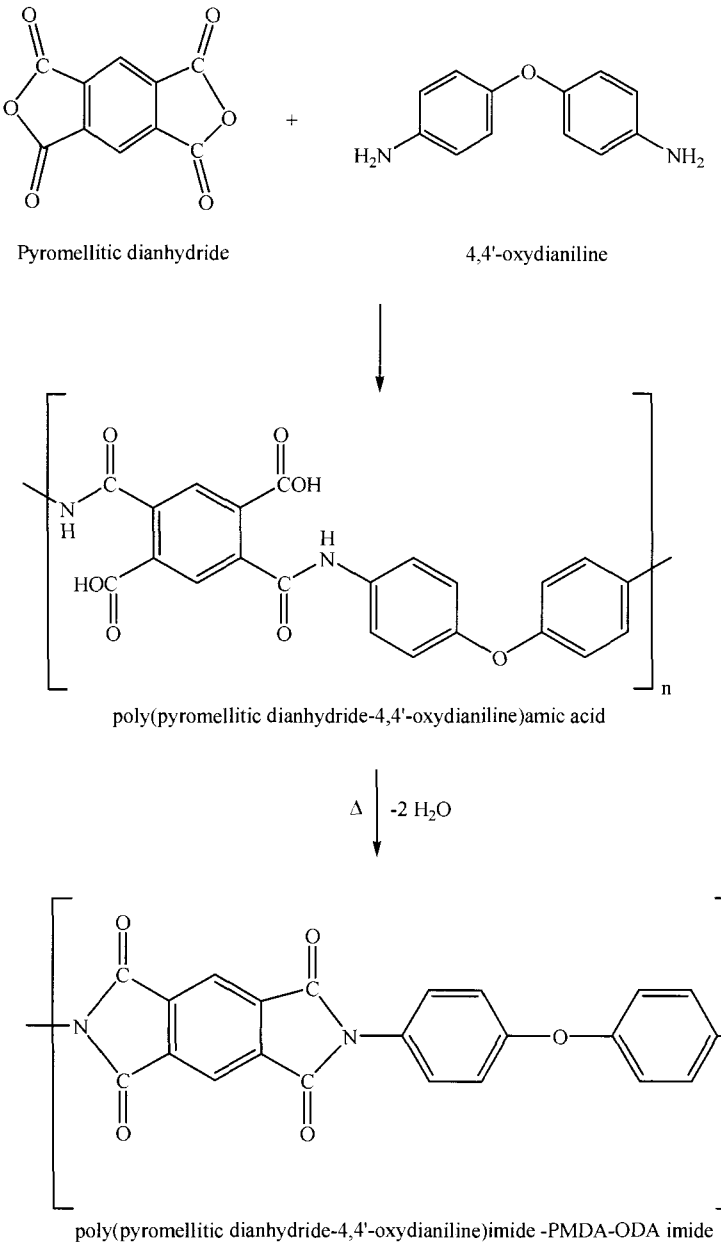

Scheme 1.14: The two-step preparation of PMDA-ODA. The first step involves the nucleophilic attack of one of the carbonyl carbon of the dianhydride by the NH_2 group of the diamine to form polyamic acid. In the second step, the polyamic acid is converted to polyimide in an intramolecular condensation reaction by heating, a process known as thermal imidization [30]

Therefore, chemical imidization is mostly used for the preparation of soluble polyimides [30] PMDA-ODA polyimide is highly insoluble in most solvents and therefore thermal imidization is primarily preferred in its preparation from PMDA-ODA polyamic acid and is utilized for all studies. A temperature range of 250-300°C is reported in literature for the thermal imidization of polyamic acid to polyimide.[30-32] However, thermal imidization does not achieve 100% conversion of polyamic acid to polyimide. Full imidization can be achieved through chemical processes. [30] In addition side reactions are possible between polyamic acid or polyimide chains and free or terminal NH_2 groups at these elevated temperatures. The side reactions are presented in Scheme 1.15. However, the occurrence of these reactions leads to the formation of crosslinks that contribute to the overall complex chemistry and strength of the polymer.

1.4.2.2 Chemical Stability PMDA-ODA polyimide in Acid and Bases

One application of interest is the use of polyimide/carbon/metal composites developed in this study as anode or cathode electrode materials in photoelectrochemical cells (PECs) and fuels cells containing acid electrolytes in continuous contact with the electrode. The chemical and thermal stability of PMDA-ODA polyimide in dilute acids makes it an attractive material for elevated temperature applications in acidic mediums. In contrast, the use of polyimide/carbon/metal composites in alkaline electrolytes is limited by the fact that PMDA-ODA polyimide reacts with dilute alkaline solutions, resulting in a ring opening reaction forming the PMDA-ODA polyamic acid salt. [33-35] The reaction between potassium hydroxide (KOH) and PMDA-ODA polyimide is presented in Scheme 1.16. This reaction is widely used as a surface etching technique for polyimide to improve metal or metal oxide particle adhesion to the surface of the

polymer.[33, 34, 36] Surface modification of polyimides using bases is highly effective and can be achieved with concentrations as low as 0.1M and within relatively short periods of 1-2 minutes.[33]

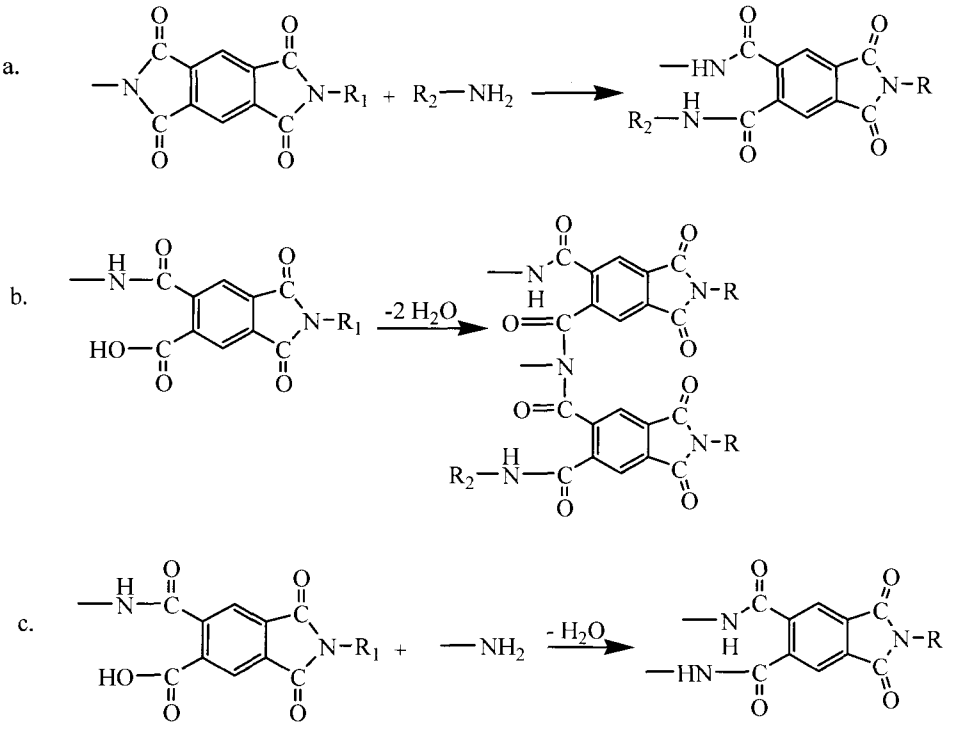

Scheme 1.15: Possible crosslinking side reactions during thermal imidization at elevated temperature. a.) Reaction between the imide ring and terminal amine groups b.) Imidization cross linking between two polyamic acid molecules with no ring formation c.) Reaction between polyamic acid with free amino groups [30]

Although polyimide is chemically stable in dilute acid, sulfonation of the aromatic rings in the polyimide films using fuming sulfuric acid has also been investigated. [33] However, sulfonation in these studies is only achieved at high acid concentrations (65%

w/w). Sulfonation of aromatic ring in PMDA-ODA polyimide should be limited because only dilute concentrations of H_2SO_4 are utilized in the studies presented.

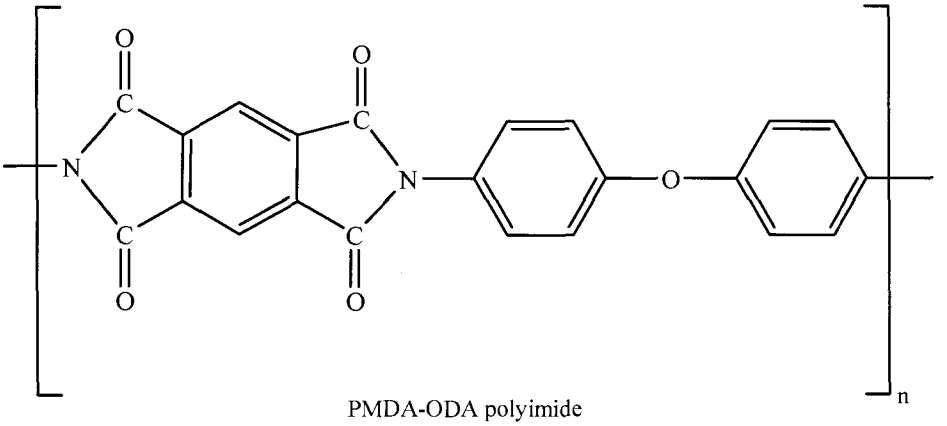

PMDA-ODA polyimide

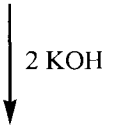

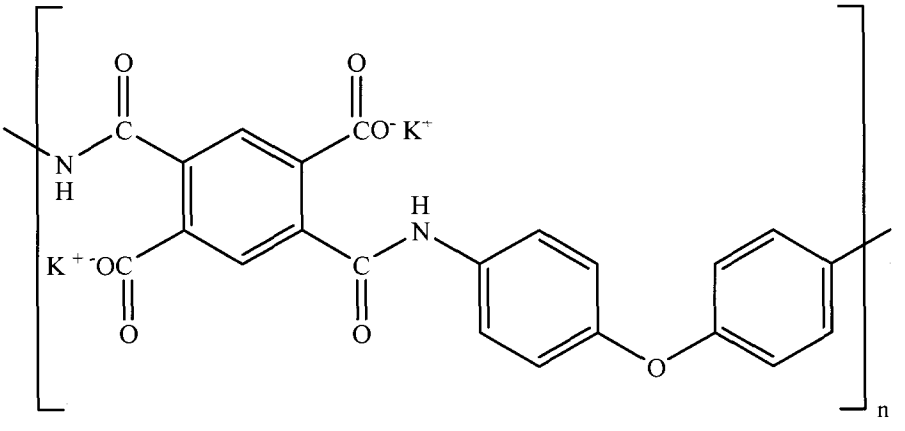

PMDA-ODA polyamic acid

Scheme 1.16: Reaction between PMDA-ODA polyimide and KOH to form a polyamate salt

1.4.2.3 Solubility of PMDA-ODA polyimide

PMDA-ODA polyimide is insoluble in many organic solvents. The lack of good solubility makes it difficult to cast or process polyimide into films wtih variable thickness. However, PMDA-ODA polyamic acid precursor allows for better processability due to its good solubility properties in polar aprotic solvents such as N,N-dimethylformide (DMF), N-methyl-2-pyrrolidone (NMP), methyl glycol (MG), N,N-dimethylacetamide (DMAC), tetramethyl urea (TMU) and dimethyl sulfoxide (DMSO).[28, 32, 37, 38] The improved solubility is derived from the presence of the proton of the PMDA-ODA polyamic acid. The carboxylic acid groups provide solvation sites at which the positively charged protons interact with the negative dipole of polar aprotic solvent molecules leading to ion/dipole interactions.[39] Therefore, for PMDA-ODA polyimide applications, the precursor is applied or molded onto substrates prior to thermal imidization. In this project a 15% (w/w) PMDA-ODA polyamic acid solution in a 80/20 percent NMP/Aromatic hydrocarbon solvent system under the trade name Pyre ML® RC5057 is used (Industrial Summit Technologies Corp.). Pyre-ML is a highly viscous liquid and in most cases requires further dilution prior to processing. to and during thermal imidization. This is especially true for DMSO and NMP. Gradual and total removal of the solvent is critical, as it can influence the mechanical and physical integrity of the resulting polyimide film. Rapid removal of the solvent at the high imidization temperatures can lead to formation of air pockets and fractures caused by uneven stress on the film. Furthermore, if these solvents are used to dilute polyamic acid, large periods of time are required to ensure the gradual evaporation and removal of the solvent from the PI films.

Traditional solvents used in the dilution of PMDA-ODA polyamic have low volatility due to their relatively high boiling points and are therefore difficult to remove them prior to and during imidization. To solve the problems associated with the low volatility of solvent, an aprotic polar solvent system that consists of acetone and DMSO is used. While PMDA-ODA polyamic acid is soluble in DMSO, it precipitates from solution containing only acetone. However, the precursor is readily soluble in a 5:1 binary solvent system containing acetone and DMSO, respectively. In addition, since the solvent system contains large amounts of highly volatile acetone and small amounts DMSO, larger solvent volumes for polyamic acid processing can be used. The high volatility of acetone ensures that the time required for the removal of solvent prior to thermal imidization is reasonable. In addition, large solvent volumes are useful in the minimization of carbon aggregation during the formation of PMDA-ODA polyamic acid/carbon precursor films.

1.4.3 Carbon Incorporation into Polyimide Matrix

Carbon black is an inexpensive, common material used in polyimides, providing a conductive material embedded within the polymer matrix.[27, 40, 41] The carbon black forms fibrous aggregates with chain-like connections that allow electrons to flow through the polymer. In most cases, carbon is incorporated into a polyamic acid solution prior to thermal imidization to provide a more homogeneous distribution of the carbon.

The use of carbon black as conductive fillers in polymers is not limited to polyimide. The incorporation of carbon black into polymers such as high density polyethylene (HDPE), ethylnene-proylenediene monomer (EPDM) rubber, and acrylonitrile butadiene rubber (NBR) has also been reported.[42, 43] Recent studies have examined both single walled carbon nanotubes (SWNT) and multi walled carbon nanotubes (MWNT) as

polyimide filler materials. Both have demonstrated superior electrical conductivity in comparison to carbon blacks.[44-48] In addition, polyimide/carbon nanotube composites such as AURUMTM® by Mitsui are now commercially available. However, the high cost of carbon nanotubes is the main drawback to the bulk production and application of conductive polyimide/carbon nanotube composites.

PI/carbon films are prepared using a method provided by Lin et. al. [28] In their study, they investigated the influence of morphology on electrical conductivity characteristics of polyimide films filled with five different carbon blacks. Based on this study, conductex® SC carbon black offered superior conductivity when compared to the rest of the carbon fillers. This carbon material is therefore chosen for all the PI/carbon/metal composite studies.

A standard operating procedure for preparing PI/carbon films of varying thickness and uniform carbon dispersion on glass substrates using layer by layer application of a precursor/carbon solution is developed in this project. The polyamic acid/carbon precursor films are imidized using a step-wise temperature ramp to form the polyimide/carbon films. In addition, curing studies have been performed to evaluate the influence of solvent composition on the PI/carbon composite films. These curing studies demonstrate that the gradual and complete removal of the less volatile DMSO and NMP is critical to ensuring that the mechanical integrity of the films is maintained.

1.4.4 Metal Incorporation into Polyimide/Carbon

The use of polyimide-metal composites in microelectronics and biosensor applications has been reported. [49, 50] The formation of polyimide/metal composites has been limited to sol gel processes, photoirradiation and chemical vapor deposition

techniques due to the insulating properties of polyimide substrates. [37, 51-57] However, metal deposition at free standing polyimide substrates has not been extensively studied. The majority of studies for the electrochemical deposition of metal onto polyimide surfaces have been conducted after polyimide is coated onto an electroactive substrate.[37, 50] Polyimide films are often grafted using other methods such as photo irradiation of the precursor onto a conductive substrate. The properties of the resulting laminate polyimide are then probed electrochemically. [58, 59] The electrodeposition of PAA/metal salt solution into an electrode surface to create PAA/metal hybrids has also been documented. [58-60] Andrescu et al. investigated the incorporation of Au and Ag nanoparticles into electrochemically deposited PAA to form a PAA/metal composite by taking advantage of PAA's affinity to reduce incorporated cations. Specifically, when the carboxyl group of the PAA reacts with triethylamine, a polyamate salt is formed with a cation that readily exchanges for the metal cation. The metal cation is then thermally or electrochemically reduced to metallic form.

1.4.5 Conductive Polyimide/Carbon/Metal Composites - Focus and Envisioned Applications

Although methods exist for the chemical insertion of metal into polyimide, there have been no documented examples of the direct deposition of metals where the conducting polyimide/carbon composites are utilized directly as an electrode. In this study the direct electrochemical deposition of gold, platinum and palladium metals on the surface of polyimide/carbon composites to form polyimide/carbon/metal composites is explored. The suitability of these polyimide/carbon/metal composites as working electrodes used to probe electrochemical reactions is also investigated. Additionally, the polyimide cure

procedure, polyamic acid-to-solvent ratios and carbon loading are optimized to produce uniform conductive PI/carbon composites. For comparison, gold metal is also deposited using chemical vapor deposition (CVD) on PI/carbon substrates, and the electrochemical properties are compared. Finally, the chemical and mechanical properties of the PI/carbon/metal composites are evaluated.

The characterization of the physical, chemical, and mechanical properties after incorporation of carbon and metal deposition onto the surface of PMDA-ODA polyimide are investigated using a host of analytical techniques. The thermal stability of PMDA-ODA polyimide prior and after incorporation of carbon and metal is studied using thermal analysis techniques, specifically differential scanning calorimetry (DSC) and thermal gravimetric analysis (TGA). The presence and distribution of metal on the surface of the polyimide carbon composites are investigated using x-ray photoelectron spectroscopy (XPS) and scanning electron microscopy (SEM).

Electrochemical methods, including cyclic voltammetry, are used for the deposition of metal and probing electrochemical interactions at the surface of the PI/carbon/metal electrodes. Specifically, the electrooxidation of alcohols such as, methanol at the surface of the PI/carbon/metal (i.e. platinum and palladium) in acidic or alkaline media are investigated.[61, 62] Platinum or platinum-ruthenium electrocatalysts embedded or on the surface of the anode material of direct methanol fuel cells (DMFC) facilitate the oxidation of methanol, the half reaction occurring at the anode side of the fuel cell.[63] However, a 50:50 atomic ratio binary mixture of a platinum-ruthenium electrocatalyst is preferred over platinum since it is less prone to carbon monoxide poisoning. Carbon monoxide, an intermediate of the methanol oxidation reaction, strongly adsorbs on the

platinum electrode surface, diminishing the efficiency of platinum to catalyze methanol oxidation. Hydroxyl groups adsorbed on the ruthenium particles catalyze the electrooxidation of the adsorbed CO species, therefore freeing the platinum sites for methanol oxidation. For the cathode side, platinum or a platinum-chromium electrocatalysts are used as electrodes. A schematic of a DMFC is presented in Figure 1 with the half reactions and overall reaction presented as follows:

Anode: $CH_3OH + H_20 \rightarrow CO_2 + 6H^+ + 6e^-$

Cathode: $1.5O_2 + 6H^+ + 6e^- \rightarrow 3H_20$

Overall: $CH_3OH + 1.5O_2 \rightarrow CO_2 + H_20$

Protons are shuttled to the cathode through a polyelectrolyte material such as Nafion® while electrons are shuttled through an external circuit to the cathode in addition to powering connected electronic devices.

Although outside the scope of this study, further applications could be investigated for PI/carbon/Pt and PI. For example, evaluation of the performance of PI/carbon/Pt(or Pd) composite as an electrocatalyst in the methanol oxidation reactions under elevated temperatures can be explored. It has been shown that the efficiency of Pt and Pt-Ru catalysts increases with elevated temperature. [64-68] In addition, further modification of PI to include sulfonate groups could be investigated. Previous studies, though sparse, have shown that sulfonated polyimide membranes offer good swelling properties and ionic conductivities which enhance the transport of protons across the polyelectrolyte, making them good candidates for polyelectrolyte materials.[69, 70] Sulfonated PI can then laminated to sulfonated PI/carbon/Pt electrodes to fabricate a PI based DMFC.

Present DMFC operation is constrained to temperatures below 80°C because

Nafion®'s mechanical and proton conducting properties deteriorate at temperatures above 80°C. The ability to construct the electrode material and the polyelectrolyte from sulfonated PI/carbon/Pt (or Pd) composites and sulfonated PI respectively for DMFC construction could allow higher operating temperatures above 80°C.

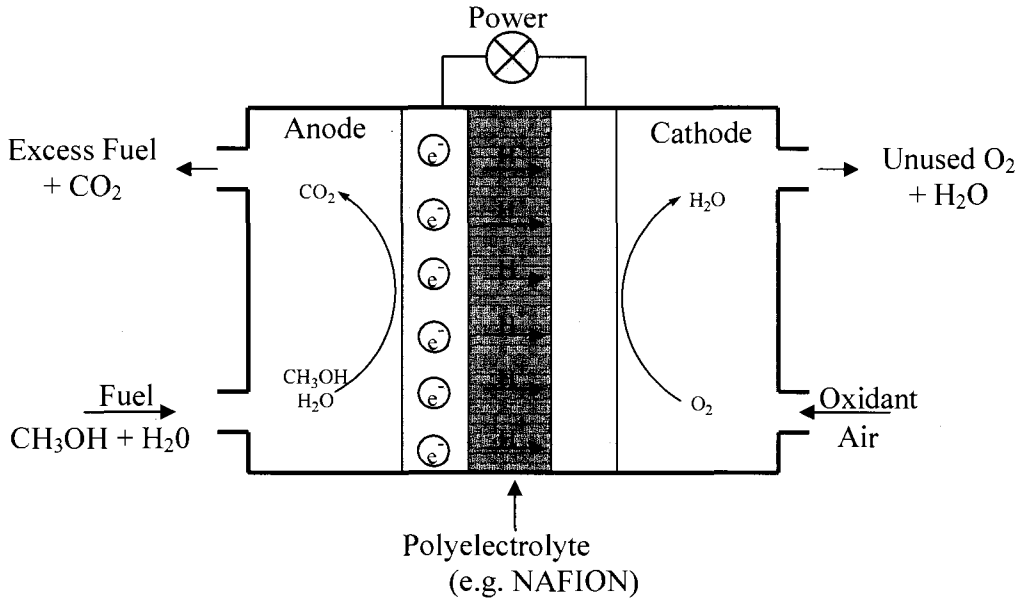

Figure1.1: Schematic of a Direct Methanol Fuel Cell (DMFC)

Similarly, the PI/carbon/Pt(Pd) electrodes can be explored for applications in hydrogen fuel cells to catalyze the electrooxidation of hydrogen. The fabrication and design of a hydrogen fuel cell is very similar to that of a DMFC except in this case the fuel is hydrogen instead of methanol. A schematic of a hydrogen fuel cell is presented in Figure 1.2. The half cell and overall reactions of a hydrogen fuel cell are presented as follows:

Anode: $H_2 \rightarrow 2H^+ + 2e^-$

Cathode: $0.5O_2 + 2H^+ + 2e^- \rightarrow H_20$

Overall: $2H_2 + O_2 \rightarrow 2H_20$

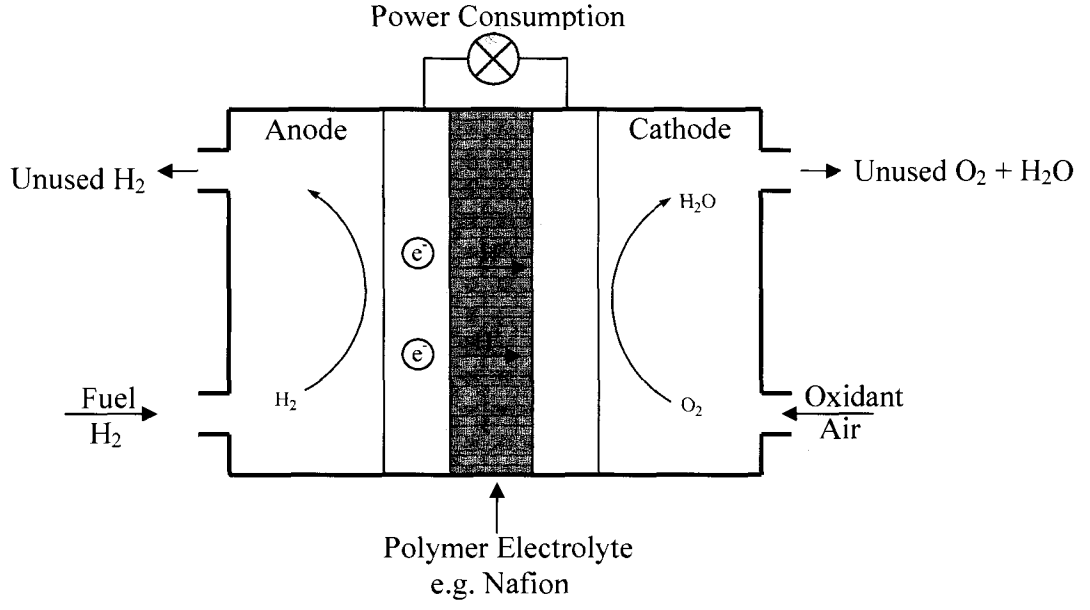

Figure 1.2: Schematic of a Hydrogen Fuel Cell

Another conceived application for PI/carbon/Pt(Pd) composites is to use them as electron donor layers in polymer based solar cells. The general layout of a polymer solar cell is presented on figure 1.3. Conjugated polymers are one class of materials used as electron donor materials in polymer cells.[71-73] Electrons in a conjugated polymer system are excited from the highest occupied molecular orbital (HOMO) to the lowest unoccupied molecular orbital (LUMO) by incoming photons. Delocalized electrons act as charge carriers by shuttling across the polymer backbone leading to the inherent electrical conductivity of conjugated polymers. In the case of PMDA/ODA polyimide, HOMO to LUMO excitations by photons are possible due to the presence of benzene and cyclic imide rings repeating units of the polyimide. Although not inherently conducting, the

presence of carbon and metal particles could act as charge carriers in the polyimide matrix leads to an electrically conductivity composite. These properties afforded by a modified electrically conducting PMDA/ODA polyimide could be exploited for its use as an electron donor layer in polymer solar cells.

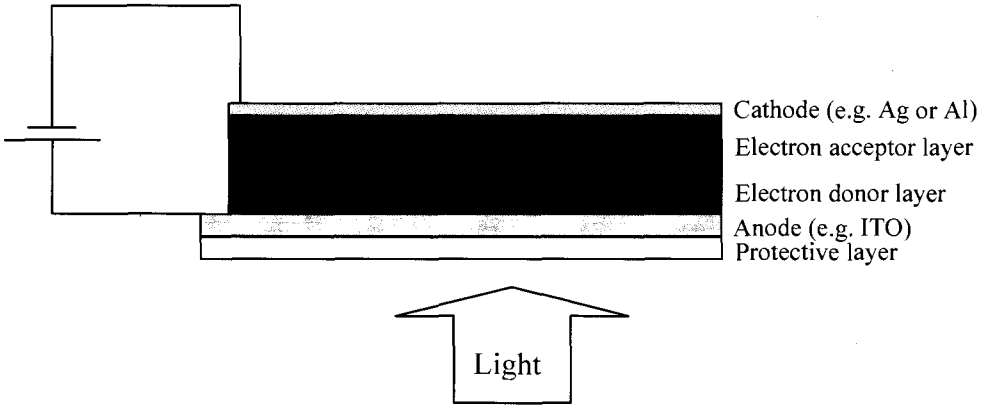

Figure 1.3: General Schematic of an Organic Solar Cell

Polyimides have found use as gate insulators in thin film organic field effect transistors (OFETS) because of their mechanical flexibility, thermal stability and excellent insulating properties.[74-77] OFETS are aimed at replacing traditionally used rigid silicon based mixed oxide semiconductor field effect transistors (MOSFETS). One further application can be envisioned for PI/carbon/Au is in the manufacture of contact electrodes for OFETS. A typical field emission transistor constitutes of three electrodes that include a voltage source, voltage drain and a gate. The current flow across the transistor is controlled by the gate. The source and the drain are separated from the gate through an insulating layer. Gold electrode channels making up the source and the drain electrodes are pattered on the insulator using electroplating methods or chemical vapor

deposition. By layering PI/carbon on the channel pattern imprinted on a PI insulating layer gold can then be electrochemically deposited on the PI/carbon layer as envisioned in Figure 1.4.

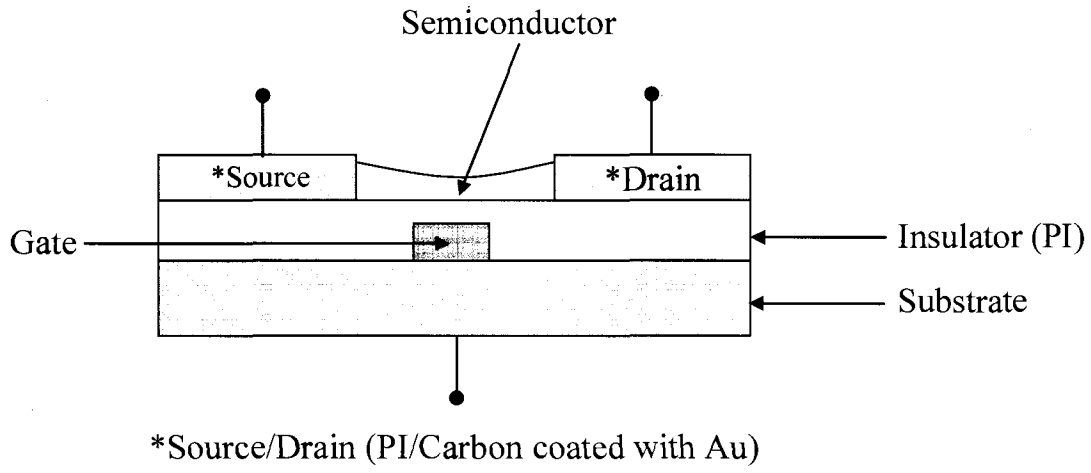

Figure 1.4: Envisioned PI/carbon/Au layered OFET [76, 77]

1.5 References

1. Grunbauer, H.J.M. and Folmer, J.C.W., *Polymer morphology of CO2 blown rigid polyurethane foams: its fractal nature.* Journal of Applied Polymer Science, 1994. **54**: p. 935-949.

2. Pielichowski, K., Kulesza, K., and Pearce, E.M., *Thermal degradation studies on rigid polyurethane foams blown with pentane.* Journal of Applied Polymer Science, 2003. **88**: p. 2319-2330.

3. Prociak, A., Pielichowski, J., and Sterzynski, T., *Thermal diffusivity of rigid polyurethane foams blown with different hydrocarbons.* Polymer Testing, 2000. **19**: p. 705-712.

4. Seo, W.J., Jung, H.C., Hyun, J.C., Kim, W.N., Lee, Y.B., Choe, K.H., and Kim, S.B., *Mechanical, morphological, and thermal properties of rigid polyurethane foams blown by distilled water.* Journal of Applied Polymer Science, 2003. **90**(1): p. 12-21.

5. Broberg, K., Tinnerberg, H., Axmon, A., Warholm, M., Rannug, A., and Littorin, M., *Influence of genetic factors on toluene diisocyanate-related symptoms: evidence from a cross-sectional study.* Environmental Health, 2008. **7**(15).

6. Banks, D.E., Rando, R.J., and Barkman, H.W., *Persistence Of Toluene Diisocyanate-induced Asthma Despite Negligible Workplace Exposures. .* Chest, 1990. **97**(1): p. 121-125.

7. Bello, D., Herrick, C.A., Smith, T.J., Woskie, S.R., Streicher, R.P., Cullen, M.R., Liu, Y.C., and Redlich, C.A., *Skin exposure to isocyanates: Reasons for concern.* Environmental Health Perspectives, 2007. **115**(3): p. 328-335.

8. Hatchett, D.W., Kodippili, G., Kinyanjui, J.M., Benincasa, F., and Sapochak, L., *FTIR analysis of thermally processed PU foam.* Polymer Degredation and Stability, 2005. **87**: p. 555-561.

9. McElhanon, J.R., Russick, E.M., Wheeler, D.R., Loy, D.A., and Aubert, J.H., *Removable foams based on an epoxy resin incorporating reversible Diels-Alder adducts.* Journal of Applied Polymer Science, 2002. **85**: p. 1496-1502.

10. Russick, E.M. and Rand, P.B., *Development and characterization of a new epoxy foam encapusulant as ablefoam replacement.*, in *Sandia Report:SAND98-2538*. 1998, Sandia National Laboratories.

11. Aubert, J., *Thermally removable epoxy adhesives incorporating thermally reversible Diels-Alder adducts.* Journal of Adhesion, 2003. **79**: p. 609-616.

12. Aubert, J.H., Tallant, D.R., Sawyer, P.S., and Garcia, M.J. *Synthesis and formulation of a removable conformal coating using Diels-Alder thermally-reversible adducts. ACS Fall National Meeting, Poly, PMSE and FSCT preprints.* 8/22-26, 2004. Philadelphia, PA.

13. Brown, R.F., *Organic Chemistry.* 1975, Belmont, CA: Wadsworth Publishing Company, Inc.

14. Chang, T.C., Wu, K.H., Liao, C.L., Lin, S.T., and Wang, G.P., *Thermo-oxidative degradation of siloxane-containing polyimide and unmodified polyimide.* Polymer Degradation and Stability, 1998. **62**: p. 299-305.

15. Lin, S.-T. and Huang, S.K., *Thermal degradation study of siloxane-DGEBA epoxy copolymers.* European Polymer Journal, 1997. **33**: p. 365-373.

16. Dvornic, P.R., Perpall, H.J., Uden, P.C., and Lenz, R.W., *Exactly alternating silarylene-siloxane polymers. VII. Thermal Stabilityand degradation behavior of p-silphenylene-siloxane polymers with methyl, vinyl, hydrido, and/or fluoralky side groups.* Journal of Polymer Science: Part A: Polymer Chemistry, 1989. **27**: p. 3503-3514.

17. Barthel, H. and Nikitina, E., *INS and IR Study of Intermolecular Interactions at the Fumed Silica-Polydimethylsiloxane Interphase. Part 3 Silica-Siloxane Adsorption Complexes.* Silicon Chemistry, 2004. **1**(4): p. 261-279.

18. Petrov, P., Bozukov, M., Burkhardt, M., Muthukrishnan, S., Muller, A.H.E., and Tsvetanov, C.B., *Stabilization of polymeric micelles with a mixed poly(ethylene oxide)/poly(2-hydroxyethyl methacrylate) shell by formation of poly(pentaerythritol tetraacrylate) nanonetworks within the micelles.* Journal of Materials Chemistry, 2006. **16**(22): p. 2192-2199.

19. Kim, Y.B., Kim, H.K., and Hong, J.W., *UV-curable methacrylic epoxy dispersions for cationic electrodeposition coating.* Journal of Applied Polymer Science, 2006. **102**(6): p. 5566-5570.

20. Gibson, L.J. and Ashby, M.F., *Cellular solids: structure and properties.* 1997, Cambridge: Cambridge University Press.

21. Dupont. *Kapton® HN.* 2007 [cited; Available from: http://www2.dupont.com/Kapton/en_US/assets/downloads/pdf/HN_datasheet.pdf.

22. Kaufmann C.A., Neisser A., Klenk R., and R., S., *Transfer of Cu(In,Ga)Se2 thin film solar cells to flexible substrates using an in situ process control.* Thin Solid Films, 2005. **480-481**: p. 515-519.

23. Kessler F. and Rudmann D., *Technological aspects of flexible CIGS solar cells and modules* Solar Energy, 2004. 77(6): p. 685-695.

24. Southward R.E., Thompson D.S., Thompson D.W., Caplan M.L., and A.K., S.C., *Synthesis of Reflective Polyimide Films via In Situ Silver (I) Reduction.* Chemistry of Materials, 1995. 7: p. 2171-2180.

25. Tiwari A.N., Romeo A., Baetzner D., and Zogg H., *Flexible CdTe solar cells on polymer films.* Progress in Photovoltaics: Research and Applications, 2001. **9**(3): p. 211-215.

26. Vijh A., Yang X., Du W., and Deng, X. *Film adhesion in triple junction a-Si solar cells on polyimide substrates.* in *Photovoltaic Specialists Conference.* 2005: IEEE XPLORE.

27. Bower, G.M. and Frost, L.W., *Aromatic polyimides.* Journal of Polymer Science Part A: General Papers, 1963. **1**(10): p. 3135-3150.

28. Lin J-S. and Chiu H-T., *Preparation and Properties of Conductive Polyimide films.* Journal of Polymer Research, 2002. **9**: p. 189-194.

29. Srividhya, A. and Reddy, B.S.R., *Synthesis and characterization of polyimide containing PEG/PDMS amphiphilic conetworks by hydrosilylation: Correlation between structure and properties.* Journal of Polymer Science Part a-Polymer Chemistry, 2007. **45**(9): p. 1707-1726.

30. Kricheldorf H.R., Nuyken O., and Swift G., *Handbook of Polymer Synthesis.* 2005, New York: Marcel Dekker.

31. Li, L., Qinghua, L., Jie, Y., Xuefeng, Q., Wenkai, W., Zikang, Z., and Zongguang, W., *Photosensitive polyimide (PSPI) materials containing inorganic nano particles (I)PSPI/TiO2 hybrid materials by sol-gel process.* Materials Chemistry and Physics, 2002. **74**(2): p. 210-213.

32. Zhai, Y., Yang, Q., Zhu, R.Q., and Gu, Y., *The study on imidization degree of polyamic acid in solution and ordering degree of its polyimide film.* Journal of Materials Science, 2008. **43**(1): p. 338-344.

33. Ranucci, E., Sandgren, A., Andronova, N., and Albertsson, A.C., *Improved polyimide/metal adhesion by chemical modification approaches.* Journal of Applied Polymer Science, 2001. **82**(8): p. 1971-1985.

34. Lee, K.W., Kowalczyk, S.P., and Shaw, J.M., *Surface Modification Of PMDA-ODA Polyimide - Surface-Structure Adhesion Relationship.* Macromolecules, 1990. **23**(7): p. 2097-2100.

35. Zhao, Y., Lu, Q.H., Chen, D.S., and Wei, Y., *Superhydrophobic modification of polyimide films based on gold-coated porous silver nanostructures and self-assembled monolayers.* Journal of Materials Chemistry, 2006. **16**(46): p. 4504-4509.

36. Huang, X.D., Bhangale, S.M., Moran, P.M., Yakovlev, N.L., and Pan, J.S. *Surface modification studies of Kapton (R) HN polyimide films.* 2003: John Wiley & Sons Ltd.

37. Ghosh M.K. and Mittal K.L., eds. *Polyimides.* 1996, Marcel Dekker: New York.

38. Lee, T., Park, S.S., Jung, Y., Han, S., Han, D., Kim, I., and Ha, C.-S., *Preparation and characterization of polyimide/mesoporous silica hybrid nanocomposites based on water-soluble poly(amic acid) ammonium salt.* European Polymer Journal, 2009. **45**(1): p. 19-29.

39. Sorrell, T.N., *Organic Chemistry.* 2 ed. 2006, Sausalito, CA.: University Science Books.

40. Imai Y., Fueki T., Inoue T., and M-A., K., *A New Direct Preparation of Electroconductive Polyimide/Carbon Composite Via Polycondensation of Nylon-Salt Type Monomer/Carbon Black Mixture* Journal of Polymer Science: Part A:Polymer Chemistry, 1998. **36**: p. 1031-1034.

41. Pantea D., Darmstadt H., Kaliaguine S., and Roy C., *Electrical conductivity of conductive carbon blacks:influence of surface chemistry and topology.* Applied Surface Science, 2003. **217**: p. 181-193.

42. Luo S. and Wong C.P., *Study on effect of acrbon black on behavior of conductive polymer composites with positive temperature coefficient.* IEEE Transactions on Components and Packaging Technologies, 200. **23**(1): p. 151-156.

43. Zhang W., Dehghani-Sanij, A.A., and Blackburn R.S., *Carbon based conductive polymer composites.* Journal of Materials Science, 2007. **42**: p. 3408-3418.

44. Hill D., Lin Y., Qu L., Kitagorodskiy A., Connell J.W., Allard L.F., and Y-P., S., *Functionalization of Carbon nanotubes with Derivatized Polyimide.* Macromolecules, 2005. **38**: p. 7670-7675.

45. Jiang X., Bin Y., and Matsuo M., *Electrical and Mechanical Properties of Polyimide-Carbon Nanotubes Composites Fabricated by In Situ Polymerization.* Polymer, 2005. **46**: p. 7418-7424.

46. Shigeta M., Komatsu M., and Nakashima N., *Individual Solubilization of Single-Walled Carbon Nanotubes Using Totally Aromatic Polyimide.* Chemical Physics Letters, 2006. **418**: p. 115-118.

47. Wise K.E., Park C., Siochi E.J., and J.S., H., *Stable Dispersion of single Wall Carbon Nanotubes in Polyimide: The Role of Covalent Interactions.* Chemical Physics Letters 2004. **391**: p. 207-211.

48. Zhu B-K., Xie S-H., Xu Z-K., and Y-Y, X., *Preparation and Properties of the Polyimide/Multi-Walled Carbon Nanotubes (MWNTs) Nanocomposites.* Composites Science and Technology, 2005. **66** p. 548–554.

49. Harrington C.B., Harrington M.I., Sultan M.F., and J.R., T., *Durable Platinum /Poyimide Sensing Structures*, Office, U.S.P., Editor. 1998, General Motors Corporation: United States.

50. Metz S., Heuschkel M.O., Avila B.V., Holzer R., Bertrand D., and P., R. *Microelectrodes with Three-Dimensional Structures for Improved Neural Interfacing.* in *Proceedings of the 23rd Annual EMBS International Conference.* 2001. Instabul, Turkey.

51. Bergmeister J.J., Rnacourt J.D., and Taylor L.T., *Synthesis and Characterization of Magnetic Iron Modified Polyimide Films.* Chemistry of Materials, 1990. **2**: p. 640-641.

52. Cardoso, J., GomezDaza, O., Ixtlilco, L., Nair, M.T.S., and Nair, P.K., *Conductive copper sulfide thin films on polyimide foils.* Semiconductor Science and Technology, 2001. **16**(2): p. 123-127.

53. Horn K., Bradshaw A.M. , Doblhofer K., Krause S. , Weinberg G., Seidenspinner H.M. , and R., S., *A Study of the Adhesion of Copper to Polyimide Foils using Surface Analytical Techniques.* Fresenius Z Anal Chem, 1989. **333**: p. 590-595.

54. Maggioni G., Carturan S., Boscarino D., G., D.M., and U., P., *Polyimide and platinum containing polyimide thin films obtained by vapour deposition polymerization; effects of thermal treatments.* Materials Letters, 1997. **32**(2-3): p. 147-150.

55. Sawada T. and Ando S., *Synthesis, Characterization, and Optical Properties of Metal-Containing Fluorinated Polyimide Films* Chemistry of Materials, 1998. **10**: p. 3368-3378.

56. Sessler G.M., Hahn B., and Yoon D.Y., *Electrical Conduction in Polyimide Films.* Journal of Applied Physics, 1986. **60**(1): p. 318-326.

57. Yoda S., Hasegawa A., Suda H., Uchimaru Y., Haraya K., Tsujui T., and Otake K., *Preparation of a Platinum and Palladium/Polyimide Nanocomposite Film as a Precursor of Metal-Doped Carbon Molecular Sieve Membrane via Supercritical Impregnation.* Chemistry of Materials, 2004. **16**: p. 2363-2368.

58. Anderson, M.R., Davis, R.M., Taylor, C.D., Parker, M., Clark, S., Marciu, D., and Miller, M., *Thin Polyimide Films Prepared by Ionic Self Assembly.* Langmuir, 2001. **17**: p. 8380-8385.

59. Oh S-Y., Park J-K., Choi J-W., and Moon C., *Fabrication of Micro Array of Polyimide LB Film and Its Application in Bioelectronics Device.* Molecular Crystals and Liquid Crystals, 2002. **377**: p. 241-244.

60. Andreescu D., Wanekaya A.K., Sadik O.A., and J., W., *Nanostructured Polyamic Acid Membranes as Novel Electrode Materials.* Langmuir, 2005. **21**(15): p. 6891-6899.

61. Hatchett, D.W., Wijeratne R., and Kinyanjui J.M., *Reduction of $PtCl_6^{2-}$ and $PtCl_4^{2-}$ in polyaniline: Catalytic oxidation of methanol at morphologically different composites.* Journal of Electroanalytical Chemistry, 2006. **593**: p. 203-210.

62. Ye, J., Liu, J., Xu, C., Jiang, S.P., and Tong, Y., *Electrooxidation of 2-propanol on Pt, Pd and Au in alkaline medium.* Electrochemistry Communications, 2007. **9**: p. 2760-2763.

63. Haile, S.M., *Fuel cell materials and components.* Acta Materialia, 2003. **51**(19): p. 5981-6000.

64. Arico, A.S., Baglio, V., Di Blasi, A., Modica, E., Antonucci, P.L., and Antonucci, V., *Analysis of the high-temperature methanol oxidation behaviour at carbon-supported Pt-Ru catalysts.* Journal of Electroanalytical Chemistry, 2003. **557**: p. 167-176.

65. Arico, A.S., Baglio, V., Di Blasi, A., Modica, E., Monforte, G., and Antonucci, V., *Electrochemical analysis of high temperature methanol electro-oxidation at Pt-decorated Ru catalysts.* Journal of Electroanalytical Chemistry, 2005. **576**(1): p. 161-169.

66. Arico, A.S., Monforte, G., Modica, E., Antonucci, P.L., and Antonucci, V., *Investigation of unsupported Pt-Ru catalysts for high temperature methanol electro-oxidation.* Electrochemistry Communications, 2000. **2**(7): p. 466-470.

67. Dickinson, A.J., Carrette, L.P.L., Collins, J.A., Friedrich, K.A., and Stimming, U., *Performance of methanol oxidation catalysts with varying Pt : Ru ratio as a function of temperature.* Journal of Applied Electrochemistry, 2004. **34**(10): p. 975-980.

68. Umeda, M., Sugii, H., and Uchida, I., *Alcohol electrooxidation at Pt and Pt-Ru sputtered electrodes under elevated temperature and pressurized conditions.* Journal of Power Sources, 2008. **179**(2): p. 489-496.

69. Gebel, G., Meyer, G., Gonon, L., Capron, P., Marscaq, D., Marestin, C., and Mercier, R., *Degradation of sulfonated polyimide membranes in fuel cell conditions.* Journal of Power Sources|Journal of Power Sources, 2006. **157**(1): p. 293-301.

70. Okamoto, K., *Sulfonated polyimides for polymer electrolyte membrane fuel cell.* Journal of Photopolymer Science and Technology, 2003. **16**(2): p. 247-254.

71. Hertel, D. and Bassler, H., *Photoconduction in amorphous organic solids.* ChemPhysChem, 2008. **9**(5): p. 666-688.

72. Mayer, A.C., Scully, S.R., Hardin, B.E., Rowell, M.W., and McGehee, M.D., *Polymer-based solar cells.* Materials Today, 2007. **10**(11): p. 28-33.

73. Brabec, C.J., Dyakonov, V., Parisi, C.J., ;, and Sariciftci, N.S., *Organic Photovoltaics; Concepts and Realization.* 2003, New York: Springer-Verlag.

74. Ahn, T., Choi, Y., Jung, H.M., and Yi, M., *Fully aromatic polyimide gate insulators with low temperature processability for pentacene organic thin-film transistors.* Organic Electronics, 2009. **10**(1): p. 12-17.

75. Zhen, L.J., Guan, W.H., Shang, L.W., Liu, M., and Liu, G. *Organic thin-film transistor memory with gold nanocrystals embedded in polyimide gate dielectric.* 2008: Iop Publishing Ltd.

76. Yusaku, K., Shingo, I., Ryohei, T., Tsuyoshi, S., Takao, S., Hiroshi, K., and Takayasu, S., *High mobility of pentacene field-effect transistors with polyimide gate dielectric layers.* Applied Physics Letters, 2004. **84**(19): p. 3789-3791.

77. Horowitz, G., *Organic field-effect transistors.* Advanced Materials, 1998. **10**(5): p. 365-377.

CHAPTER 2

EXPERIMENTAL

2.1 Characterization Methodology: Polyurethane Foam

2.1.1 Chemicals and Solutions

PU Foam: The PU foam was prepared using Voranol 490 (Dow Chemical Company, Midland MI), DC 193 Surfactant (Dow Corning Corporation, Taylor, MI), Polycat 17 amine catalyst (Air Products, New Milford, CT), distilled water, and Rubinate 1680 (Huntsman Polyurethanes, Geismar, LA). The mass of each component was selected to produce a target foam density of 0.1g/cc.

2.1.2 Polyurethane Foam Synthesis

A Model D700, a two-reactant mixing system by Decker Industries was used to automatically mix and dispense the components used to formulate the PU foam. The Voranol, amine catalyst, surfactant and water were pre-mixed at a ratio (by volume) of 86.96: 2.03: 0.55: 1.00 respectively to make up a two-and-half gallon batch. This mixture was then added to the "poly" compartment of the mixing system. An equal volume of rubinate was added to the "iso" compartment.

During the dispensing process, the components were metered, mixed, and injected into eight 28.7 mm inner diameter, 143 mm tall, cylindrical aluminum molds using a shot time of ~2 seconds. The molds were capped at the bottom and open at the top to allow the foam to rise and expand freely. A sufficient amount of the formula was injected into each

mold to produce a small mushroom on the top of each cylinder. Mold release (PTM and W Industries #PA0801) was applied to the inside of each cylindrical mold to help in extracting the foam once it was cured. The samples were processed at controlled temperatures of 25°C, 45°C, 65°C and 85°C for a period of 30 minutes. Post-curing of all foam samples was conducted at 66°C for four hours in a convection oven.

The samples were removed from the molds after processing and the mushroom top was removed from each molded foam sample. The remaining portion was sectioned into pieces with a band saw. To assure sample consistency, each sample was cut and sanded to a height of 25.4 mm and a volume of 16.4 cm^3. The PU foam samples were then bored (6 mm diameter by 4 mm thick) from the side, middle and center of the same sample and characterized by photoacoustic FTIR spectroscopy. The areas that were used are denoted by the white circles in the Scheme 2.

Side Middle Center

Scheme 2: Core samples used for FTIR testing (6 mm diameter, 4 mm thick)

2.1.3 FTIR Spectroscopy of PU Foam

All FTIR measurements were performed using a Digilab, FTS-7000 spectrometer using a photoacoustic detector (MTEC). Each sample was scanned 64 times with a resolution setting of 4 cm^{-1} and averaged to produce each spectrum. To ensure consistency, all samples used in FTIR measurements were removed from the second section from the top of the molded PU samples. It is important to note that the vertical

foam sections did not differ appreciably. It is somewhat surprising that there is little difference in the chemistry in the vertical sections of the mold. It is possible the vertical expansion of the mold minimizes the thermal differences vertically in the mold. However, changes in the radial distribution of species in the mold were consistent in the mold. The data were normalized using the technique described by Bhattacharjee et al. for the integration and quantifying of isocyanurate and isocyanate conversion in PU foams using FTIR spectra.[1] A minimum of five samples were used for each temperature at the side, middle, and center position. All reported integration values have a relative error of less than two percent for the sample group (not shown on plots).

2.2 Characterization Methodology: Removable Epoxy Foam

2.2.1 Epoxy Foam Synthesis

Foam cylinders were prepared at Sandia National Laboratory in a stainless steel cylindrical mold by injecting the mixed resins, curatives, surfactant, and blowing agent into the mold. The foam formulation is shown in Table 2.1. A Stochiometric mix was utilized with a ratio of 1:0.565 part A to part B, respectively. After injection into the mold, the foam expanded within the mold and was packed to the desired density of approximately 0.17 g/cm^3 (with a packing factor of approximately 2). The foams were treated with a two step cure (65 °C for 2 hrs / 75 °C for 22 hrs). The top and bottom of each foam cylinder was removed and then the remainder was sectioned using a band saw. To assure sample consistency, each sample was cut and sanded to a height of 25.4 mm for each section and a volume of 16.4 cm^3.

PART A	PART B
Epon®8121: 40% (epoxy resin)	Ancamine 2049: 38.1%(diamine)
RER 1: 48%	Ancamine 2205: 15.0% (diamine)
RER2: 12%	Fluorinert FC-72: 44.2% (blowing agent)
	DC193: 1.8% (surfactant)
	Cab-O-Sil M5: 0.9% (nucleating agent)

Table 2.1: Removable Epoxy Foam Formulation

2.2.2 Thermal Cycling

Epoxy foam sections were placed in a Lindberg-Blue MO1420A gravity oven at 95 °C and maintained at this temperature for 24 hours. The temperature control accuracy provided by the manufacturer for the oven is ±0.5% and chamber temperature uniformity of ±1% at 100°C. The oven was then allowed to return to room temperature and the foam equilibrated for an additional 24 hour period. The process of heating and cooling was designated as one thermal cycle. Samples were treated and removed at 1, 5 and 10 cycles. A minimum of 5 sections were used for each thermal cycle. In addition, five untreated foam sections were used as a baseline for the study and denoted as the 0 cycle specimens.

2.2.3 FTIR Spectroscopy of Epoxy Foam

All FTIR measurements were performed using a Digilab FTS-7000 spectrometer coupled with a Digilab UMA-600 IR microscope. In-situ FTIR measurements were conducted using an untreated foam sample placed on a gold mica substrate affixed to a

heating stage. The stage is equipped with a thermostat and thermocouple to ensure the accuracy of the temperature within ± 10 °C. The in-situ samples were examined after equilibrating at a given temperature for five minutes. For these measurements the difference spectra were obtained using the pristine foam as the background. Any change in the FTIR properties of the foam appear as positive or negative bands as their composition increases or decreases, respectively. All spectra were obtained from an average of 64 scans at a resolution setting of 8 cm^{-1}. All FTIR measurements were performed on the second section from the top of the mold to ensure sample consistency. Liquid samples were analyzed using a germanium attenuated total reflectance (ATR) crystal attachment.

2.2.4 Thermal Mechanical Analysis (TMA)

Thermal mechanical analysis (TMA) was conducted using a Netzsch TMA 202 instrument. Thermal mechanical analysis experiments were run at 5 °C/min, under N_2 gas (50 ml/min) with a constant force of 5cN applied to the sample. The average length of foam material tested was 2.0 mm.

2.2.5 Mechanical Analysis of Epoxy Foams

Compression tests were performed on the cylindrical sections to obtain the modulus using a United Testing (UTM) SSTM-1 frame. In accordance with the ASTM D1621 test and specimen standard, a 4.4kN load cell at a crosshead speed of 0.127 cm/min was applied. An equal number of sections from each vertical position in the removable epoxy foam cylinders were tested.

2.2.6 Density Analysis of Epoxy Foams

The weight of the cylindrical sections was determined using an analytical balance (±

0.0001g). The weight and the volume of each section were then used to calculate the density. The average density for each thermally cycled group was calculated by averaging the densities of all sections.

2.3 Characterization Methodology: Polyimide/Carbon/Metal Composites

2.3.1 Chemicals and Solutions

Poly(pyromellitic dianhydride-co-4,4'-oxydianiline), amic acid (PAA) solution (Aldrich, 15.0 wt. % ±5 wt. % in NMP/aromatic hydrocarbons, Cat.# 575828, trade name:Pyre-M.L.® RC-5057), dimethyl sulfoxide (Aldrich, ≥99.9%, Cat.# 154938), conductex® SC carbon black (Columbian Chemical company), potassium tetrachloroplatinate, K_2PtCl_4 (Strem, 98%, Cat.# 78-1970), potassium tetrachloroaurate, $KAuCl_4$ (Aldrich, 98%, Cat.#206075), potassium tetrachloropalladate K_2PdCl_4 (Strem Chemicals, 99%, Cat.#46-2126), perchloric acid (J.T. Baker, 69-72% , Cat# 9652-33), Acetone (J.T. Baker, 99.5% , Cat.#9006-7), Potassium Ferricyanide, ($K_3Fe(CN)_6$)

2.3.2 Preparation of Polyimide/Carbon Composites

2.3.2.1 Determination of PAA Solvent System

The solubility of the precursor materials used in polyimide synthesis is low in most solvents used for traditional polymer synthesis. Low volatility Polar solvents such as N-methyl-2 pyrolidone (NMP), N,N-dimethylformanimide (DMF), dimethylsulfoxide (DMSO) or methylglycol (MG) are used to dissolve polyamic acid. For example, Pyre ML® is supplied as a highly viscous liquid that contains 15-16% PMDA/ODA amic acid in NMP. Uniform dispersion of secondary components such as carbon black or metal cations in this solution is difficult due to the high viscosity. Therefore, dilution with

suitable solvent is required prior to casting thin films or the introduction of carbon filler materials.

In contrast, the removal of all solvent from the cast film prior to the imidization is an important step in preventing fractures in the film due to heat-related evaporation stress. Therefore a more volatile solvent system is required to maintain polymer precursor solubility prior to casting and facilitate evaporation during the curing stage prior to imidization.

The choice of acetone as a desirable polar aprotic solvent for PAA was based on its high volatility, relatively low health risks as compared to other solvents used for PAA. A small amount of PAA solution was added to 20 ml of acetone. The PAA precipitated immediately upon addition and did not dissolve even after 24 hours of stirring. However, the PAA became soluble in the solution upon mixing 5 ml of DMSO to 20 ml of acetone prior to adding PAA. Although PAA was soluble upon adding only 1ml DMSO to 20 ml acetone, PAA was found to precipitate out of solution after sitting for about 48 hours. This was also observed for PAA/carbon solution where precipitation occurred immediately after stirring was stopped. Therefore, a 1:5 DMSO to Acetone solvent system was used for all studies.

2.3.2.2 PAA Solution Preparation (10% Carbon Content)

In a sealable plastic container, 5.45 g of conductex sc carbon was added to 100 ml acetone. The carbon/acetone mixture was left stirring for 24 hours and then sonicated in a water bath at room temperature for about 3 hours. In a fume hood, 54.5g of polyamic acid (PAA) was weighed in a separate container. 20 ml of DMSO was added to the PAA solution. The PAA/DMSO mixture was thoroughly mixed for five minutes at 2000 rpm

using a VWR general purpose mixer. While still mixing at the maximum mixer speed, the carbon/acetone mixture was added very slowly to the PAA solution. After adding all the carbon mixture to PAA mixture was allowed to mix for about 20 minutes. The mixture was then visually inspected for uniformity.

The order of adding carbon/acetone and PAA/DMSO mixtures was found to influence the uniformity of the resulting mixture. For example, adding the DMSO/PAA to carbon/acetone led to immediate precipitation of PAA. However, on adding carbon/acetone to DMSO/PAA, PAA precipitation did not occur. Therefore, the latter sequence was followed in preparing all PAA/carbon solutions.

2.3.2.3 PAA Solution Application on a glass substrate

A small amount PAA/Carbon mixture was poured near the outer edge of the glass substrate. Using a glass slide of the same width as the substrate, the mixture was spread evenly on the substrate. This procedure was repeated until the whole glass substrate was covered. The applied layer was allowed to dry for a period of 24 hours before applying the next layer. This procedure was repeated for a total of five applications. For PAA/carbon films used for fabricating PI/Carbon/Pt films, a mixture containing 1ml $2x10^{-2}M$ $K_2PtCl_6^{2-}$ dissolved in water and 10ml of PAA/Carbon solution was applied as a final layer. The film was then allowed to dry in a fume hood for 48 hours.

2.3.2.4 PAA Film Curing and Imidization

The glass substrate containing the PAA/Carbon film was inserted into a vacuum oven. The film was left to dry at a temperature at about 80°C and vacuum setting of about 20 mmHg for a period one week. This was a very critical step to ensure maximum removal of residual low volatility DMSO and NMP solvents from the film. Failure to

remove residual DMSO led to fracturing of the film during the imidization stage. Thermal gravimetric analysis (TGA) was used to confirm removal of NMP and DMSO.

The film was then peeled from the glass substrate and sandwiched between two glass substrates clipped together. This step was taken to ensure that the film did not curl during imidization. The film was then inserted into a Lindberg-Blue model MO1420A recirculation oven preheated to a temperature of 100°C and left to heat for a period of 30 minutes. The temperature was increased to 150°C and heated for 30 minutes. This temperature program was repeated at 200 °C, 250°C and at the imidization temperature of 280°C. The oven was then set for 25°C and allowed to gradually cool down to this temperature prior to removal.

2.3.3 Metal Deposition on PI/Carbon

2.3.3.1 Deposition of Pt, Au and Pd by Cyclic Voltammetry

Platinum, gold and palladium were electrochemically deposited on the surface of the PI/Carbon composite using cyclic voltammetry. Deposition on a freestanding PI/Carbon working electrode is achieved using potential cycles that encompass the reduction of $PtCl_4^{2-}$, $AuCl_4^-$, $PdCl_4^{2-}$ ion to Pt, Au and Pd metals respectively. A schematic showing the three-electrode electrochemical cell used for the cyclic voltammetry experiments is shown in Figure 2.1. The cell was connected to a CH instruments model 760C potentiostat.

Pt, Au and Pd deposition were carried out using $2x10^{-2}$M K_2PtCl_4, $KAuCl_4$ and K_2PdCl_4 all dissolved in 1M $HClO_4$ respectively. All solutions were purged with nitrogen for a minimum of 10 minutes prior to deposition. An Ag/AgCl electrode filled with 3M KCl was used as a reference electrode while a platinum sheet was used as counter

electrode.

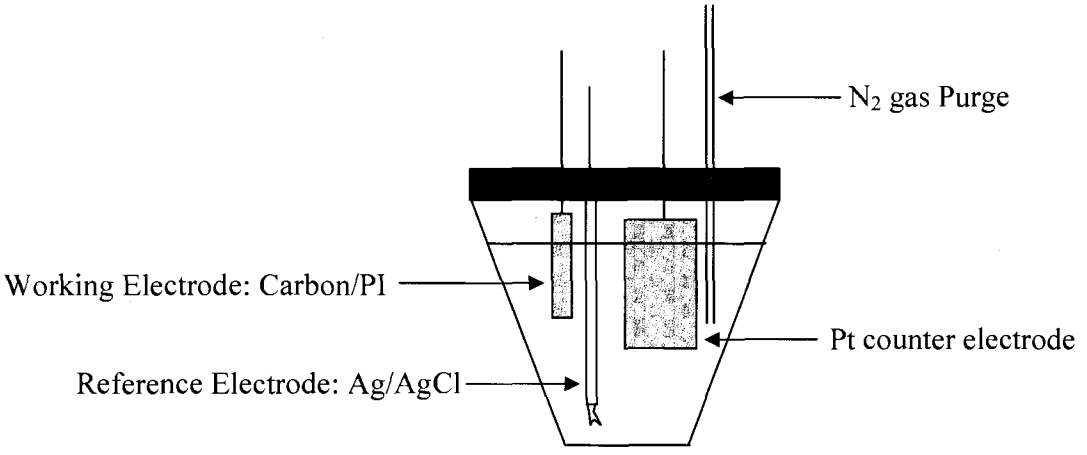

Figure 2.1: Three-electrode electrochemical cell used for cyclic voltammetry

2.3.3.2 Chemical Vapor Deposition of Au on PI/Carbon

Gold deposition on cleaved mica and PI/Carbon was performed in a Denton DV-502A high vacuum carbon filament evaporator accessorized with an Inficon XTM/2 quartz crystal oscillator thickness monitor. A chamber vacuum pressure of $4x10^{-6}$ Torr and an average deposition rate of 3 Å/sec were maintained during the deposition period.

2.3.4 Characterization

2.3.4.1 X-Ray Photoelectron Spectroscopy

X-ray photoelectron spectroscopy was employed to identify the oxidation state of platinum in the PI/Carbon/Platinum composites. XPS measurements were performed using a Specs PHOIBOS 150MCD electron analyzer with both Mg Kα and Al Kα X-ray sources. The base pressure was in the 10^{-10} mbar range for all measurements. The electron spectrometer was calibrated using XPS and Auger line positions of different metals (Cu, Ag, and Au).[2]

2.3.4.2 Simultaneous Thermal Analysis and Determination of Platinum Loading in PI/Carbon/Pt Films

Simultaneous Thermal Analysis (STA) was conducted using a Netzsch STA449C thermal analyzer. Simultaneous differential scanning calorimetry (DSC) and thermal gravimetric analysis (TGA) were performed on PAA, PI, PI/Carbon and PI/Carbon/Pt under air as both the purge (50ml/min) and protective (20 ml/min) gas at a heating rate of 10 °C/min. Samples were placed in alumina pans and covered with an alumina lid with a centered pin-hole. The furnace was evacuated to about 10^{-3} torr prior to introducing purge and protective gases.

Platinum loading in the PI/carbon/Platinum composites with a uniform carbon loading of 10% was estimated using TGA. The composite was heated to a temperature of about 900°C at which all the PI/carbon organic component of the composite was decomposed. All mass loss was assigned to the decomposition of the organic component. The remaining mass in the test crucible at the end of the experiment was then used to estimate the metal content for the composite material. For statistics, a minimum of three runs were performed at all platinum loadings examined.

2.3.4.3 Scanning Electron Microscopy

SEM images of PANI/Au composites were obtained using a JEOL 5600 electron microscope equipped with a backscattered electron (BSE) detector. The films were affixed to the sample holder using carbon tape and measurements were performed at an acceleration voltage of 15 kV. Metal shadowing was not required prior to SEM measurement.

2.3.4.4 Conductivity Characterization

Contacts with PI/Carbon and PI/Carbon/Pt films were made using a Cascade Microtech C4S-64/50 probe head with tungsten carbide electrodes. The four point probe sheet resistance of each film was then measured at locations across the surface of the pellet using an Agilent 34401A Digital Multimeter connected through a Cascade Microtech CPS-05 probe station. Constant pressure for each measurement was maintained for the probe head contacting the substrate. A total of five measurements at different locations, measured twice, are presented with representative standard deviations and relative standard deviations for the measurements.

2.3.4.5 Fourier Transform Infrared (FTIR) Spectroscopy measurements

All FTIR measurements were performed using a Digilab, FTS-7000 spectrometer using a photoacoustic detector (MTEC) on pristine samples. Each sample was scanned 64 times with a resolution setting of 4 cm^{-1} and averaged to produce each spectrum.

2.3.4.6 Cyclic voltammetry: PI/Carbon/Au characterization in Ferricyanide

Experiments to probe the ferricyanide redox couple using PI/Carbon/Au composite films as working electrodes were performed in 0.01M potassium ferricyanide [$K_3Fe(CN)_6$] in 1M KNO_3. A cyclic voltammetry assembly identical to Figure 2.1 was used for the experiment. A total of four working electrodes were used for the experiment as follows:

1. Carbon/PI with no Au layer.
2. Carbon/PI/Au containing Au deposited Carbon/PI using cyclic voltammetry.
3. Carbon/PI/Au with 100Å Au layer deposited on Carbon/PI using CVD.

4. A "reference" working Au planar electrode with 3000Å deposited on cleaved mica using CVD.

2.4 References

1. Bhattacharjee, D. and Engineer, R., *An improved technique for the determination of isocyanurate and isocyanate conversion by photoacoustic chemistry.* Journal of Cellular Plastics, 1996. **32**: p. 261-273.

2. Briggs, D. and Seah, M.P., *Practical Surface Analysis.* Vol. 1. 1990, New York Wiley.

CHAPTER 3

FTIR CHARACTERIZATION OF POLYURETHANE FOAM

3.1 Introduction

Polyurethanes have been used in wide variety of applications including insulating panels, coatings, sealants and adhesives. The continued use of rigid polyurethane (PU) foams in industrial applications is primarily based on insulating properties and low thermal conductivity of the materials. In contrast, the materials mechanical properties are more important for applications including thermal coatings, sealants and adhesives.[1-3] The application determines the degree of rigid (hard structure) versus flexible (soft structure) units that should be employed. [4]

Polyurethanes are extremely versatile materials employing diverse chemical functional groups that are incorporated into the polymer matrix during the reaction of the polyol with isocyanate. This reaction forms the structural backbone of the polymer and the flexibility or rigidity of the PU foam is based on the chemical constituents of the reactants. Typical diisocyanates include 2, 4- and 2, 6-toluene diisocyanate (TDI), 4, 4'-methylene diphenyl diisocyanate (MDI), and 1, 6-hexamethylene diisocyanate (HDI). However, each of these diisocyantes is hazardous if handled improperly. To minimize the hazard of common diisocyanates, a partially polymerized MDI was developed by Huntsman Chemical. The partially polymerized MDI (Rubinate 1680) contains chemical structures that can then be incorporated into the polymer matrix during the formation of

the PU foam. For example, Rubinate 1680 has been previously shown to include uretoneimine linkages based on the following structure. Degradation of the uretoneimine structure (bonds in bold) provides equimolar concentrations of carbodiimide and diisocyanate functional groups in the polymer. The diisocyanate groups can continue to react reducing its composition in comparison to the carbodiimide functional groups created from the degradation of the uretoneimine structure.

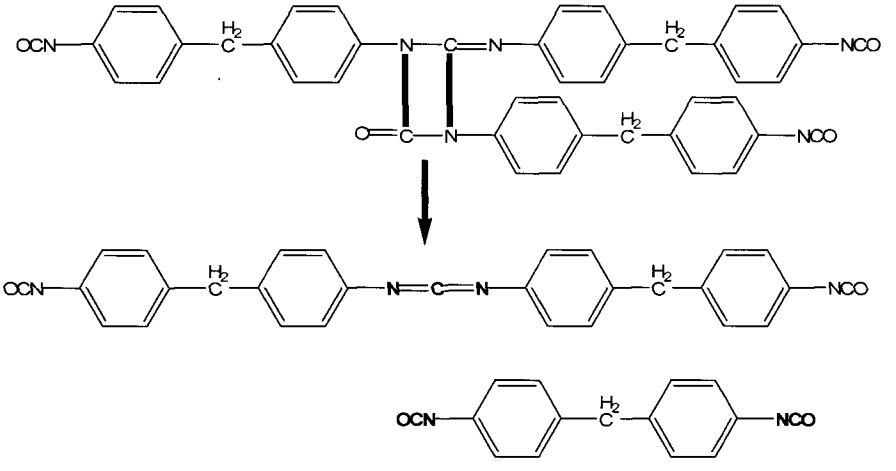

Scheme 3.1: Thermally initiated decomposition of the uretoneimine linkage in Rubinate 1680 to form carbodiimide and diisocyanate species (bold)

The formation of PU foams can be classified by the reaction of isocyanate and polyols (gel reaction) coupled with a gas generation reaction (foaming reaction) based on the addition of a blowing agent. A variety of blowing agents can be used in the production of PU foams with different microstructure and properties. [1, 5-7]For example, water can act as a blowing agent through the formation and decomposition of carbamic acid groups to form a primary amine and carbon dioxide. The foaming process causes the polymer foam to expand and fill the mold. The diisocyanate can continue to

react in the foaming process forming additional chemical functional groups such as urea, uretoneimine, iso-alophonate, biuret, carbodiimide and uretidinedione, which all contribute to the overall structure and rigidity of the material.[3, 4, 8] Rigid PU foams offer a very low thermal conductivity giving them the highest insulating value among all conventional insulating materials that are commercially available. Moreover, the trapped gas within the closed cell structure of the polymer matrix further reduces heat transfer that might occur by conduction.[9, 10] These factors produce regions of thermal isolation within the molded PU foam.

The complex microstructure, heterogeneity and mechanical characteristics of PU foams produced using the modified MDI have been examined previously.[11] The correlation of the physical, mechanical and chemical changes that occur in this foam when exposed to different processing conditions for a variety of mold geometries has also been examined.[12] The study demonstrated that the average density and radial density decreases with increasing processing temperature and larger mold geometry. In addition, the morphology of the foam is directly influenced by the processing temperature. The density, collapse strength, and Young's modulus have been used primarily to characterize the physical properties and rigidity of the molded PU foam in these studies. This research has focused on correlating the physical, mechanical and chemical properties of the foam to provide a more thorough understanding of processes that occur during preparation, processing, and curing of the material.[13]

The effect of thermal gradients in molded PU foams has largely been ignored in the literature. The exothermic nature of the reactions implies that internal thermal gradients may be present in the complex foam system. In addition, the foaming reaction creates

thermal isolated regions within the foam causing a certain degree of thermal segregation within molds. In previous studies of PU foams prepared using Rubinate 1680 it has been show that increasing processing temperature causes a significant decrease in the uretoneimine linkages in the polymer and a corresponding decrease in the density and modulus. [11-13] However, analysis of the heterogeneity of the chemistry with respect to the mold and position within the mold was not addressed. In the preparation of the PU foam, the foaming reaction is exothermic expanding up and out toward the wall of the mold. The reaction creates thermal gradients within the reaction mixture due to differences in the rate of heat transfer at the center and the side of the molded foam. The highest temperature should be at the center of the mold, decreasing in intensity as one moves toward the outer surface. In addition, the mold provides a surface for thermal convection reducing the temperature of the foam at the surface relative to the center. The influence of these processes on the chemistry of the molded polyurethane foam is the focus of this study.

In this study, the chemical composition (radially from side to center) of molded PU foam at different processing temperatures is explored using FTIR/PAS spectroscopy. Specifically, the concentration of the uretoneimine linkages, carbodiimide functional groups, and unreacted isocyanate groups are examined as a function of processing temperatures (25°C, 45°C, 65°C and 85°C). Quantitative analysis of the complex foam samples is obtained by examining the emergence and depletion of chemical species in the FTIR/PAS spectra. The resulting chemical gradients are identified and quantified with respect to radial position of the mold. The data is used to determine how thermal and chemical gradients influence the homogeneity and morphology of PU foam in a simple

cylindrical mold.

3.2 Results and Discussion

3.2.1 Photoacoustic FTIR (FTIR/PAS) Analysis of PU Foam

FTIR is a useful tool for determining the chemical composition of the complex PU foam. The PU foam is comprised of a complex mixture of unreacted starting materials and emerging chemical functional groups associated with the polymerization reaction. The functional groups that exhibit IR absorption bands can be monitored provided they can be isolated from other bands. The identification of the thermally sensitive functional groups within the polymer matrix is also critical to the analysis of the degradation properties of the material. FTIR/PAS is also a non-destructive measurement of pristine samples requiring no pre-treatment or grinding of the material into a KBr pellet which allows archival and future measurement of samples. Therefore, quantitative analysis of chemical species of interest can be performed using the characteristic bands exhibited by the unique functional groups within the foam provided experimental parameters are kept constant for each measurement. The measurements can be made over extended periods of time consistent with the normal degradation routines of the polymer [14].

This project is particularly interested in the qualitative and quantitative analysis of the bands associated with cross-linked structures (uretoneimine, 1379 cm^{-1} and 1726 cm^{-1}), unreacted isocyanate (2320 cm^{-1}), and emerging carbodiimide (2134 cm^{-1} and 2098 cm^{-1}) bands associated with degradation of the uretoneimine structures, Figure 3.1. The carbodiimide and isocyanate species generated from the degradation of the uretoneimine can be monitored and compared.

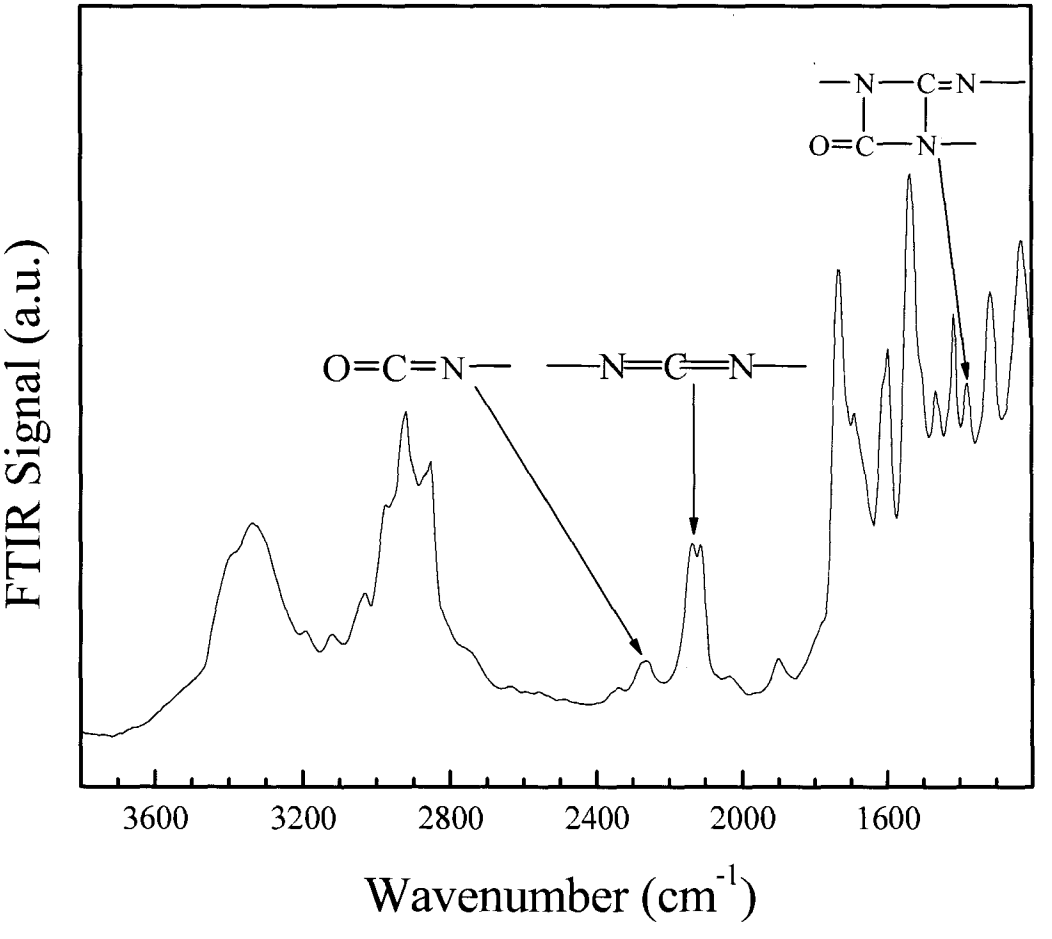

Figure 3.1: FTIR/PAS spectra of PU foam processed at 85°C with the isocyanate, carbodiimide, and uretoneimine groups labeled for clarity

The decomposition of uretoneimine structure in the "rubinate" isocyanate material is signaled by the decreases in the FTIR bands at 1726 cm^{-1} (carbonyl) and 1379 cm^{-1} (CN). However, the band at 1726 cm^{-1} will not be used to characterize the uretoneimine structure since it overlaps with bands corresponding to urethane and ester groups of the PU foam.[15, 16]

Figure 3.2a – 3.2c provides the FTIR data for the side, middle, and center molded PU foam at processing temperatures of 25, 45, 65, and 85°C. The FTIR response at ~ 1380 cm^{-1} is largest in Figure 3.2a (side) for the sample processed at 25°C decreasing as the processing temperature reaches 85°C. The uretoneimine intensity from the FTIR spectra for the side sample processed at 25°C will be considered as the baseline for the PU foams. The FTIR bands decrease as the processing temperature increases for the side samples which is consistent with the degradation of the uretoneimine structure in the polymer. There are two factors concerning the thermal degradation that need to be considered based on the data presented in Figure 3.2a – 3.2c. First, the thermal processing of the PU foam degrades uretonimine structures in all sections of the mold at all temperatures with exception to the side of the mold for the foam processed at 25°C. Second, the exothermic PU reaction and formation of the cellular structure cause a thermal gradient to exist as one move from the center of the mold to the side causing degradation of the uretoneimine structure, for all processing temperatures indicating that the foaming reaction reaches temperatures above the degradation temperature of uretoneimine groups at 40°C. In addition as one traverses the mold from the side to the middle and then the center, a decrease in the uretoneimine band is also observed.

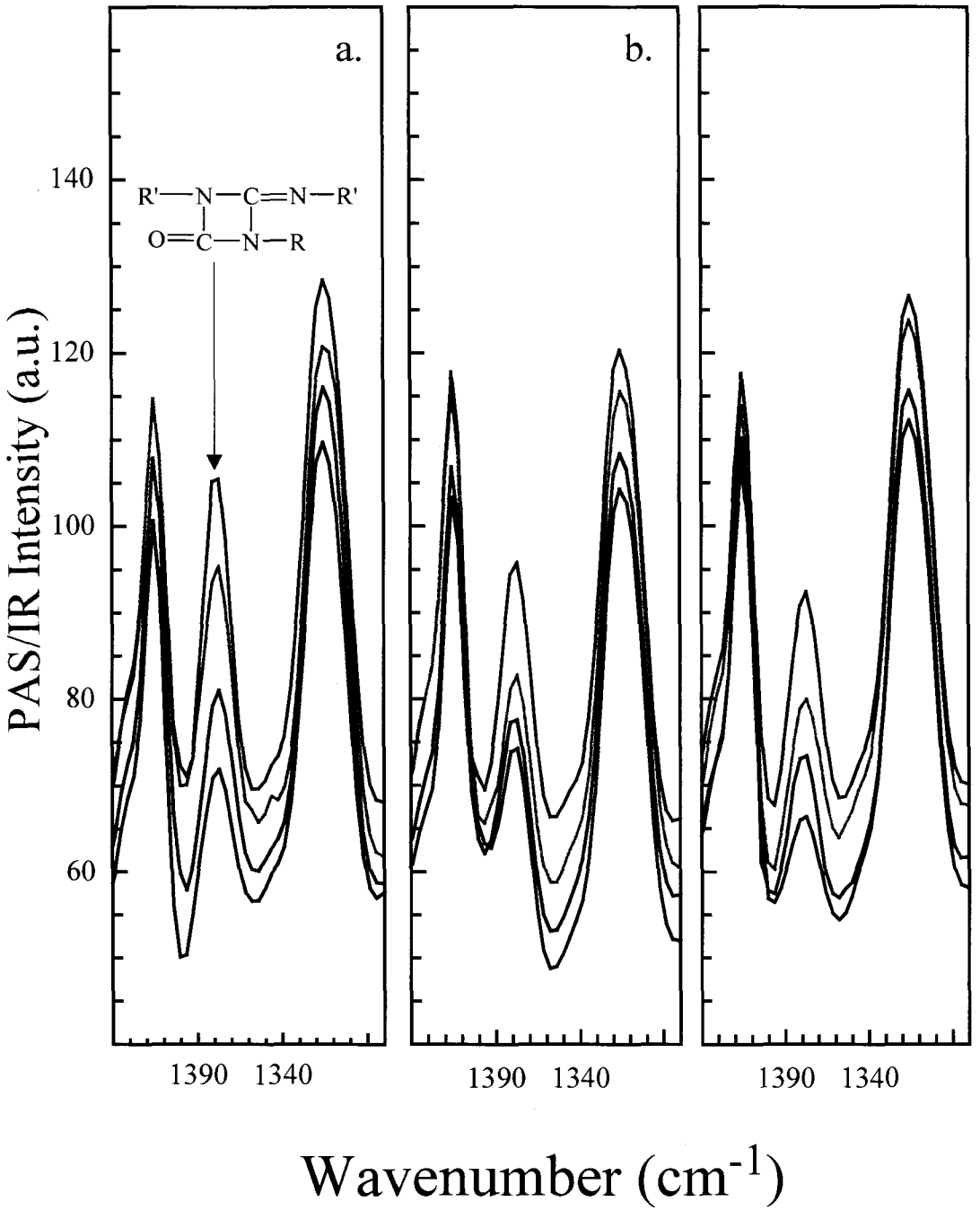

Figure 3.2: FTIR/PAS spectra highlighting the uretoneimine structure for molded PU foam processed at 25°C (Black), 45°C (Green), 65°C (Red), and 85°C (Blue) at the a. side, b. middle, and, c. center of the cylindrical mold

Finally, the side of the mold is in part, thermally isolated from the center of the mold and the exothermic foaming reaction causing less degradation of the uretoneimine structure for all processing temperatures.

The FTIR spectra for the isocyanate and carbodiimide between 1900 cm^{-1} - 2500 cm^{-1} is presented in Figure 3.3a – 3.3c, for the side, middle, and center of the molded PU foam (see experimental section) processed at temperatures of 25°C, 45°C, 65°C and 85°C. In Figure 3.3a, the side sample processed at 25°C shows very little in the spectral signal associated with the carbodiimide structure at 2134 cm^{-1} and 2098 cm^{-1}. This supports choosing the side sample processed at 25°C as the baseline value for the uretoneimine structure in Figure 3.2a. In addition, the unreacted isocyanate (~2320 cm^{-1}) for the side sample processed at 25°C is the largest for all samples examined.

There are a few trends that can be observed for the samples with respect to the carbodiimide and isocyanate functional groups. The carbodiimide increases in intensity for the side, middle, and center of the mold as the processing temperature increases. In contrast, the isocyanate band decreases for the side, middle, and center of the mold. These results are consistent with the degradation properties associated with uretoneimine structures in the polymer and the increases reactivity of isocyanate as processing temperatures are increased.

3.2.2 FTIR Analysis of Functional Groups in PU Foam.

Integration of the uretonimine, carbodiimide, and isocyanate bands from a minimum of five samples in Figure 3.4a – 3.4c provides a summary of the FTIR results.The side, middle, and center samples are denoted by the filled squares, filled circles, and filled triangles, respectively.

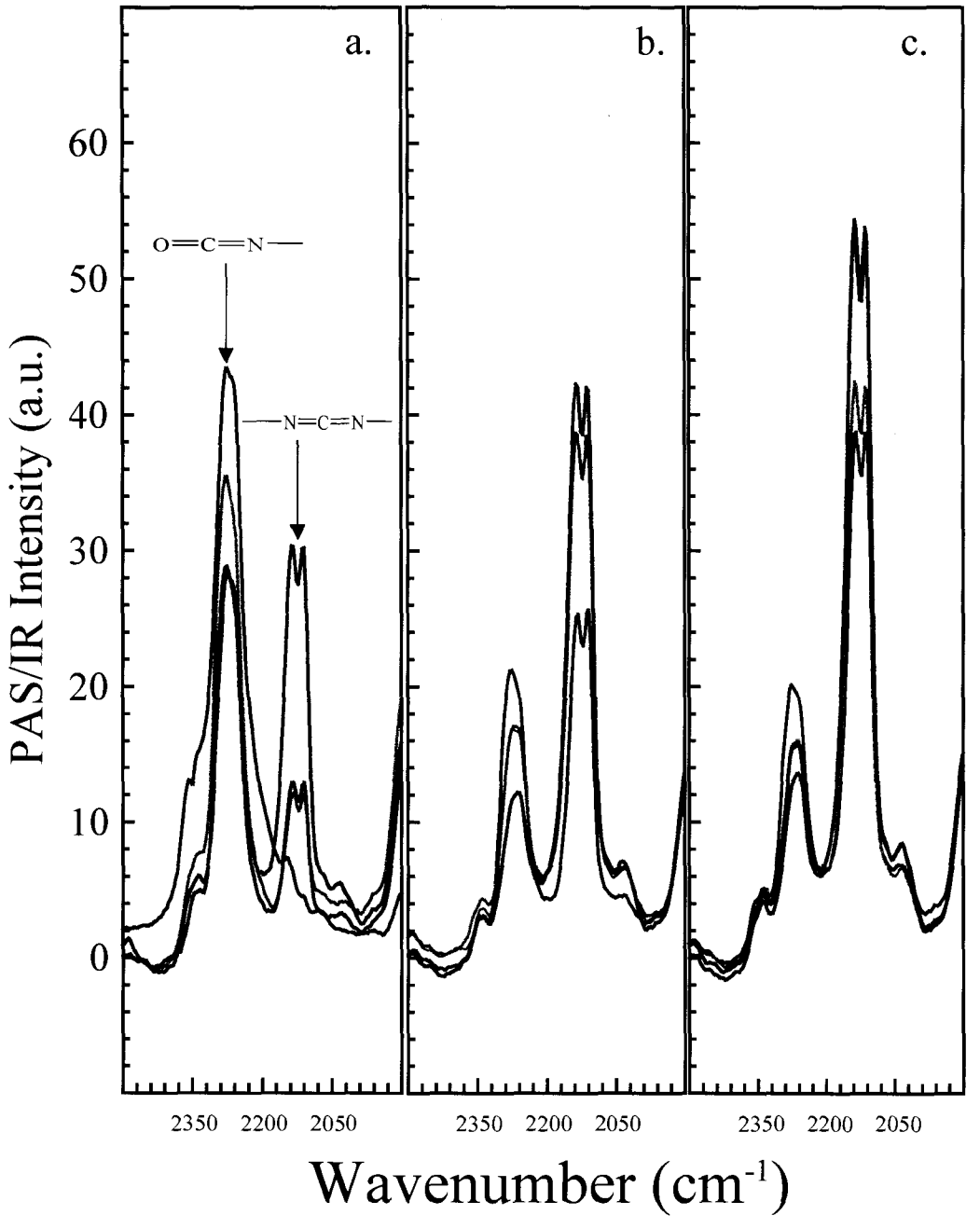

Figure 3.3: FTIR/PAS spectra highlighting the isocyanate and carbodiimide structures for molded PU foam processed at 25°C (Black), 45°C (Green), 65°C (Red), and 85°C (Blue) at the **a.** side, b. middle, and, **c.** center of the cylindrical mold

In Figure 3.4a, the side, middle and center of the mold show the characteristic decrease in intensity for the uretoneimine band as the mold is traversed from side to the center. In addition, for each position within the mold, the uretoneimine functional groups decrease with increasing processing temperature.

The emergence of carbodiimide functional groups within the polymer is based on the decomposition of the uretoneimine bonds. Therefore the carbodiimide functional groups should increase as a function of mold position as one traverses the mold from side to the center and with respect to increasing temperature. In Figure 3.4b, the carbodiimide intensity is near zero for the sample processed at 25°C at the side of the mold. The integrated values increase for the carbodiimide functional group at 25°C for the middle and center of the mold. The same trend is observed for all processing temperatures studied. The data indicates that both the loss of uretoneimine functional groups and the emergence of carbodiimide can be monitored using FTIR spectroscopy. In addition the data provides information concerning chemical gradients that emerge during the foaming reaction and secondary curing processes. The trends highlight the chemical gradients that exist within the simple mold at temperatures sufficient to degrade the structure within the polymer. The data indicates that under the processing conditions used all materials appear to be inhomogeneous.

The results also confirm the inhomogenous nature of the polymer for all temperatures employed in this study. The data indicates that the thermal insulation due to the cellular nature of the foam provides a degree of isolation that can be observed spectroscopically even with simple molds.

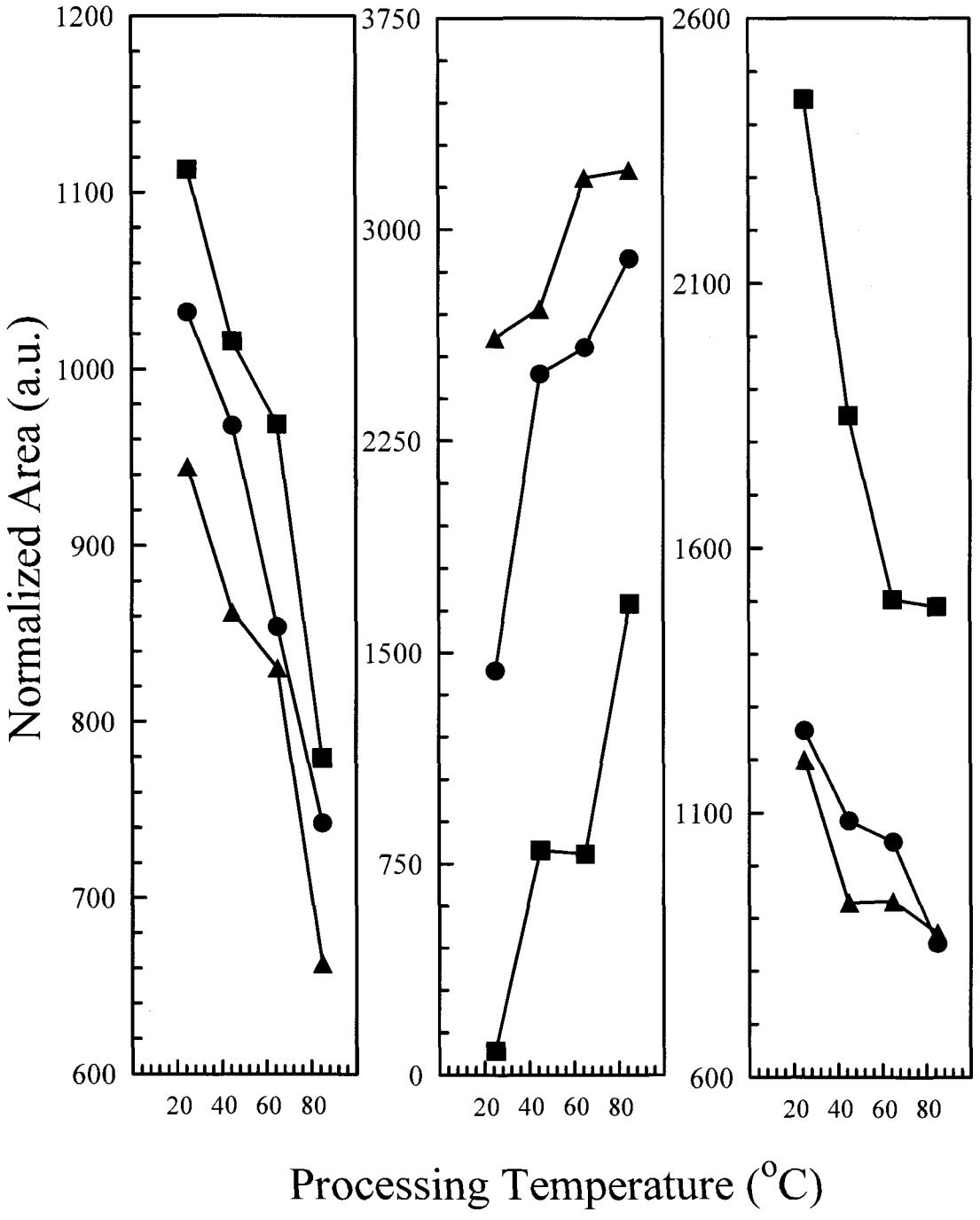

Figure 3.4: Integrated FTIR/PAS bands for a. uretoneimine, b.carbodiimide, and c. isocyanate groups as a function of mold position (■ – side, ● – middle, ▲ – center). Bands areas are normalized versus the area of the phenyl C=C band located at 1600 cm^{-1}

The center and side of the samples show the largest difference due to thermal activation during foaming process and because heat flow is limited due to low thermal conductivity of the cellular foam.

A secondary indication of chemical differences that exist within the foam can be observed through the change in composition of unreacted isocyanate in Figure 3.4c. The data indicates that the largest concentration of unreacted isocyanate exists in the foam processed at 25°C in the side position of the mold. The concentration of unreacted isocyanate at the middle and center of the mold decreases appreciably relative to the side of the mold. In addition, a decrease in the isocyanate is observed for all positions as a function of increasing processing temperature. The data indicates that a greater amount of unreacted material is present in the foam if the processing temperatures are lower. The composition of isocyanate at the side of the mold never reaches values comparable to either the middle or center of the foam. The data indicates that the side of the mold is not at thermal equilibrium with the sample. This suggests that the thermal properties of the mold and the ability of the mold to act as a thermal conductor influence the composition of all three of functional groups identified in this study.

3.2.3 Imaging of PU Foam

The FTIR data indicates that thermal gradients exist within the molded PU foam regardless of the processing temperatures employed. The emergence of chemical gradients in PU foams due to thermal gradients can also influence the morphology of the molded PU foam. Previously studies have shown that increasing temperatures used during thermal processing decreases the density of the foam through thermal expansion and evolution of CO_2 during the foaming process. Decreasing density can be attributed

to increasing cell dimension as observed in Figure 3.5. This figure shows optical images of PU foam as a function of position and processing temperature providing a qualitative assessment of the influence of thermal gradients on the cell morphology.

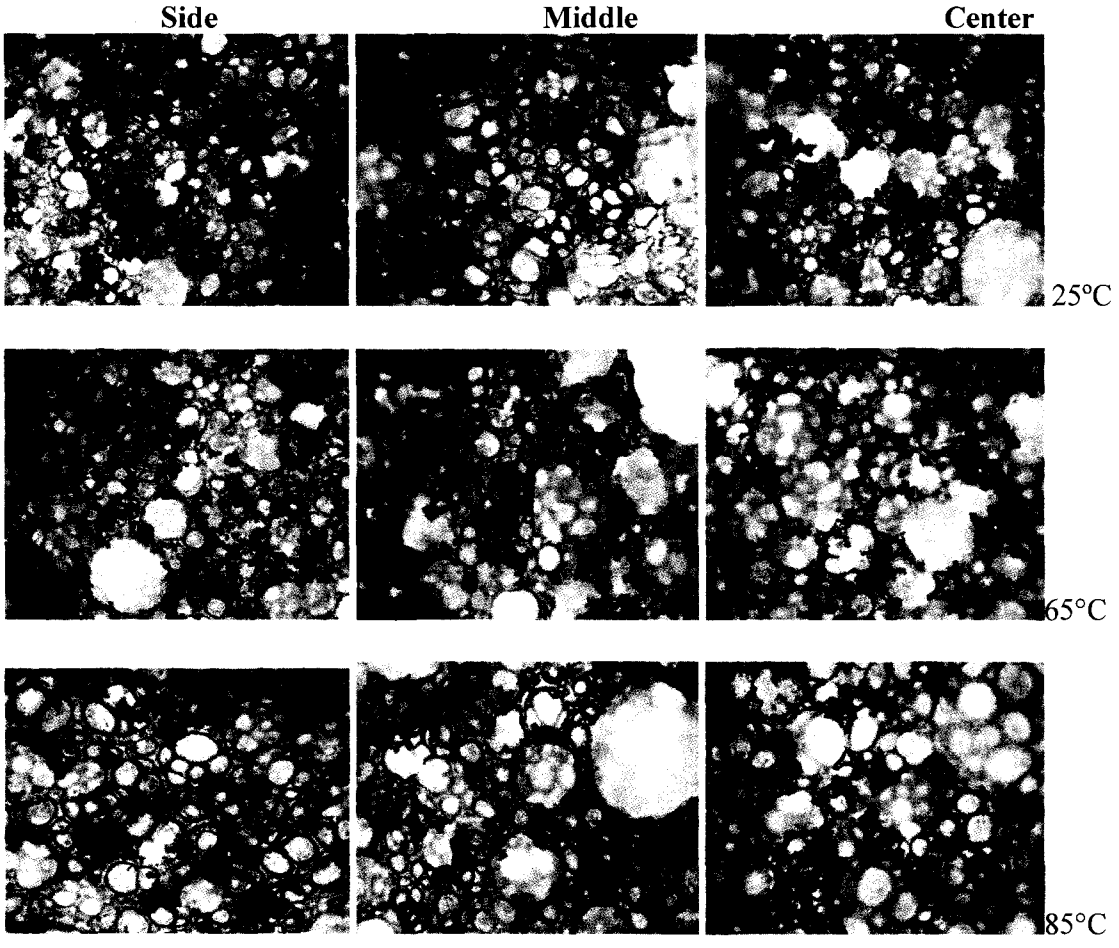

Figure 3.5: Optical images of PU foam as a function of position and processing temperature

The PU foam processed at 25°C has the smallest cell distribution for the side of the mold. The cell dimensions increase from the side to center of the foam processed at

25°C. Larger dimension cells are predominantly observed in the center of the mold with a few appearing in the middle for the foam processed at 25°C. Increasing cell dimensions are observed as one increases the processing temperature for all positions in the molded PU foam. The same trend is observed as a function of increasing processing temperature with the center sample processed at 65°C and 85°C showing the largest cell dimension and distribution. The images are consistent with the decrease in cross-link structures (uretoneimine) observed in the FTIR data and the thermal activation of the foaming process.

3.3 References

1. Gupta, T. and Adhikari, B., *Thermal degradation of HTPB-based polyurethane and polyurethane ureas.* Thermochimica Acta, 2003. **402**: p. 169-181.

2. Harbron, D.R., Paige, C.J., and Scarrow, R.K., *Methods of minimizing density gradients in rigid polyurethane foams* Journal of Cellular Plastics, 2001. **37**: p. 43-57.

3. Szycher, M., *Szycher's Handbook of polyurethanes.* 1999, New York, NY: CRC Press.

4. Pompe, G., Pohlers, A., Pötschke, P., and Pionteck, J., *Influence of processing conditions on the multiphase structure of segmented polyurethanes.* Polymer, 1998. **39**: p. 5147-5153.

5. Grunbauer, H.J.M. and Folmer, J.C.W., *Polymer morphology of CO2 blown rigid polyurethane foams: its fractal nature.* Journal of Applied Polymer Science, 1994. **54**: p. 935-949.

6. Pielichowski, K., Kulesza, K., and Pearce, E.M., *Thermal degradation studies on rigid polyurethane foams blown with pentane.* Journal of Applied Polymer Science, 2003. **88**: p. 2319-2330.

7. Seo, W.J., Jung, H.C., Hyun, J.C., Kim, W.N., Lee, Y.B., Choe, K.H., and Kim, S.B., *Mechanical, morphological, and thermal properties of rigid polyurethane foams blown by distilled water.* Journal of Applied Polymer Science, 2003. **90**(1): p. 12-21.

8. Chattopadhyay, D.K., Sreedhar, B., and Raju, K.V.S.N., *Thermal stability of chemically crosslinked moisture-cured polyurethane coatings.* Journal of Applied Polymer Science, 2005. **95**: p. 1509-1518.

9. Biedermann, A., Kudoke, C., Merten, A., Minogue, E., Rotermund, U., Ebert, H.P., Hienemann, U., and Fricke, J., *Analysis of heat transfer mechanisms in polyurethane rigid foam.* Journal of Cellular Plastics, 2001. **37**: p. 467-483.

10. Prociak, A., Pielichowski, J., and Sterzynski, T., *Thermal diffusivity of rigid polyurethane foams blown with different hydrocarbons.* Polymer Testing, 2000. **19**(6): p. 705-712.

11. Hawkins, M.C., O'Toole, B., and Jackovich, D., *Cell morphology and mechanical properties of rigid polyurethane foam.* Journal of Cellular Plastics, 2005. **41**: p. 267-285.

12. Jackovich, D., O'Toole, B., and Hawkins, M.C., *Temperature and mold size effects on physical and mechanical properties of a polyurethane foam.* Journal of Cellular Plastics, 2005. **41**: p. 153-168.

13. Hatchett, D.W., Kodippili, G., Kinyanjui, J.M., Benincasa, F., and Sapochak, L., *FTIR analysis of thermally processed PU foam.* Polymer Degredation and Stability, 2005. **87**: p. 555-561.

14. Bhattacharjee, D. and Engineer, R., *An improved technique for the determination of isocyanurate and isocyanate conversion by photoacoustic chemistry.* Journal of Cellular Plastics, 1996. **32**: p. 261-273.

15. Dillon, J.G., *Infrared Spectroscopic Atlas of Polyurethanes.* 1989, Lancaster, PA.: Technomic Publishing Co.

16. Silverstein, R.M. and Webster, F.X., *Spectrometric identification of organic compounds.* 1998, New York: John Wiley & Sons.

CHAPTER 4

CHEMICAL AND THERMAL STABILITY OF A DIELS-ALDER EPOXY FOAM

4.1 Introduction

Polymeric foams are versatile materials that have been used for a broad range of applications based on their chemical, physical and mechanical properties. The synthetic conditions can be varied to provide rigid or flexible foams with variable densities and mechanical strength. For example polyurethane (PU) foams can be prepared as rigid impact resistance materials or flexible memory materials that can retain shape after decompression by changing chemical substituent groups in the PU polymer chain. Chemical cross links are often utilized to provide more rigid foams. Rigid (PU) foams have been used to encapsulate electro-mechanical components and provide shock isolation and impact resistance. The foam can be injected into a cavity where it expands encapsulating the component. The PU foam adheres strongly to the component providing shock isolation. Although PU foams have high mechanical strength required for shock isolation, the material is extremely difficult to remove without damaging the encapsulated component. Strong adhesion of PU foams to surfaces requires that harsh methods such as sand blasting or chemical reactions with strong bases be used to remove the foam from components. Damage or corrosion of sensitive electrical components can occur using these methods. Therefore repair of components that have been previously encapsulated is unlikely. Foam systems that can be easily removed using less harsh methods while

maintaining the integrity of the encapsulated components are required.

Removable epoxy foams (**REFs**) have been developed as a possible replacement for traditional rigid PU foams currently used to encapsulate sensitive components. **REFs** have been proposed as replacements for PU foams because they provide a simple chemical method to remove the foam from the encapsulated components for repair, replacement of damaged parts, or dismantlement and disposal. Reversible Diels-Alder linkages are incorporated into the foam which can thermally degrade to facilitate dissolution. The foam dissolves in the presence of suitable solvent under more benign conditions than required for removing PU foams, minimizing any damage to the encapsulated components. Moreover, **REFs** have similar properties when compared to PU foams. They can easily expand to fill complicated geometric shapes with good adhesion to provide shock isolation.

The incorporation of chemical groups that enhance the removal of the foam is an important factor when considering the utility of the foam system. However, **REFs** must have similar mechanical properties when compared to PU foams to be useful for a wide range of applications. Previously it was demonstrated that the mechanical properties of PU foams degrade with time and exposure to elevated temperature.[1, 2] Decreases in Young's modulus and density of PU foams are common when exposed to elevated temperatures and multiple thermal cycles due to chemical changes in the foam. Therefore, **REFs** must have comparable thermal and mechanical stability to be used as replacements for PU foams in encapsulation applications.

The synthesis of removable epoxy foams is achieved through the incorporation of Diels-Alder bonds in the structure. The simplest Diels-Alder reaction between furan and

maleimide is shown in reaction scheme 4.1. A higher yield of the exo species is obtained relative to the endo species during the reaction. The formation of the Diels-Alder species is favored below 60 °C. The reverse reaction becomes more prominent as the temperature is increased above 90 °C, resulting in thermal degradation of the Diels-Alder bonds. Removable resins and foams based on reversible Diels-Alder chemistry have been prepared and utilized for a variety of applications including adhesives and potting of electronic components.[3-6] The epoxy resins incorporate Diels-Alder chemistry directly into the **REFs** structure. The reversibility of the Diels-Alder bonds has not been extensively studied for **REFs**. More importantly, questions remain with respect to the influence of thermal exposure on the overall chemical and mechanical stability of **REFs**.

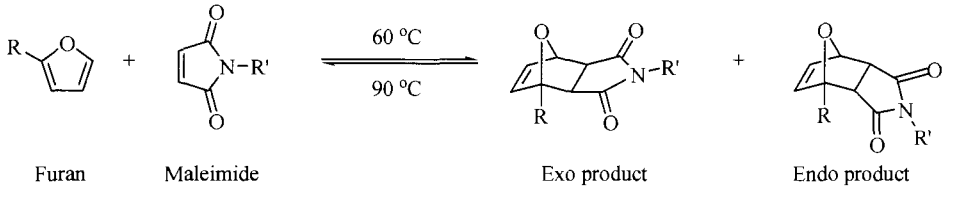

Scheme 4.1: The general Diels-Alder reaction between Furan and Maleimide

The role of other reactions within the epoxy based foams is also extremely important. These reactions within the epoxy resin based foams can also be influenced by thermal exposure changing both the chemistry and structure of the foam. For example, the formation of chemical cross links within the foam occurs when epoxy resins are reacted with diamines or polyamines. The process is commonly referred to as amine curing. Curing results in a highly crosslinked solid with superior adhesion and mechanical

properties. A simplified cure reaction between the epoxide group of an epoxy resin and a primary amine is presented in Scheme 4.2. The secondary amine can subsequently react with another epoxide group to form a tertiary amine. The reactions between epoxide and amine groups form chemical crosslinks which increases the rigidity of the foam.[7, 8]

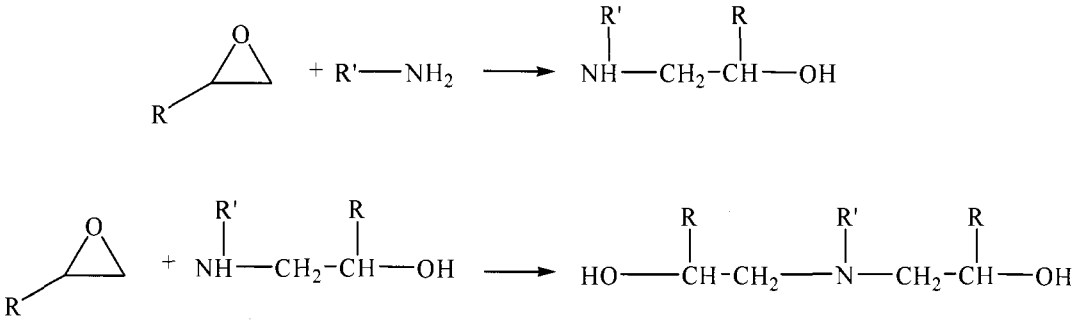

Scheme 4.2: Epoxide Group Reaction with a Primary Amine

The formation of the epoxy foam is achieved with the addition of blowing agent and surfactant during the amine curing reaction. The incorporation of the Diels-Alder adducts provides linkages that can be broken to facilitate removal of the resin, coating or foam through simple thermal treatment. However, additional modification of the epoxy resin backbone with specific functional groups can lead to a large number of resins with tailored interactions and properties. For example, in previous studies, siloxane tethers have been incorporated to the resin backbone to improve the thermal stability of Diels-Alder based foam.[3-6] Specifically, siloxane oligomers have been shown to improve the thermal stability of siloxane-modified bisphenol-A diglycidyl ether epoxy (ESDG) copolymers.[9] Furthermore, phenyl enriched siloxane oligomers further increase the

degradation temperature of the bisphenol-A diglycidyl ether (DGEBA) resin over dimethyl siloxane oligomers.

Although the synthetic process for preparing Diels-Alder based removable epoxy resins and foams is well documented, the characterization of the chemical and mechanical properties of **REFs** under thermal conditions that should encompass the degradation of the Diels-Alder adduct has not been extensively studied. In addition, the repeated thermal cycling of **REFs** and the chemical reversibility of Diels-Alder adduct formation/decomposition has not been addressed in terms of the materials stability. A search of the literature provide a single high temperature investigation of a heat transfer model to study the effect of heat fluxes on Diels-Alder **REFs** from room temperature to about 900°C.[10] However, there is limited experimental data to accompany this study. In addition, the theoretical studies do not explore the influence of thermal cycling on the chemical and mechanical properties of the materials.

The present study focuses on Diels-Alder **REFs** synthesized from a mixture of epoxy resins that include a commercial epoxy resin, Epon® 8121, and two removable Diels-Alder epoxy resins. The first removable epoxy resins was prepared through the reaction of octamethyltetrasiloxane with di-4,1-phenoxy-bismaleimide. This species was then reacted with two furfuryl glycidyl ether units. This product is referred to as **Removable Epoxy Resin 1** or, **RER1**. The second epoxy resin, **RER2**, was prepared using the same procedure used to prepare **RER1**, substituting 1,3-phenoxy dimaleimide for di-4,1-phenoxy-bismaleimide octamethyltetrasiloxane. The second step in the preparation of **RER1 and RER2** is presented in Scheme 4.3a and 4.3b respectively. Scheme 4.3c represents the structure of bisphenol-A diglycidyl ether which is the active constituent of

Epon® 8121. The epoxy foam prepared from this resin mixture was subjected to between two and ten thermal cycles. In this study, one thermal cycle is denoted by 24 hours of thermal exposure at 95 °C followed by a 24 hours cooling period.

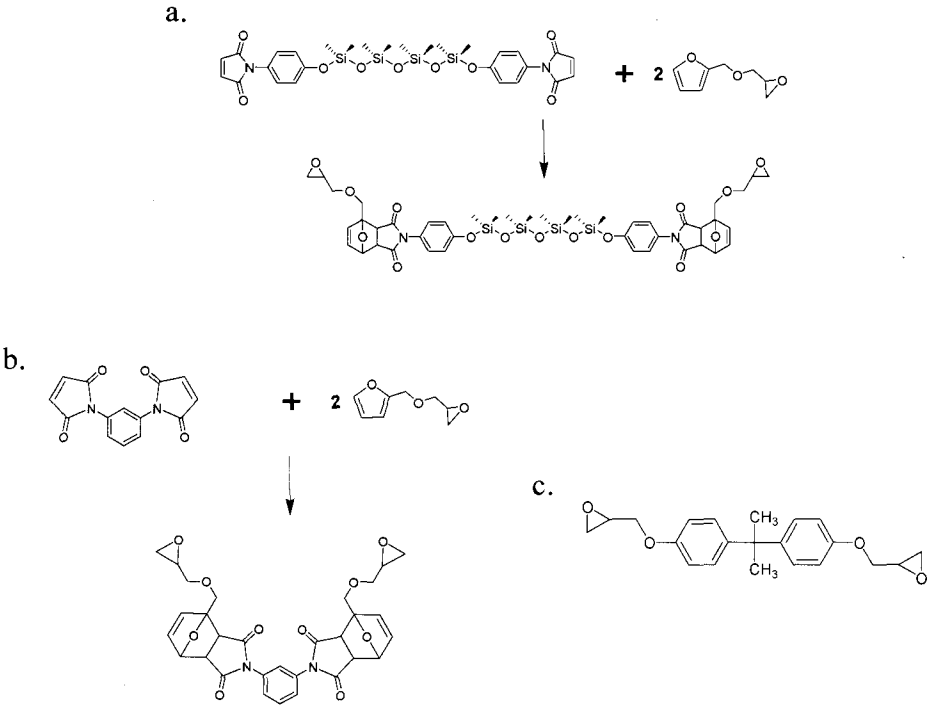

Scheme 4.3: (a) Preparation of RER1 resin (b) Preparation of RER2 resin
(c) bisphenol-A diglycidyl ether the active constituent of Shell Epon® 8121 resin

This study examines the effect of thermal exposure and cycling on the chemistry, physical, and mechanical properties of the removable epoxy foam. In addition, the reversibility of thermally induced changes in the chemistry and the mechanical properties of epoxy foams were evaluated with respect to repeated thermal cycling. The temperature range exceeds the temperature for the formation and breakage of Diels-Alder

bonds and the inter-chain physical interactions between functional groups in the polymeric resin chains such as hydrogen bonding and polar interactions. The physical interactions and packing of the siloxane groups in the RER1 adduct can be influenced at temperatures well below the degradation of the Diels-Alder bonds. In addition, siloxane groups are known to exhibit high chemical stability well above the temperatures used in this study.[9, 11, 12] The influence of thermal exposure on the chemical, physical and mechanical properties of removable epoxy foams was examined using Fourier transform infrared (FTIR) microsampling analysis and thermal mechanical analysis (TMA). In addition, the density and Young's modulus were examined as an indication of thermal expansion and changes in the mechanical properties of the thermally cycled **REFs**.

4.2 Results and Discussion

4.2.1 FTIR Analysis

Analysis of the chemical properties of complex foam systems requires an understanding of the FTIR characteristics of the individual components used in the preparation. This is particularly important in the fingerprint region (1000 – 2000 cm^{-1}), which contains multiple bands that can be used to identify constituent functional groups. This region can also be used to monitor changes in chemical composition and structure of the epoxy foam during thermal exposure, provided the functional groups can be identified. The FTIR spectra of the foam building blocks, furfuryl alcohol, furfuryl glycidyl ether, di-4,1-phenoxy-bismaleimide octamethyltetrasiloxane, and the **RER1** resin (di-4,1-phenoxy-bismaleimide octamethyltetrasiloxane reacted with furfuryl glycidyl ether) and epoxy foam are presented in Figure 4.1a – 4.1e, respectively.

Furfuryl alcohol is included in the study because it was present in the **RER1** resin. For clarity, Figure 4.2 and Figure 4.3 provide a more detailed plot of the IR bands for spectral ranges between 800-1350 cm^{-1} and 1350-1900 cm^{-1}, respectively. Previous studies have identified characteristic bands associated with epoxy foams using FTIR spectroscopy. [13] In this study, the IR bands associated with the adduct, including ether groups, siloxane chain extenders, C-N, and C-O functional groups have been identified. The band assignments for the foam are provided in Table 4.1. Many of the characteristic species are observed as overlapping bands in the fingerprint region encompassing C-O-C ether modes between 1000 – 1300 cm^{-1}, Si-O-Si and CH_3-Si-O modes between 1000 – 1275 cm^{-1}, C-N-C modes around 1390 cm^{-1} and C=O modes between 1650 and 1750.[14, 15]

It is impossible to evaluate the individual contribution of each functional group independently due to the high degree of overlap between the bands. However, the band at 1255 cm^{-1} in Figure 4.1c for di-4,1-phenoxy-bismaleimide octamethyltetrasiloxane is not present in either the alcohol or furfuryl glycidal ether spectra. The absence of C-O-C bands in this structure precludes assignment of this band to the ether functional group. Rather, the band is the result of the repeating CH_3-Si-O functional group typically observed at medium to high intensity between 1200 – 1270 cm^{-1}. This band appears in both the **RER1** and foam with similar intensities. This band is examined for the foam to determine if the siloxane extenders are influenced by thermal processing. The strong carbonyl band located at 1710 cm^{-1} can be attributed to the bismaleimide functional group. This band can be observed at 1714 cm^{-1} for the **RER1** resin, with the emergence of a second carbonyl band at 1774 cm^{-1}.[15, 16]

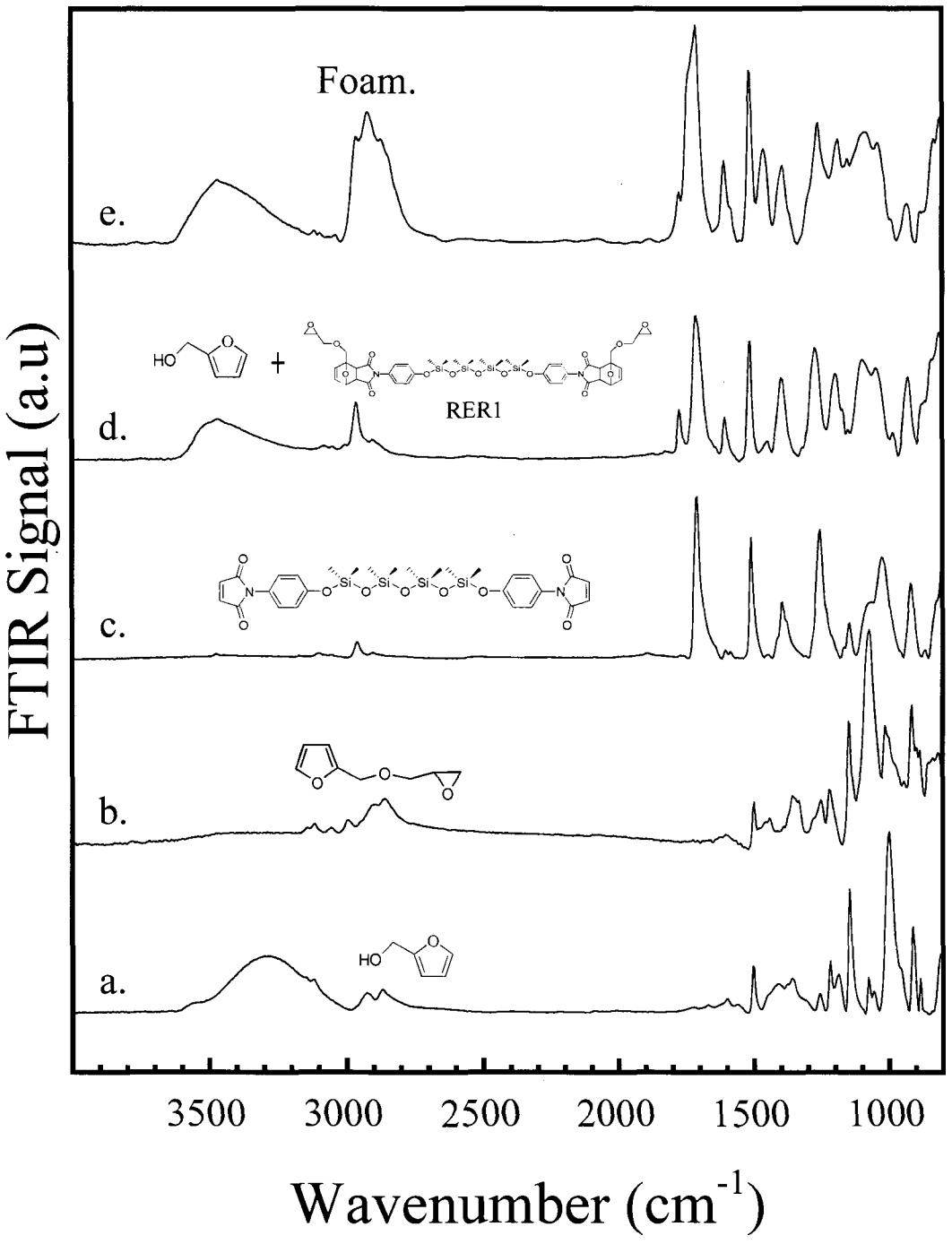

Figure 4.1: FTIR of a.) furfuryl alcohol b.) furfuryl glycidyl ether c.) di-4,1-phenoxy-bismaleimide octamethyltetrasiloxane, d.) **RER1** resin e.) epoxy foam. Spectral Range: 800-4000 cm^{-1}

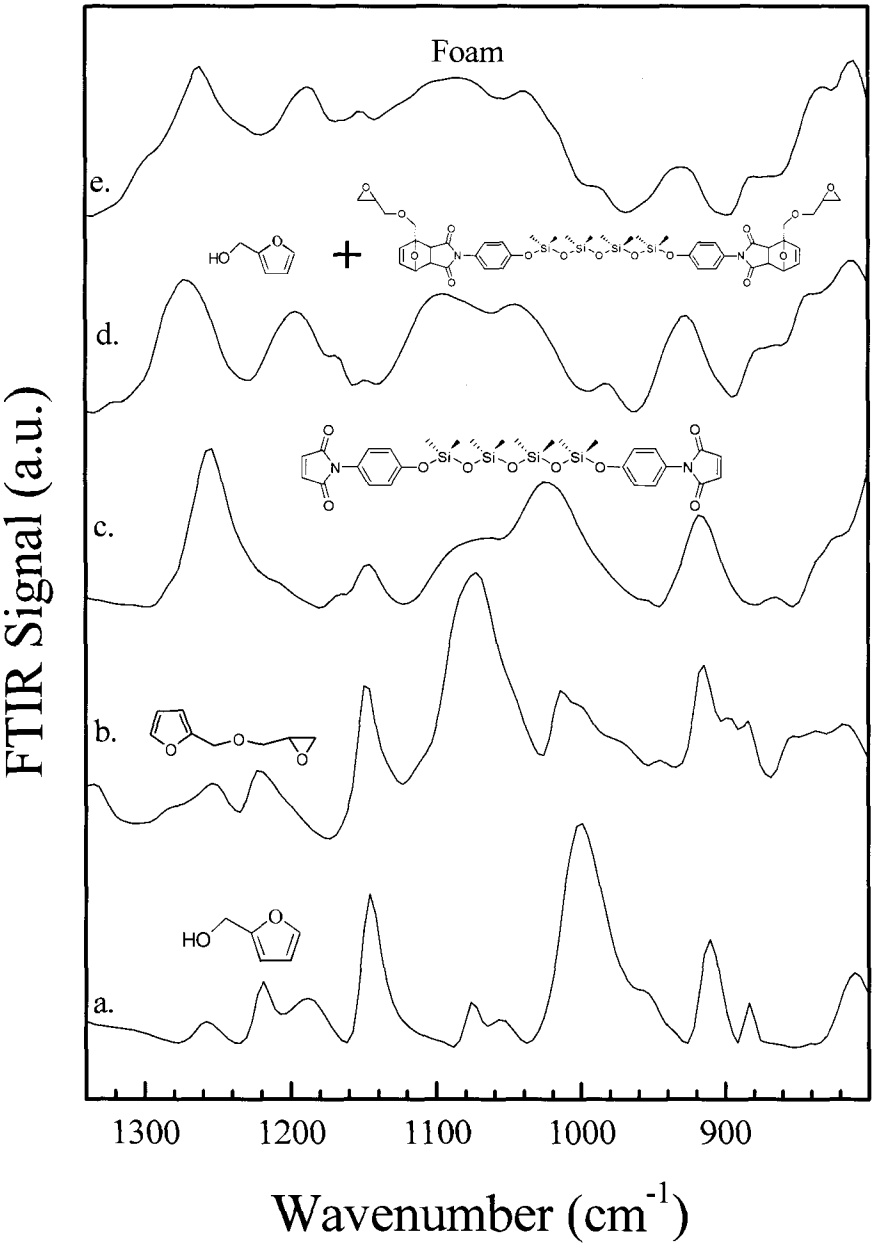

Figure 4.2: FTIR of a.) furfuryl alcohol b.) furfuryl glycidyl ether c.) di-4,1-phenoxy-bismaleimide octamethyltetrasiloxane, d.) **RER1** resin e.) epoxy foam. Spectral Range: 800-1340 cm^{-1}

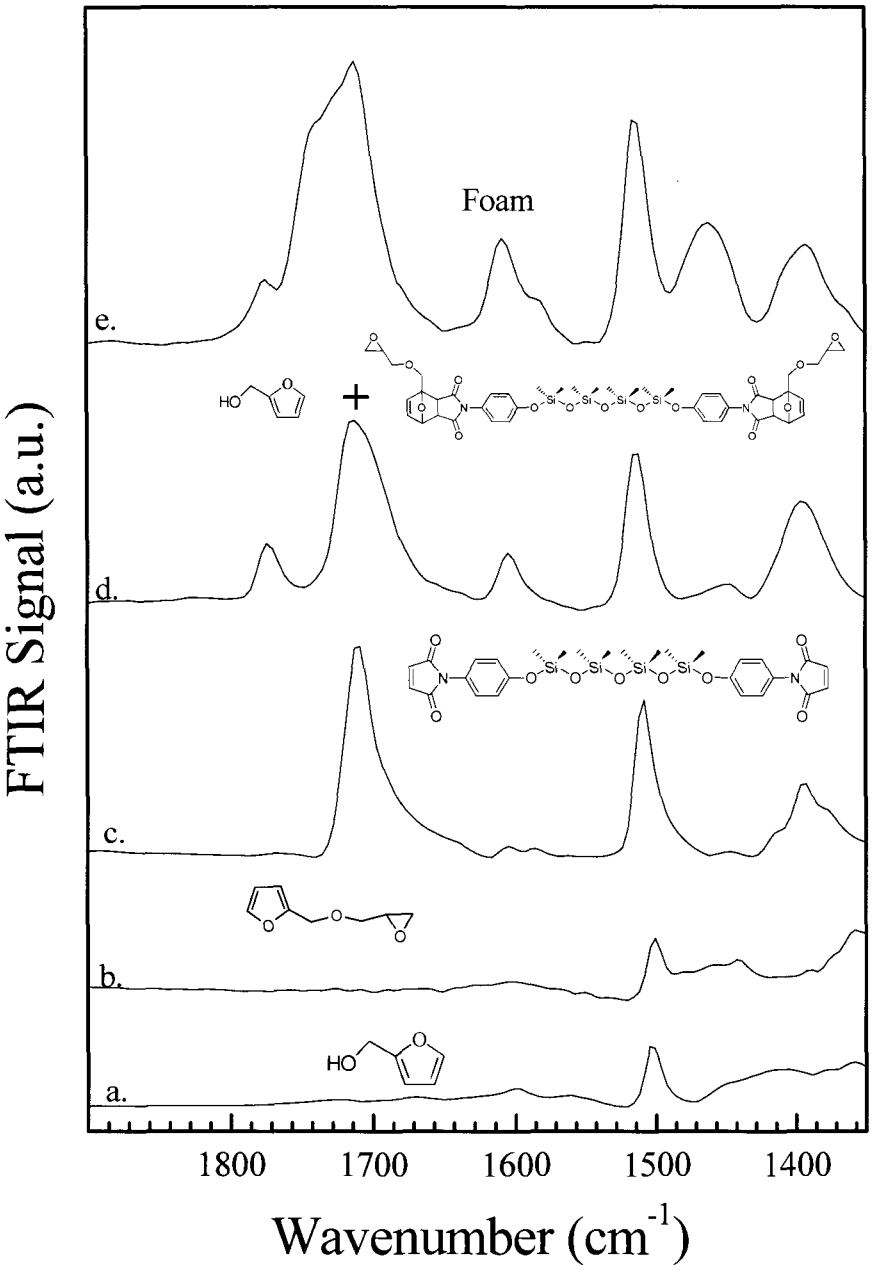

Figure 4.3: FTIR of a.) furfuryl alcohol b.) furfuryl glycidyl ether c.) di-4,1-phenoxy-bismaleimide octamethyltetrasiloxane, d.) **RER1** resin e.) epoxy foam. Spectral Range: 1350-1900 cm^{-1}

Location (cm^{-1})	Band Intensity	Assignment	Location (cm^{-1})	Band Intensity	Assignment
811	very strong	out of plane (C-H) aromatic [15],[17]	1515	strong	. C=C stretch in ring [15]
832	weak shoulder	Si-CH_3(in plane bending related to in-chain Si-CH_3 groups) [17]	1608	medium	. C=C stretch in ring [15]
879	weak shoulder	=C-H & =CH_2 bending vibrations	1713	very strong	C=O symmetric stretch - aliphatic carbonyls groups of crosslinks in Michael addition[18-20]
930	medium	916 cm^{-1} :(epoxide ring) ([15, 21], 917 cm^{-1} :Si-O-Si symmetric stretching[22] 925:(Si-OH) [23, 24]	1740	weak shoulder	C=O symmetric stretch in succinimide group
1013	very weak	C-O stretch in primary alcohol [15]	1774	weak shoulder	C=O asymmetric stretch [18-20, 25]
1040	medium shoulder	Si-O-Si asymmetric stretching [17]	1755	weak shoulder in temperature ramping study	C=O symmetric stretch in lactams[26, 27] 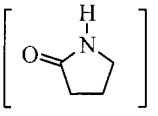
1086	wide strong	. C-O-C aliphatic ether asymmetric stretching[28]	1789	weak shoulder in temperature ramping study	C=O asymmetric stretch (lactams) [26, 27]
1151	weak	C-O-C ether furfuryl group, C-N-C stretching in maleimide[29],[30]	2873	weak shoulder (wide)	C-H asymmetric stretching (aliphatic) [23]
1167	very weak	Si-O-Si asymmetric stretching [22]	2919	strong large	C-H symmetric stretching in alkyl chain CH_2 [15]
1188	strong	C-N-C stretching in succinimide group [19]	2959	weak shoulder	C-H asymmetric stretching in alkyl chain CH_2 [23]
1262	strong	Si-CH_3 (in plane bending or scissoring, asymmetrical) [17]	3035	very weak	C-H stretching in ring [15]
1392	medium	C-N stretching [19]	3462	strong wide	OH stretch [15]
1461	medium	CH_2, CH_3 bend [15]			

Table 4.1: FTIR band assignment for Diels-Alder based Epoxy Foam

The emergence of the latter band in the **RER1** spectrum is characteristic of the formation of the succinimide groups for Diels-Alder adducts of maleimides.[20, 28] Both carbonyl bands are also present in the foam spectrum at 1713 cm^{-1} and 1775 cm^{-1} indicating the Diels-Alder adduct remains intact within the foam network prior to thermal treatment.

When the foam is subjected to thermal treatment it is possible to break the Diels-Alder bonds in the **RER1** and **RER2** resins. Thermal degradation of the Diels-Alder bonds typically occurs above 90 °C. The structure of the adduct is particularly useful for evaluating the FTIR bands that should be influenced by the loss of the furfuryl glycidyl ether from the di-4,1-phenoxy-bismaleimide octamethyltetrasiloxane and 1,3-phenoxy dimaleimide as shown in Scheme 4.4.

Thermal processing of the foam can influence the structure and physical properties of the epoxy foam. First, the degradation of the Diels-Alder adduct can decrease the rigidity of the foam, increasing thermal expansion. Molecular interactions of the siloxane groups can be disrupted during the expansion of the foam. Therefore, both chemical and structural changes in the epoxy foam can be observed during thermal cycling. The physical and chemical changes appear as changes in the FTIR signature of the foam. The structural and chemical changes in the foam were monitored using in-situ FTIR at elevated temperatures. The FTIR bands associated with the Diels-Alder and siloxane functional groups were monitored as a function of increasing and decreasing exposure temperatures in Figure 4.4. The FTIR spectrum of the untreated epoxy foam at room temperature (25 °C) is presented in Figure 4.4a. The FTIR difference spectra are provided for increasing temperatures 40, 80, and 120 °C in Figure 4.4b. The reversibility of the thermal exposure is evaluated as the temperature is decreased with FTIR

measurements obtained at 100, 80, 60, and 27 °C in Figure 4.4c.

a.

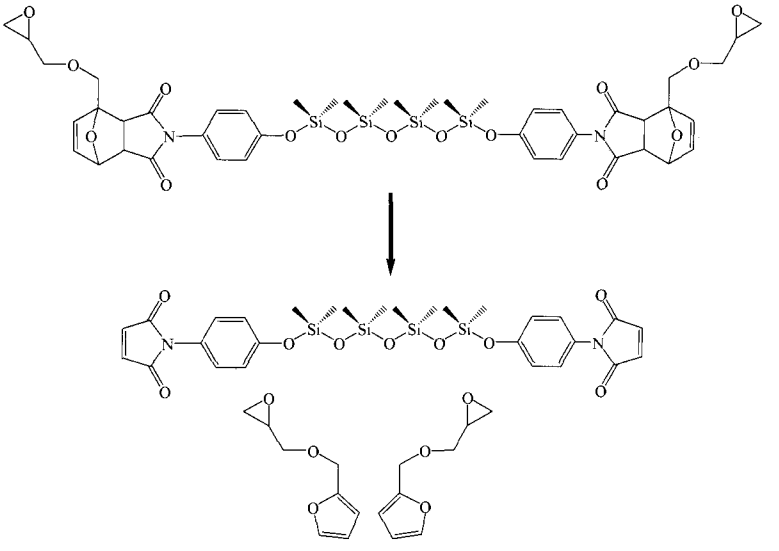

b.

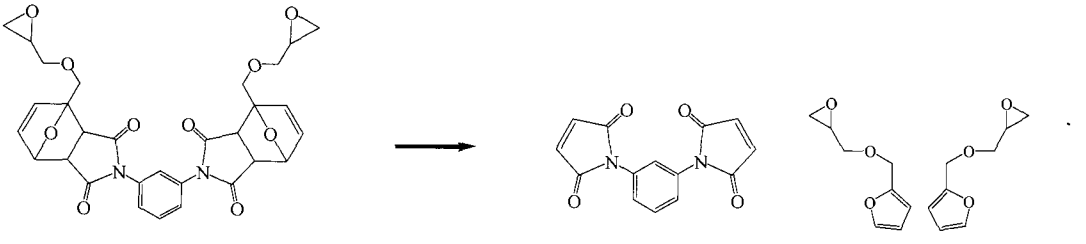

Scheme 4.4: Loss of furfuryl glycidyl ether from: a. di-4,1-phenoxy-bismaleimide octamethyltetrasiloxane b. 1,3-phenoxy dimaleimide during the reverse Diels-Alder reaction

For clarity, Figure 4.5, Figure 4.6 and Figure 4.7 provide plots for Figure 4.4 for spectral ranges 800-1395 cm^{-1}, 1350-1900 cm^{-1}, and 1900-4000 cm^{-1}, respectively.

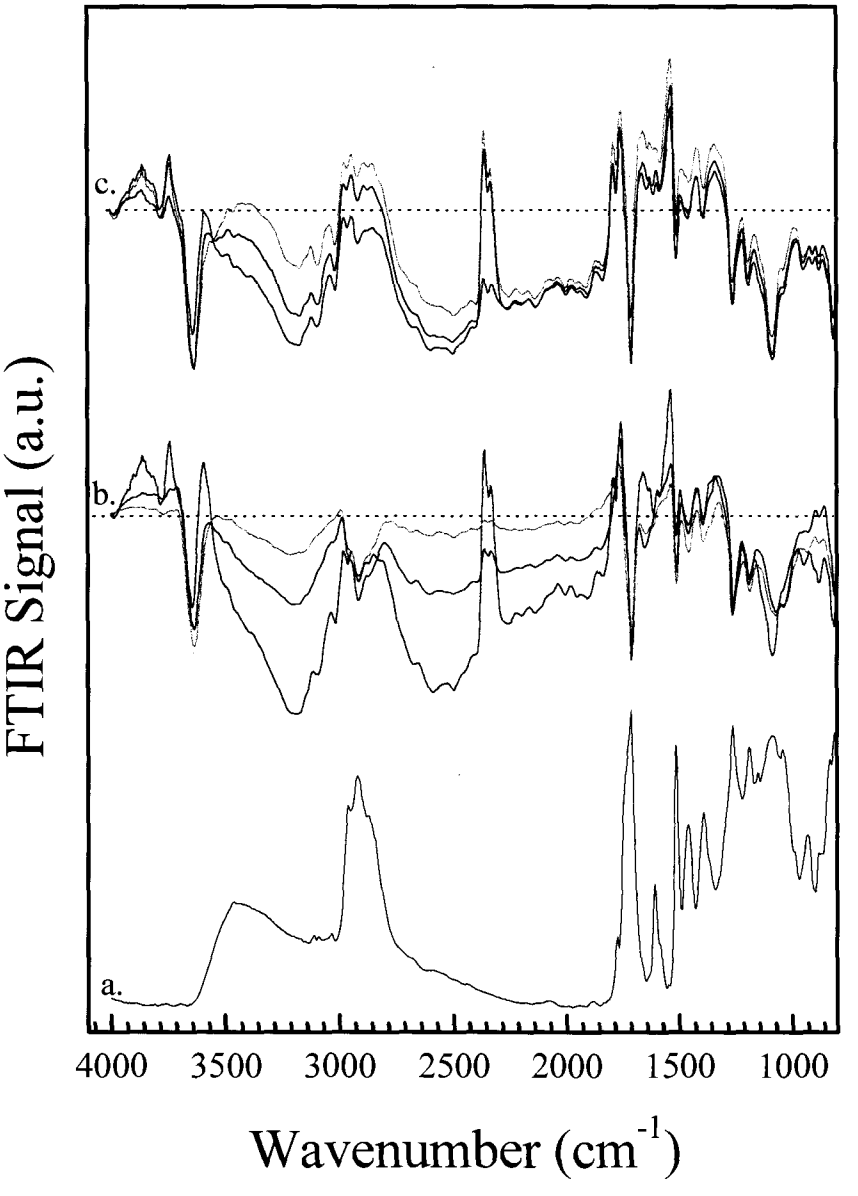

Figure 4.4: a. Normal IR spectra of pristine epoxy foam. b. Difference FTIR spectra for increasing exposure temperatures of 40 °C (Green), 80 °C (Red), and 120 °C (Blue). c. Difference FTIR spectra for decreasing exposure temperatures of 100 °C (Blue), 80 °C (Red), 60 °C (Green), and 27 °C (Yellow). Spectral Range: 800-4000cm^{-1}

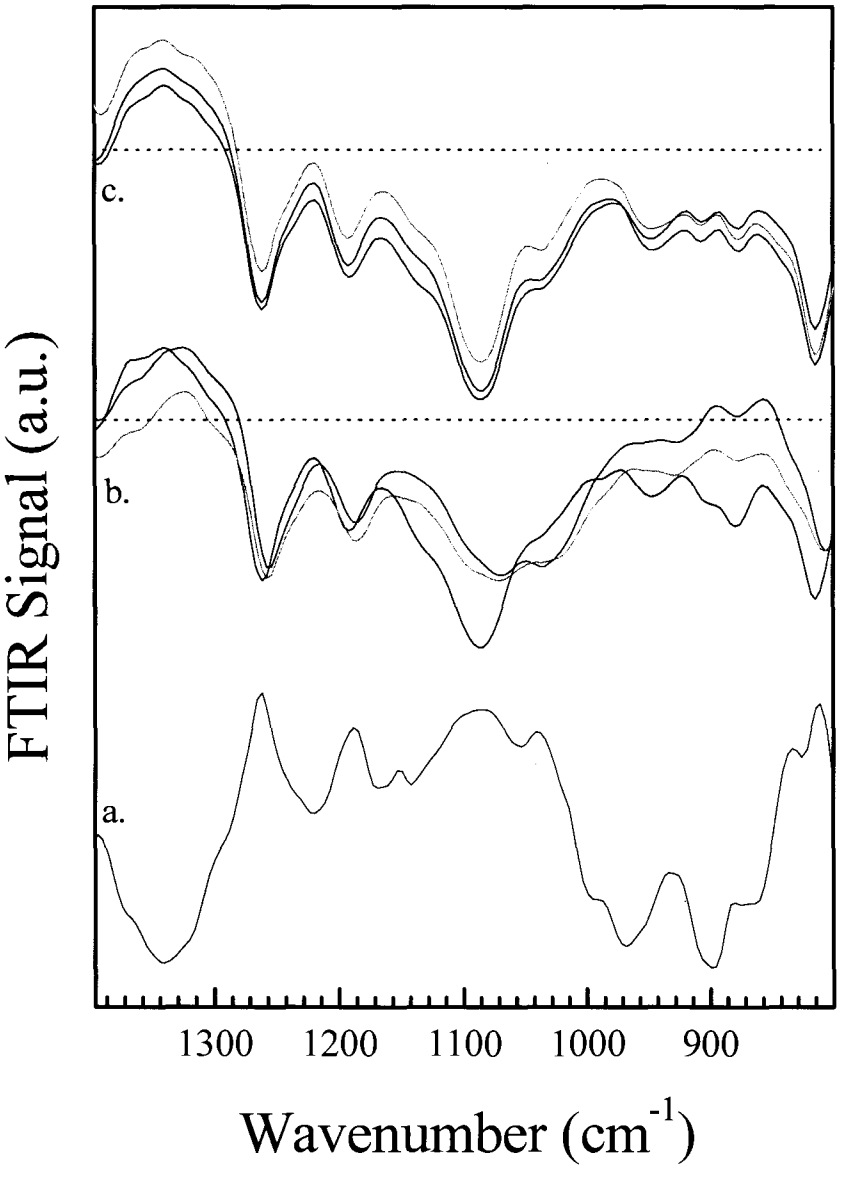

Figure 4.5: a. Normal IR spectra of pristine epoxy foam. b. Difference FTIR spectra for increasing exposure temperatures of 40 °C (Green), 80 °C (Red), and 120 °C (Blue). c. Difference FTIR spectra for decreasing exposure temperatures of 100 °C (Blue), 80 °C (Red), 60 °C (Green), and 27 °C (Yellow). Spectral Range: 800-1395cm^{-1}

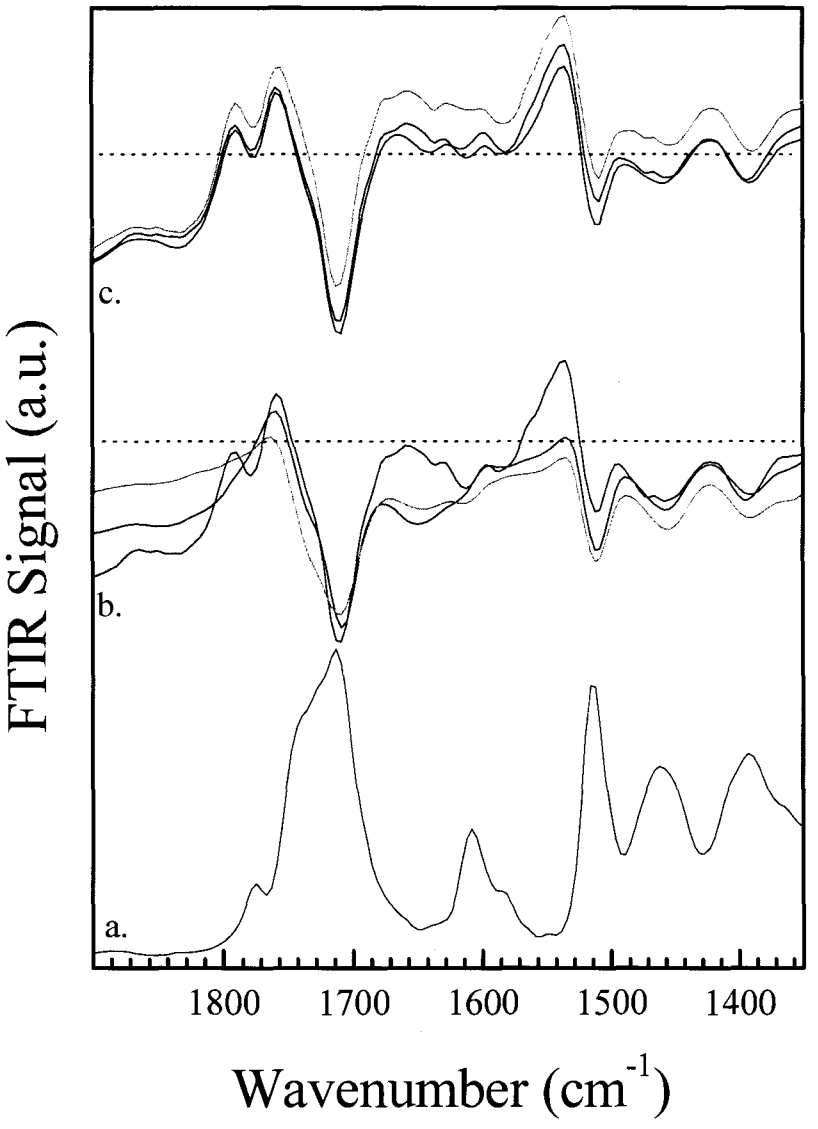

Figure 4.6: a. Normal IR spectra of pristine epoxy foam. b. Difference FTIR spectra for increasing exposure temperatures of 40 °C (Green), 80 °C (Red), and 120 °C (Blue). c. Difference FTIR spectra for decreasing exposure temperatures of 100 °C (Blue), 80 °C (Red), 60 °C (Green), and 27 °C (Yellow). Spectral Range: 1350-1900cm^{-1}

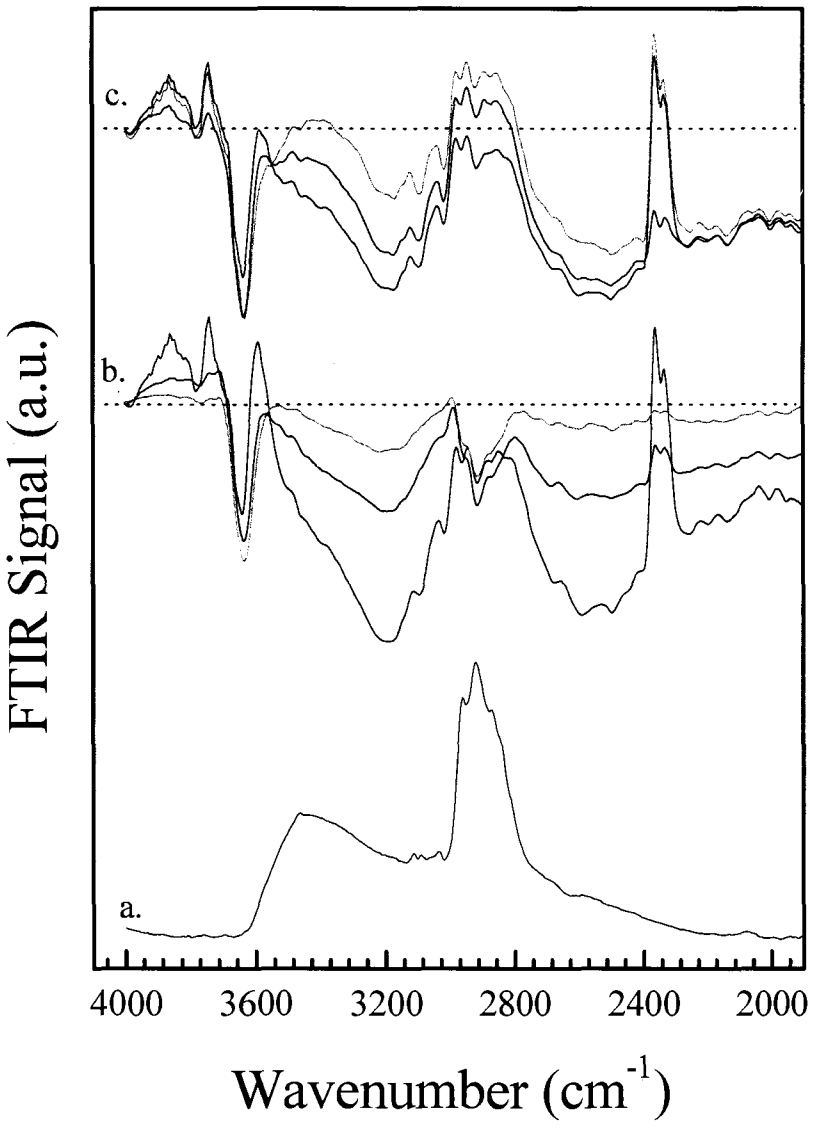

Figure 4.7: a. Normal IR spectra of pristine epoxy foam. b. Difference FTIR spectra for increasing exposure temperatures of 40 °C (Green), 80 °C (Red), and 120 °C (Blue). c. Difference FTIR spectra for decreasing exposure temperatures of 100 °C (Blue), 80 °C (Red), 60 °C (Green), and 27 °C (Yellow). Spectral Range: 1900-4000cm^{-1}

The difference FTIR spectra were obtained at temperatures encompassing the Diels-Alder bond formation and breakage. FTIR bands that show negative absorbance are indicative of a decrease in the concentration of chemical functional groups, or disruption of resonance of a given functional group due to structural changes. Positive absorbance bands appear due to increasing concentration and shifts in energy associated with chemical species during thermal changes in structure and chemistry of the system.

The trend observed for the difference spectra in Figure 4.4b is consistent with the decomposition of the Diels-Alder structures as well as changes in the siloxane functional group interactions. Specifically a wholesale decrease in band intensity is observed from 800 to 1450 cm^{-1}. This region encompasses the ether C-O-C, Si-O-Si, CH_3-Si-O (1259 cm^{-1}), and C-N-C (1390 cm^{-1}) modes. In addition, a decrease in the intensity of the C=C aromatic band at 1503 cm^{-1} is observed with a corresponding emergence of a new band at higher energy (1535 cm^{-1}). A similar trend is observed for C=O bands with decreases in intensity at 1710 cm^{-1} and an increase in the band intensity at 1755 cm^{-1}. The changes in the chemistry and structure of the epoxy foam are consistent with the loss of the furfuryl glycidyl ether and changing electron density within the two adjacent ring structures. The difference spectra for the decreasing temperatures show that the changes in the foam structure and chemistry are not reversible. None of the bands return to their pre thermal exposure intensities. It is expected that the permanent loss of Diels-Alder structures and the corresponding expansion of the foam will lower both the modulus and density of the foam. More importantly the first changes in the foam chemistry and structure were documented at 40 °C, a temperature ~50 °C lower than the thermal decomposition of the

Diels-Alder bonds. This implies that structural changes are significant at temperatures that are far below the degradation threshold of the Diels-Alder bonds.

4.2.2 Thermal Mechanical Analysis (TMA)

TMA is useful for examining thermal expansion of foams. Any change in the axial dimension of the foam is measured as function of temperature. Contraction or expansion, designated as dL, is recorded as a percentage of the original length of the sample, L_0 and plotted as a function of temperature for 0, 1, 5 and 10 thermal cycles in Figure 4.8. Pristine foam (0 thermal cycles) exhibits an expansion of ~17 % at an onset temperature of 97 °C followed by contraction at 105 °C. A much smaller, secondary expansion of the foam occurs at ~ 120 °C. Densification of the foam is not observed for this sample under the temperature range studied. In contrast, samples subjected to thermal cycles show no additional expansion with densification observed above an applied temperature of ~110 °C. The results suggest that the thermal expansion is immediate and occurs during the first thermal cycle. The foams exposed to more than one thermal cycle have undergone the bulk of the expansion prior to TMA measurements. The expansion of the pristine foam occurs after the temperature associated with the degradation of the Diels-Alder bonds has been exceeded.

Degradation of chemical bonds and changing intermolecular chain interactions within the foam matrix directly influence the expansion of the foam. These results are consistent with the changing chemistry and functional group interactions that were in the FTIR difference spectra shown in Figure 4.7. The glass transition temperature (T_g) can also be estimated from the TMA results for the foam that has been thermally cycled.

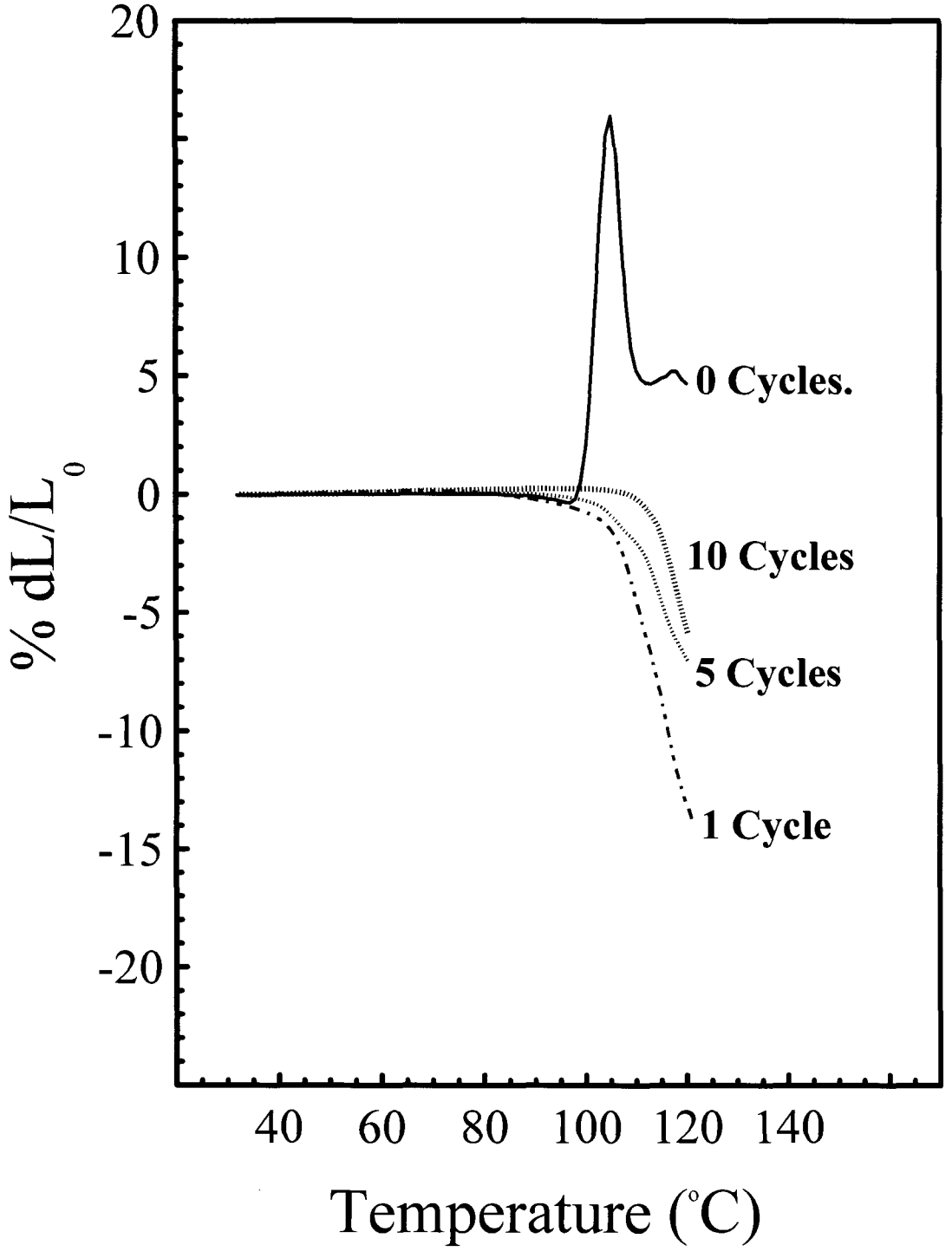

Figure 4.8: TMA curves of epoxy foam as a function of the number of thermal cycles

The inflection point for the contraction of the foam has previously been assigned to the glass transition temperature (T_g) epoxy polymer chains.[9, 31, 32] The large expansion observed for the pristine foam precludes the identification of the T_g for this sample. From the inflection point, the T_g for foam samples exposed to 1, 5, and 10 thermal cycles was determined to be 109.1 °C, 114.6 °C and 117.1 °C, respectively. The increase in the T_g values may be indicative of increased cross links between the epoxide group and the diamine curative (Scheme 4.2) as thermal cycling proceeds.[7, 31-33] The values are in agreement with T_g values reported previously for other epoxy resins. For example, the T_g for both the bisphenol-A diglycidyl ether (DGEBA) resin and siloxane modified DGEBA copolymers were estimated at 99 °C. [9, 33]

4.2.3 Foam Density Analysis

The FTIR analysis of the epoxy foam suggests that that the degradation of Diels-Alder bonds and changing molecular interactions occur during thermal exposure. In addition, TMA shows that thermal expansion occurs after the temperature required for Diels-Alder bond degradation. Based on these observations the foam density should decrease as a function of thermal cycling. A plot of the average foam density as a function of thermal cycling is presented in Figure 4.9. The plot shows the average density for foam treated for 0, 1, 5 and 10 thermal cycles. The average densities were found to be 0.13 ± 0.0075 g/cm^3 (±6 %), 0.12 ± 0.0041 g/cm^3 (± 4 %), 0.089 ±0.011 g/cm^3 (± 13 %) and 0.077 ± 0.010 g/cm^3 (±13 %), for 0, 1, 5 and 10 thermal cycles, respectively. The overall density loss observed for the sample treated to ten thermal thermal cycles is 41 % compared to the pristine foam. The decrease in density indicates that expansion occurs after the foam is exposed to increasing temperatures.

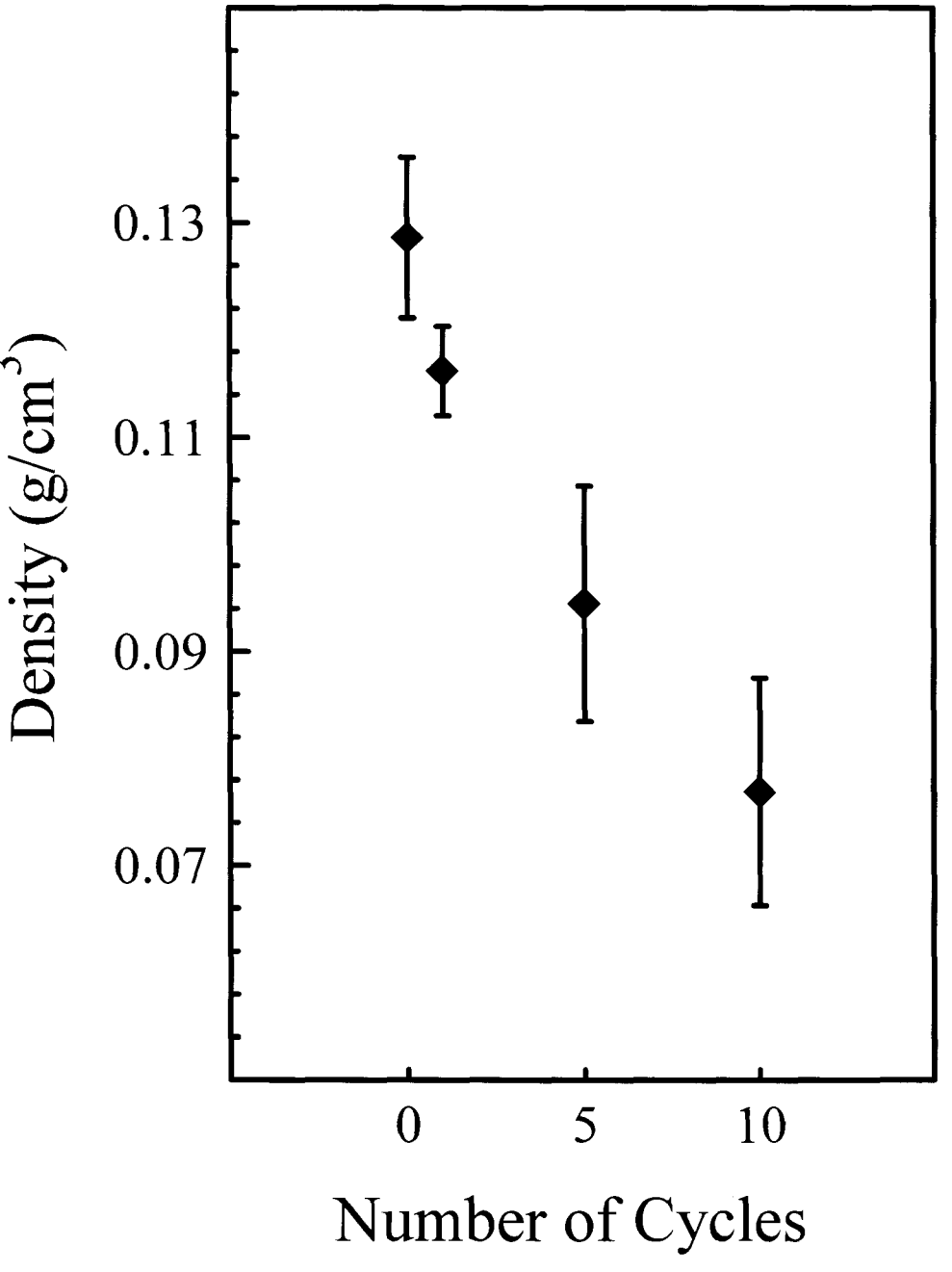

Figure 4.9: Density of the epoxy foam as a function of thermal cycling

The data indicates that the thermal expansion of the foam is not reversible and increases with increasing number of thermal cycles. However, the decrease in density may not be solely attributed to foam expansion. The decreasing density may also be due to a decrease in mass associated with the loss of trapped blowing agent or mass loss due to chemical degradation of the foam.

4.2.4 Mechanical Strength Analysis.

The decrease in density associated with thermal exposure should also influence the mechanical properties of the materials. The modulus of a foam material is highly dependent on its density with a drop in foam density accompanied by a decrease in rigidity.[33-35] A plot of Young's modulus as a function of thermal cycling is presented in Figure 4.10. A significant drop in the modulus is observed as thermal cycling progresses. For comparison, the modulus for pristine foam is approximately 30% higher than the average value of 35.6 MPa for removable epoxy foam that does not contain siloxane functional groups.[4] The difference can be attributed to differences in chain-chain interactions associated with the siloxane groups. During thermal expansion of the foam these interactions are lost and the modulus drops appreciably to values lower than foams that do not contain siloxane functional groups. The measured modulus values were 47.9 ± 6.8 MPa (±14%), 36.4 ± 3.8 MPa (± 11%), 21.2 ± 6.4 MPa (22%) and 16.5 ± 2.7 MPa (±18%) for 0, 1, 5 and 10 thermal cycles, respectively. There is a 24 %, 40 % and 68 % drop in the modulus after 1, 5 and 10 thermal cycles, respectively when compared to pristine foam.

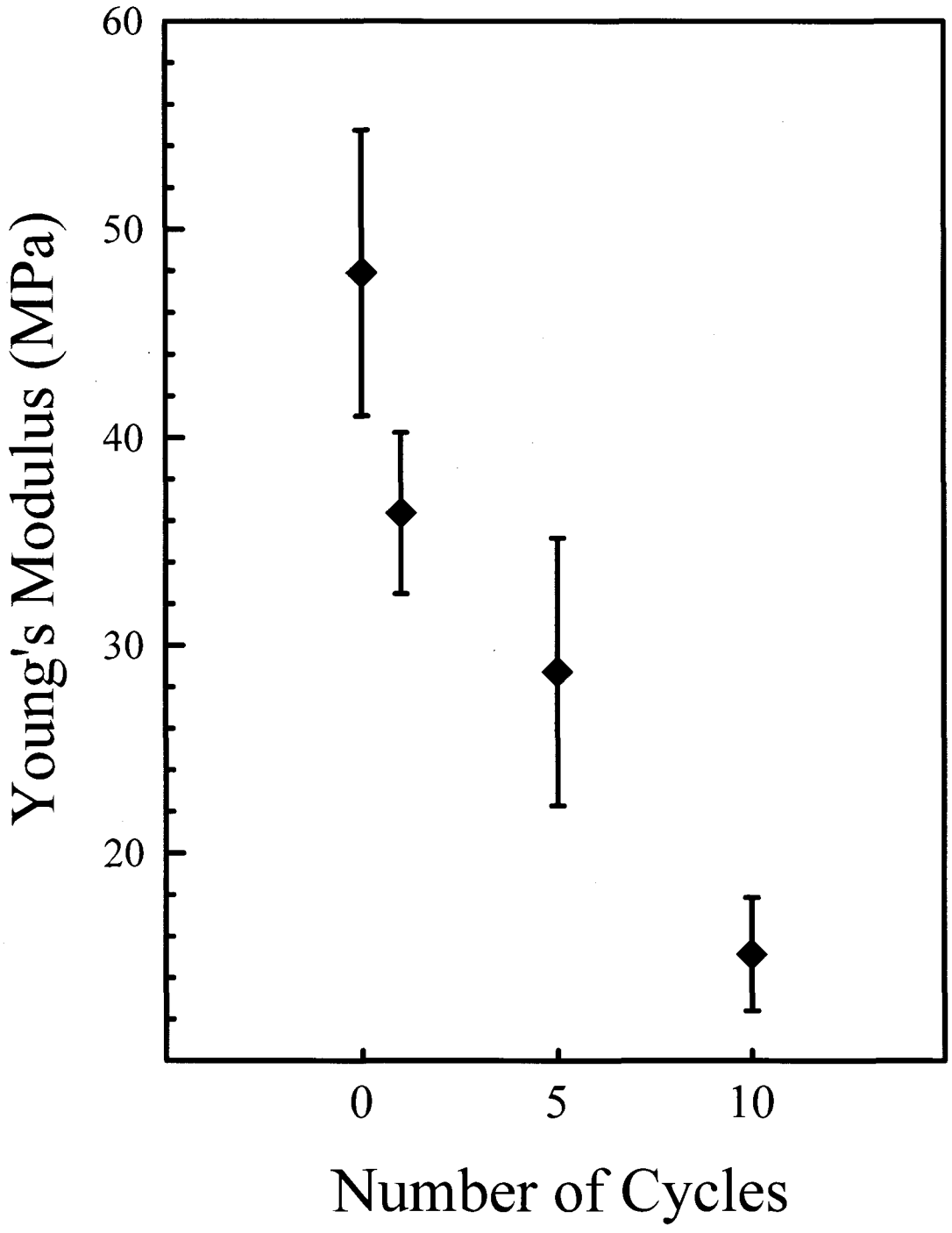

Figure 4.10: Modulus of removable epoxy foam as a function of thermal cycling

The decrease in modulus is consistent with the accompanying drop in the density based on the square rule relation between Young's modulus and density. [33-35] The Young's modulus can be estimated with respect to the density of the foam using the following non-linear equation:

$$\left(\frac{E^*}{E_s}\right) = C_1\left(\frac{\rho^*}{\rho_s}\right)^2 \qquad C_1 \approx 1$$

The terms E^*/E_s and ρ^*/ρ_s represent the relative modulus and density of the foam respectively. In this study, E^* and ρ^* represent the predicted modulus and experimental density of a thermally cycled foam sample respectively. E_s and ρ_s represent the experimental modulus and experimental density of a pristine foam material not exposed to thermal cycling respectively. The constant C_1 represents all geometric constants of proportionality and is approximated to be equal to 1.[33] A comparison of the calculated modulus and the experimental modulus obtained in this study is provided in Table 4.2.

Number of Thermal Cycles	Experimental Density (g/cm^3)	Experimental Modulus (MPa)	Predicted Modulus (MPa)
0	0.13 ± 0.0075	47.9 ± 6.8	-
1	0.12 ± 0.0041	36.4 ± 3.8	40.8
5	0.094 ± 0.011	21.2 ± 6.4	23.0
10	0.077 ± 0.011	16.5 ± 2.7	18.1

Table 4.2: Comparison of predicted and experimental modulus

The calculated modulus values are within the relative error of the experimental measurement confirming that the drop in modulus can be mainly attributed to the

decrease in density associated with thermal cycling and expansion of the epoxy foam.

4.3 References

1. Hatchett, D.W., Kinyanjui, J.M., and Sapochak, L., *FTIR analysis of chemical gradients in thermally processed molded polyurethane foam.* Journal of Cellular Plastics, 2007. **43**: p. 183-196.

2. Hatchett, D.W., Kodippili, G., Kinyanjui, J.M., Benincasa, F., and Sapochak, L., *FTIR analysis of thermally processed PU foam.* Polymer Degredation and Stability, 2005. **87**: p. 555-561.

3. Loy, D.A., Wheeler, D.R., Russick, E.M., McElhannon, J.R., and Saunders, R.S., *Method of making thermally removable epoxies.* January 2002, Sandia Corporation: USA.

4. McElhanon, J.R., Russick, E.M., Wheeler, D.R., Loy, D.A., and Aubert, J.H., *Removable foams based on an epoxy resin incorporating reversible Diels-Alder adducts.* Journal of Applied Polymer Science, 2002. **85**: p. 1496-1502.

5. Russick, E.M. and Rand, P.B., *Development and characterization of a new epoxy foam encapusulant as ablefoam replacement.*, in *Sandia Report:SAND98-2538.* 1998, Sandia National Laboratories.

6. Small, J.H., Loy, D.A., Wheeler, D.R., McElhannon, J.R., Saunders, R.S., and Randall, S., *Method of making thermally removable polymeric encapsulants*, Office, U.S.P., Editor. August 2001, Sandia National Laboratories.

7. Kent, J.A., ed. *Riegel's handbook of industrial chemistry.* 2003, Academics/Plenum Publishers: New York.

8. Sbirrazouli, N., Mititeli-Mija, A., Vincent, L., and Alzina, C., *Isoconversional kinetic analysis of stochiometric and off-stochiometric epoxy-amine cures.* Thermochimica Acta, 2006. **447**: p. 167-177.

9. Lin, S.-T. and Huang, S.K., *Thermal degradation study of siloxane-DGEBA epoxy copolymers.* European Polymer Journal, 1997. **33**: p. 365-373.

10. Hobbs, M.L., *Modeling epoxy foams exposed to fire like-heat fluxes.* Polymer Degradation and Stability, 2005. **89**: p. 353-372.

11. Chang, T.C., Wu, K.H., Liao, C.L., Lin, S.T., and Wang, G.P., *Thermo-oxidative degradation of siloxane-containing polyimide and unmodified polyimide.* Polymer Degradation and Stability, 1998. **62**: p. 299-305.

12. Dvornic, P.R., Perpall, H.J., Uden, P.C., and Lenz, R.W., *Exactly alternating silarylene-siloxane polymers. VII. Thermal Stabilityand degradation behavior of p-silphenylene-siloxane polymers with methyl, vinyl, hydrido, and/or fluoralky side groups.* Journal of Polymer Science: Part A: Polymer Chemistry, 1989. **27**: p. 3503-3514.

13. Aubert, J.H., Tallant, D.R., Sawyer, P.S., and Garcia, M.J. *Synthesis and formulation of a removable conformal coating using Diels-Alder thermally-reversible adducts. ACS Fall National Meeting, Poly, PMSE and FSCT preprints.* 8/22-26, 2004. Philadelphia, PA.

14. Pavia, D.L., Lampman, G.M., and Kriz, G.S., *Introduction to spectroscopy: a guide for students of organic chemistry.* 1979, Orlando: Saunders College Publishing.

15. Silverstein, R.M. and Webster, F.X., *Spectrometric identification of organic compounds.* 1998, New York: John Wiley & Sons.

16. Laita, H., Boufi, S., and Gandini, A., *The application of the Diels-Alder reaction to polymers bearing furan moieties. 1. Reactions with maleimides.* European Polymer Journal, 1997. **33**(8): p. 1203-1211

17. Barthel, H. and Nikitina, E., *INS and IR Study of Intermolecular Interactions at the Fumed Silica-Polydimethylsiloxane Interphase. Part 3 Silica-Siloxane Adsorption Complexes.* Silicon Chemistry, 2004. **1**(4): p. 261-279.

18. Adachi, K., Achimuthu, A.K., and Chujo, Y., *Synthesis of organic-inorganic polymer hybrids controlled by Diels-Alder reaction.* Macromolecules, 2004. **37**(26): p. 9793-9797.

19. Gousse, C., Gandini, A., and Hodge, P., *Application of the Diels-Alder reaction to polymers bearing furan moieties. 2. Diels-Alder and retro-Diels-Alder reactions involving furan rings in some styrene copolymers.* Macromolecules, 1998. **31**(2): p. 314-321.

20. Imai, Y., Itoh, H., Naka, K., and Chujo, Y., *Thermally reversible IPN organic-inorganic polymer hybrids utilizing the Diels-Alder reaction.* Macromolecules, 2000. **33**: p. 4343-4346.

21. Eidelman, N., Raghavan, D., Forster, A.M., Amis, E.J., and Karim, A. *Combinatorial approach to characterizing epoxy curing.* 2004: Wiley-V C H Verlag Gmbh.

22. Guo, X., Guo, H., Fu, L., Zhang, H., Deng, R., Sun, L., Feng, J., and Dang, S., *Novel hybrid periodic mesoporous organosilica material grafting with Tb complex: Synthesis, characterization and photoluminescence property.* Microporous and Mesoporous Materials, 2009. **119**(1-3): p. 252-258.

23. Matsumoto, T., Takayama, Y., Wada, N., Onoda, H., Kojima, K., Yamada, H., and Wakabayashi, H., *Acid-free synthesis of poly-organo-siloxane spherical particles using a W/O emulsion.* Journal of Materials Chemistry, 2003. **13**(7): p. 1764-1770.

24. Leyden, D.E., Murthy, R.S.S., Blitz, J.P., Atwater, J.B., and Rachetti, A., *Reflectance FTIR Investigations Of The Reactions Of Silanes On Silica Surfaces* Mikrochimica Acta, 1988. **2**(1-6): p. 53-56.

25. Lee, Y.J., Kim, Y.W., Ha, J.D., Oh, J.M., and Yi, M.H., *Synthesis and characterization of novel polyimides with 1-octadecyl side chains for liquid crystal alignment layers.* Polymers for Advanced Technologies, 2007. **18**(3): p. 226-234.

26. Jiang, T. and Xu, K., *FTIR study of ultradispersed diamond powder synthesized by explosive detonation.* Carbon, 1995. **33**(12): p. 1663-1671.

27. Jarrahpour, A.A., Shekarriz, M., and Taslimi, A., *Asymmetric synthesis and antimicrobial activity of some new mono and bicyclic beta-lactams.* Molecules, 2004. **9**(11): p. 939-948.

28. Aubert, J.H., *Thermally removable epoxy adhesives incorporating thermally reversible Diels-Alder adducts.* Journal of Adhesion, 2003. **79**(6): p. 609-616.

29. Aubert, J., *Thermally removable epoxy adhesives incorporating thermally reversible Diels-Alder adducts.* Journal of Adhesion, 2003. **79**: p. 609-616.

30. C. Di Giulio, M.G.B.J., *Fourier transform infrared spectroscopic characterization of aromatic bismaleimide resin cure states.* Journal of Applied Polymer Science, 1984. **29**(5): p. 1771-1779.

31. Wang, H. and Siow, K.S., *Measurement of Tg in epoxy resins by DSC-effects of residual stress.* Polymer Engineering and Science, 1999. **39**: p. 422-429.

32. Wu, C.S., *Influence of post-curing and temperature effects on bulk density, glass transition and stress strain behaviour of imidazole-cured epoxy network.* Journal of Materials Science, 1992. **27**: p. 2952-2959.

33. Gibson, L.J. and Ashby, M.F., *Cellular solids: structure and properties.* 1997, Cambridge: Cambridge University Press.

34. Hawkins, M.C., O'Toole, B., and Jackovich, D., *Cell morphology and mechanical properties of rigid polyurethane foam.* Journal of Cellular Plastics, 2005. **41**: p. 267-285.

35. Jackovich, D., O'Toole, B., and Hawkins, M.C., *Temperature and mold size effects on physical and mechanical properties of a polyurethane foam.* Journal of Cellular Plastics, 2005. **41**: p. 153-168.

CHAPTER 5

SYNTHESIS AND CHARACTERIZATION OF POLYIMIDE/CARBON/METAL COMPOSITES

5.1 Introduction

Electrically conductive poly(pyromellitic dianhydride-4,4'-oxydianiline)imide (PMDA-ODA polyimide) films are prepared by incorporating carbon into the insulating polymer matrix. Changes in the chemical composition of the polymer prior to and after carbon incorporation are investigated using a variety of analytical techniques. In addition, the conversion of PMDA-ODA polyamic acid to PMDA-ODA polyimide during thermal imidization is evaluated to determine the extent of polymerization.

Thermal analysis techniques (DSC/TGA) are used to evaluate the thermal stability for the polymer and composite after introducing carbon. TGA and DSC are also used to investigate the effectiveness of the curing process in removing solvents constituting the new binary acetone/DMSO solvent system used during the casting and curing process. These techniques are critical in evaluating the influence of the removal and residual content of the solvent prior to thermal imidization on the mechanical integrity of polyimide.

Electrochemical methods will be used to metalize the PI/carbon composite materials providing an electrochemical/catalytic interface. The Pt particle distribution on the PI/carbon surface and possible carbon aggregation at the surface are investigated

using scanning electron microscopy (SEM). X-ray-photoelectron spectroscopy (XPS) is used to determine the oxidation state of the metal deposits. For optimum electrode response, uniform metal nucleation on the surface of the PI/carbon films is desired. The goal is to provide the highest level of catalytic activity using the lowest mass of Pt metal deposited.

Finally, the use of PI/carbon composites as working electrodes is studied using various methods for producing gold coatings that include chemical vapor deposition (CVD) and electrodeposition. The quality of the gold deposits is evaluated electrochemically using the ferricyanide redox couple. The reversibility and electron transfer kinetics of the ferricyanide couple at the surface of PI/carbon/gold composites are investigated and compared to a gold planar electrode. PI/carbon/Au would be useful in fabricating flexible organic field effect transistors (OFET).

5.2 Results and Discussion

5.2.1 FTIR Analysis

The conversion of polyamic acid to polyimide resulting from thermal imidization is evaluated using FTIR photoacoustic spectroscopy.[1] Figure 5.1a-5.1d presents the FTIR spectra of PMDA/ODA polyamic acid (PAA), PMDA/ODA polyimide (PI), PMDA/ODA polyamic acid/carbon (PAA/carbon) and PMDA/ODA polyimide/carbon (PI/carbon) for the 600-1900 cm^{-1} spectral range while figure 5.2a-5.2d represent the same materials for the 1900-3700 cm^{-1} spectral range. The loss of bands related to carboxylic acid and amide functional groups specific to PAA and the appearance of imide bands specific to polyimide signify the conversion of the precursor to polyimide. Table 5.1 presents the band assignments for bands pertinent to the conversion of PAA to PI

during thermal imidization, confirming that thermal imidization occurs.

The strong broad band spanning 2500-3600 cm^{-1} is assigned to the carboxylic acid OH group as shown in the PAA spectrum (Figure 5.2a). In addition, characteristic secondary amide NH stretch bands occurring as multiple bands are observed in the same region between 3065-3300 cm^{-1}. [2] Both OH and NH bands are also observed for PAA/carbon as shown in Figure 5.2c although their size is diminished as compared to PAA. The diminished size of the OH and NH band intensities in the PAA/carbon spectrum possibly results from interference by carbon and has been previously reported for plastic/carbon composites. [3] A carbon black reference is used to obtain the baseline in FTIR-PAS at high carbon loadings. However, carbon black can impede diffusion of the thermal wave from the sample to the surrounding helium gas, therefore leading to a lower signal output from the PAS detector. The OH and NH bands are absent in both PI and PI/carbon spectra as seen in Figure 5.2c and 5.2d respectively confirming the conversion of PAA to PI. In addition to these bands, a medium sized band located at 1550 cm^{-1} overlapping with the aromatic C=C stretch band attributed to the secondary amide C-NH group in PAA is observed for both PAA and PAA/carbon. This band is greatly diminished in intensity for both PI and PI/carbon indicating the loss of the amide group in PAA with the formation of a cyclic imide in PI following thermal imidization.

The appearance of bands related to the imide functional group signify the formation of PI. For example, the C=O asymmetric stretch band located at around 1780 cm^{-1} is indicative and specific to the imide group marking the formation of polyimide with thermal imidization.

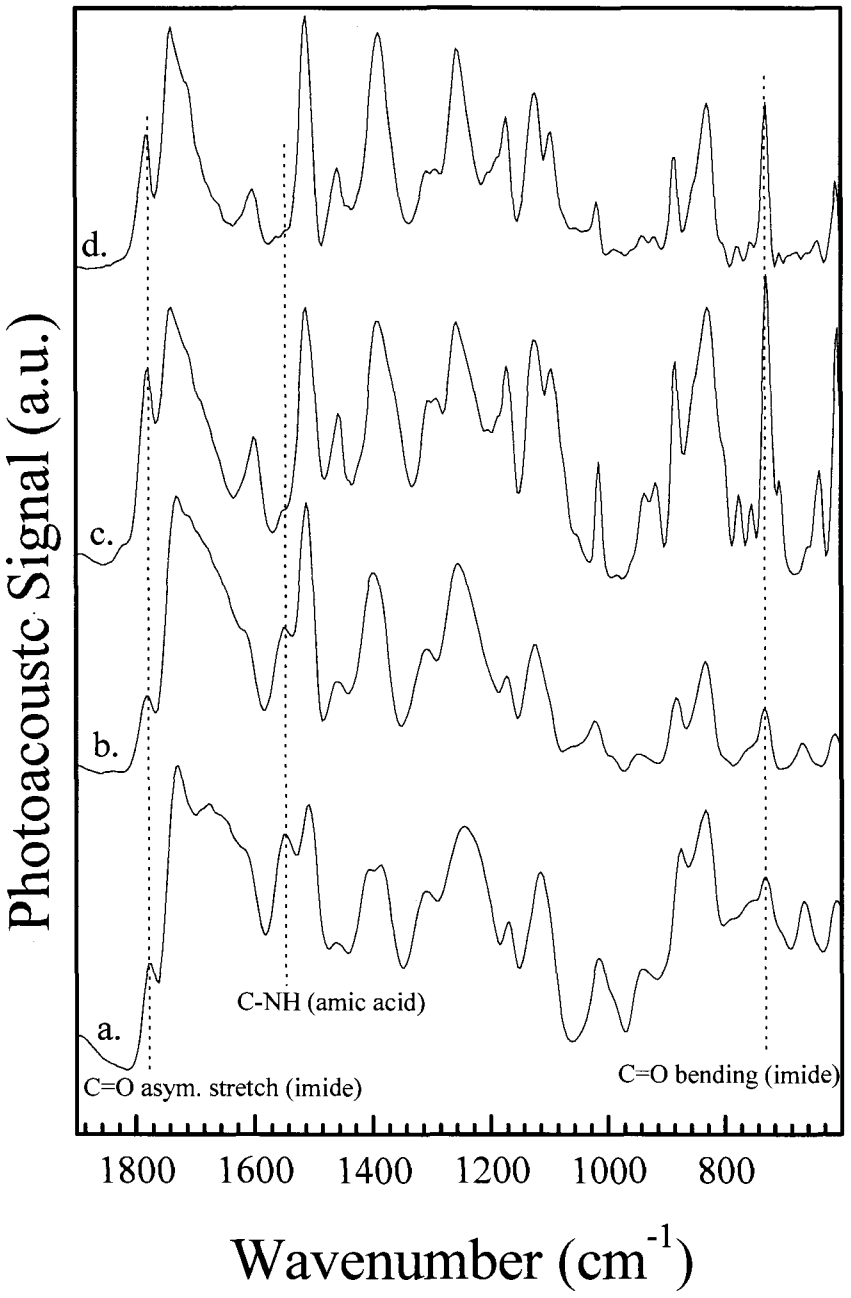

Figure 5.1: Photoacoustic FTIR spectra of a.) Polyamic acid (PAA) b.) Polyamic acid/carbon (PAA/carbon) c.) Polyimide (PI) d.) Polyimide/carbon (PI/carbon). Spectra range: (600-1900 cm^{-1})

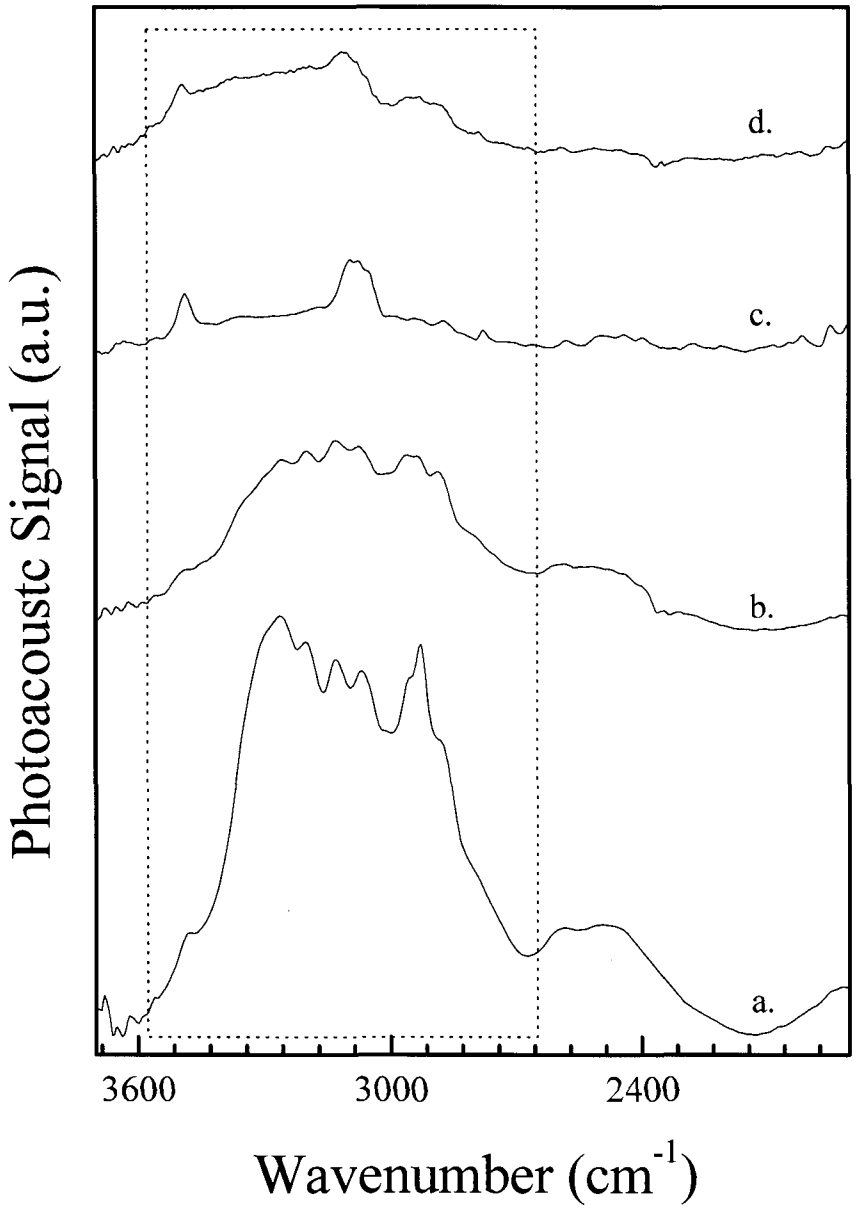

Figure 5.2: Photoacoustic FTIR spectra of a.) Polyamic acid (PAA) b.) Polyamic acid/carbon (PAA/carbon) c.) Polyimide (PI) d.) Polyimide/carbon (PI/carbon). Spectra range: (1900-3700 cm^{-1}). The boxed region highlights loss of OH and NH bands of polyamic acid with the conversion of PAA to PI

	PAA	PI	PAA/Carbon	PI/Carbon
PI Bands				
C=O bending Band intensity	731 cm^{-1} weak	729 cm^{-1} strong (sharp)	731 cm^{-1} weak	729 cm^{-1} strong (sharp)
C=O symmetric stretch (imide CONCO Band intensity		1740 cm^{-1} strong broad		1740 cm^{-1} strong broad
C=O asymmetric stretch (imide) Band intensity	1780 cm^{-1} weak	1780 cm^{-1} medium	1780 cm^{-1} weak	1780 cm^{-1} medium
PAA bands				
C=O (COOH) Band intensity	1729 cm^{-1} strong broad		1730 cm^{-1} strong broad	
C-NH Band intensity	1550 cm^{-1} medium	1552 cm^{-1} very weak	1550 cm^{-1} medium	1550 cm^{-1} very weak
OH (COOH), N-H (CONHC) Band intensity	2924-3267 cm^{-1} very strong	2924-3267 cm^{-1} very weak	2924-3267 cm^{-1} medium	2924-3267 cm^{-1} very weak

Table 5.1: Summary of FTIR bands pertinent to the conversion of polyamic acid to polyimide during thermal imidization [1, 4-6]

This band is present and located as at 1780 cm^{-1} for both PI and PI/carbon and occurs as a medium sized shoulder on the broad C=O symmetric stretch band centered at 1740 cm^{-1} for both PI and PI/carbon. In addition, a strong sharp band located at around 729 cm^{-1} assigned to imide C=O bending appears in both PI and PI/carbon. However, weak bands occurring at the same location as the C=O asymmetric stretch and C=O bending are also

observed for both PAA and PAA/carbon. This could signify that residual starting dianhydride might be present in the supplied PAA solution. Pyromellitic dianhydride exhibits the C=O asymmetric stretch at 1780 cm^{-1} and C=O bending at 720 cm^{-1}, which are very proximate to those of polyimide carbonyl groups.

5.2.2 Influence of carbon loading on PMDA/ODA Polyimide

The influence of the carbon content on the electrical conductivity of PI is evaluated and presented in Figure 5.3. Carbon loading is reported as based on % mass of carbon/mass of polyamic acid. Significant changes are observed as the amount of carbon introduced into the polyimide matrix is increased. A 7000 fold jump in the conductivity of PI is recorded as the carbon loading is increased between 2.5 percent and 5 percent. The drastic jump in conductivity is attributed to formation of fibrous chain-like carbon networks in the polymer matrix and has been previously reported for polyimide/carbon black composites. [7, 8] These networks are formed after particles reach a critical mass leading to coagulation and contact between the particles. [7-9] One theory describing this phenomenon is the percolation theory which states that after a critical carbon content (also referred to percolation threshold) is reached, the composite is converted from an insulator to a conductor.[10, 11]

After 5% carbon loading, the conductivity of the membrane improves gradually and does not change drastically after 10% carbon content is reached as seen in Figure 5.3 (inset). However, the mechanical stability of the films is compromised when the carbon content is 12.5% with fractures developing and flexibility decreasing. For this reason, composites with 10% carbon loading were used for all studies.

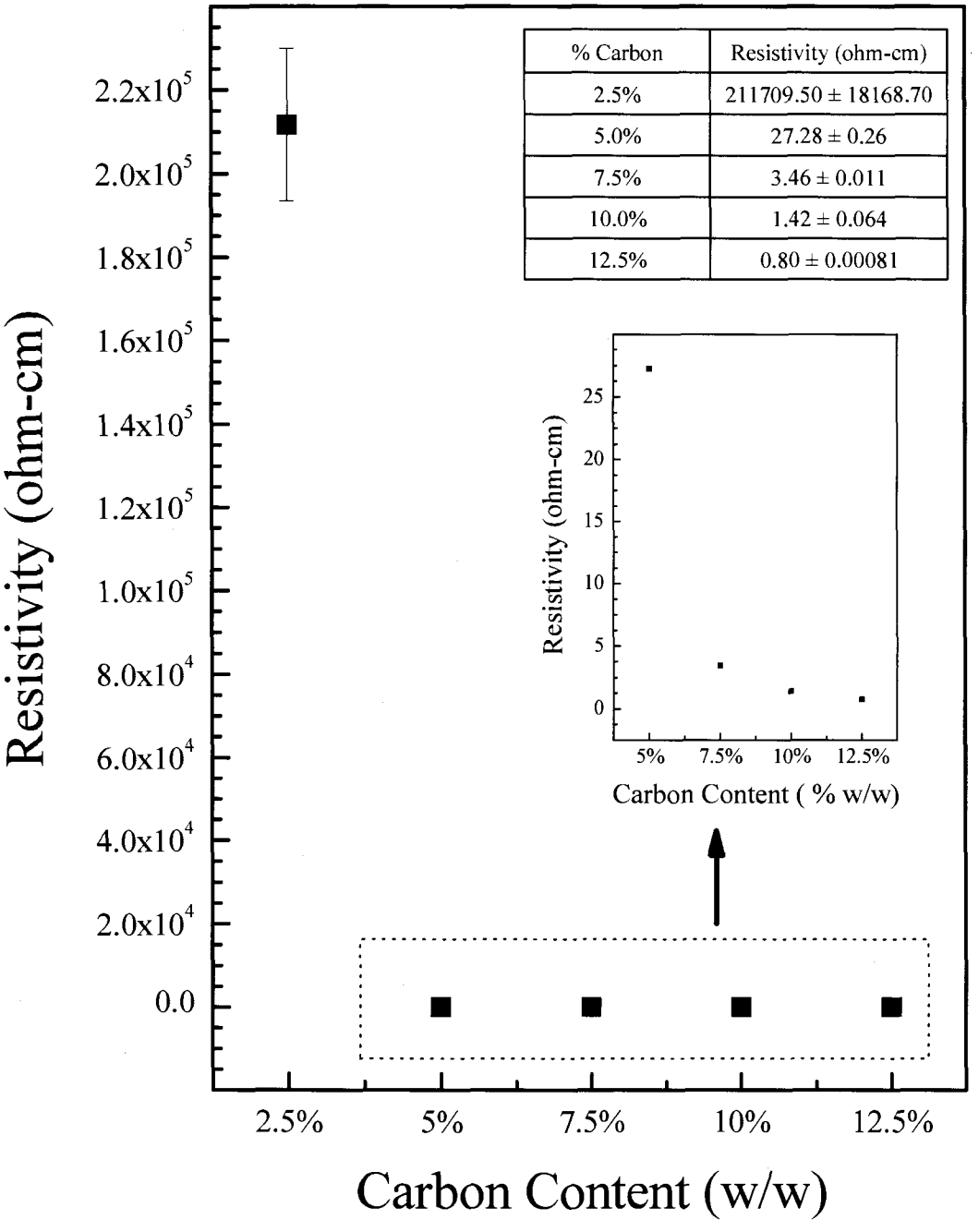

Figure 5.3: Effect of carbon loading on electrical conductivity of polyimide

The factors that influence the conductivity of polymer/carbon black composites are related to the composition of the carbon and aggregation and distribution in the polymer matrix. Factors such as variations in the density and particle size of the carbon filler play a role.[8, 9, 11-13] Increasing the density of the carbon filler allows more compact aggregation and packing leading to enhanced electrical conductivity and a lower percolation threshold. For example, highly crystallized graphite (HCG) exhibits a higher conductivity and a lower percolation threshold over carbon blacks because of its high density as compared to carbon blacks. In addition, small carbon particle size enhances conductivity since smaller particles can form more aggregates per unit volume leading to smaller gaps between the carbon centers.[11] Changes in temperature can also play a role due to thermal expansion and phase transitions in the form of melting and crystallization of the polymer which influence the resistivity of the composite. These changes can gradually or abruptly disrupt or enhance the continuity of the carbon aggregate network leading to an overall change in the conductivity of the film.

5.2.3 Thermal Analysis of Carbon/PI films

Differential scanning calorimetry (DSC) and thermal gravimetric analysis (TGA) are used to examine the effect of imidization and carbon incorporation on the thermal stability of PI. Thermal analysis techniques provide information on enthalpy changes (DSC) and mass loss (TGA) associated with exposing a sample to a temperature program. The DSC curves of representative PAA, PAA/Carbon, PI/carbon and PI samples are presented in Figure 5.4a-d respectively.

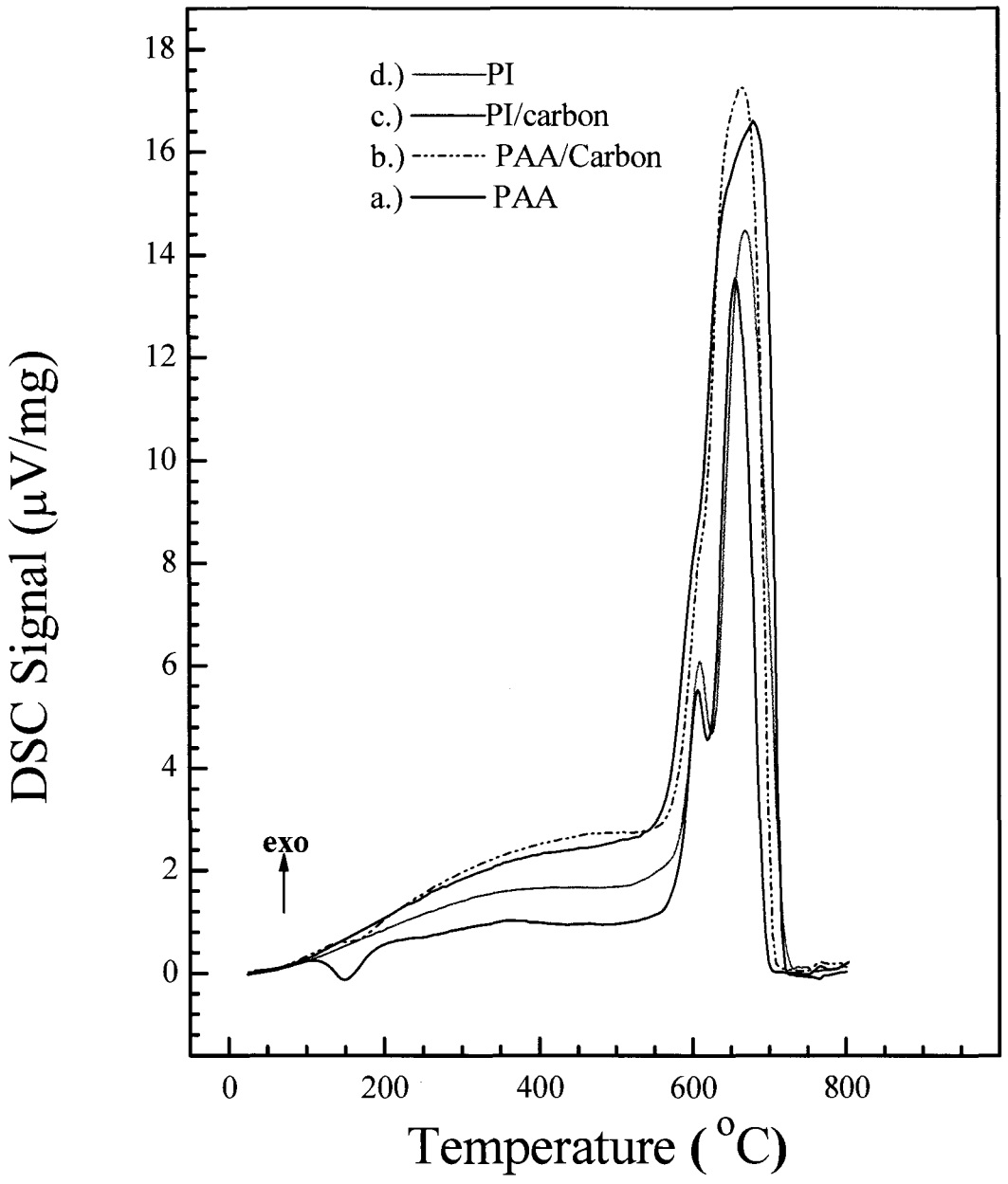

Figure 5.4: Differential Scanning Calorimetry (DSC) curves of (a.) PAA (b.) PAA/Carbon (10%) (c.) PI/carbon (10%) (d.) PI (Heating rate 10 K/min)

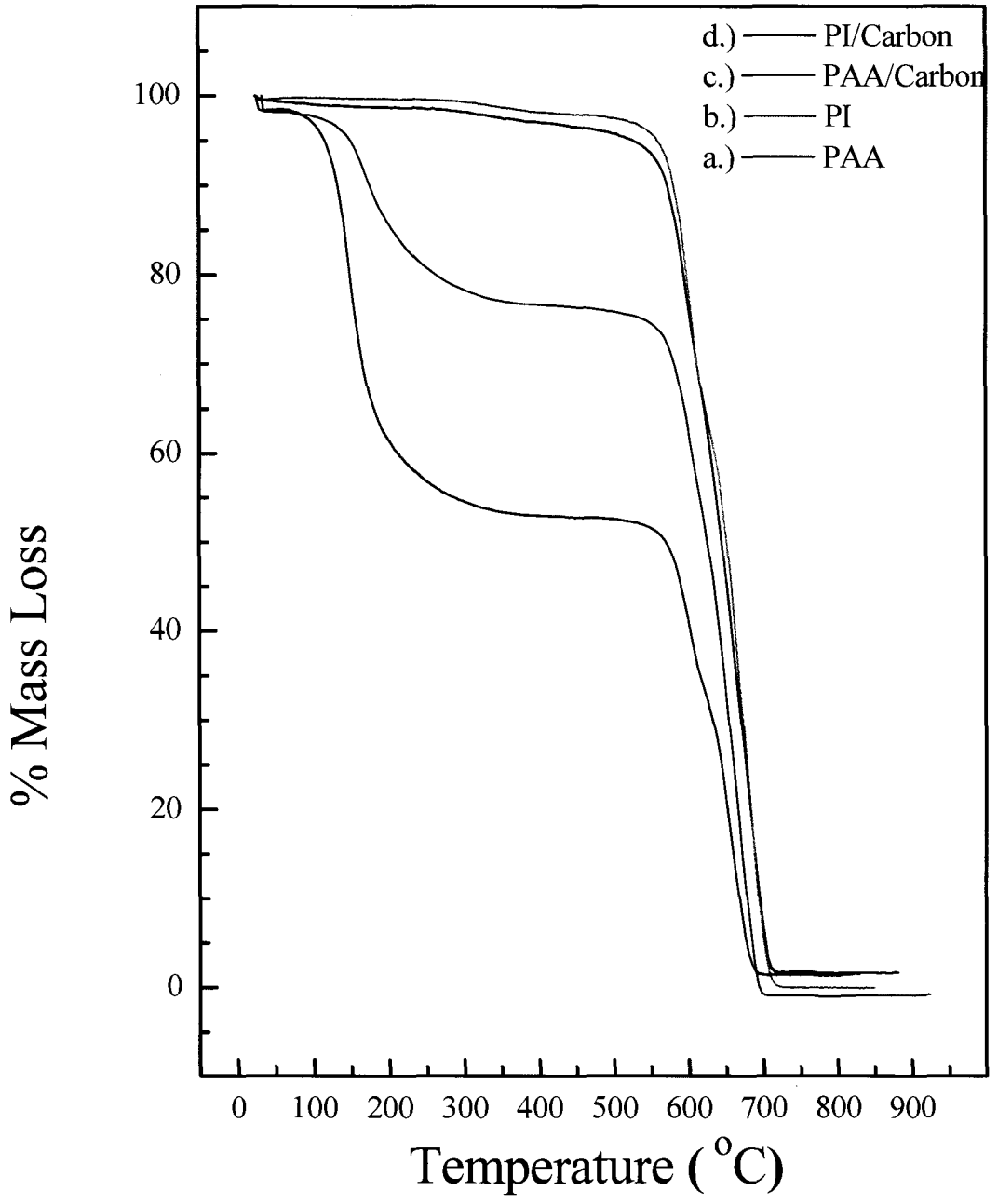

Figure 5.5: Thermal Gravimetric Analysis (TGA) curves of (a.) PAA (b.) PI. (c.) PAA/Carbon (d.) PI/carbon Heating rate: 10 K/min

The thermal stability temperature of the samples is measured at the onset of the decomposition of the organic component which is represented by the emergence of a decomposition exotherm in the case of DSC and a corresponding mass loss in the case of TGA. Figure 5.5a-d represents the TGA curves of PAA, PI, PAA/carbon and PI/carbon, respectively. Thermal stability temperatures for these materials are independently calculated from both DSC and TGA and are presented in Table 5.2. The thermal stability of PI is maintained following imidization in addition to the incorporation of carbon into the polymer. Values obtained from both techniques for PI before and after carbon incorporation are close with only a small decrease in the decomposition onset temperature for PI/carbon as compared to PI. Very close thermal stability temperatures of 568°C (DSC) and 570°C (TGA) are obtained for PI/carbon. These values are slightly lower but not appreciably different from those obtained for pristine PI.

	DSC decomposition onset temperature (°C)	TGA decomposition onset temperature (°C)
PAA	579	575
PAA/carbon	579	576
PI	576	576
PI/carbon	568	570

Table 5.2: Decomposition temperatures for PI and PI/carbon based on DSC and TGA

The TGA and DSC curves of PAA and PAA/Carbon can be used to determine temperatures that have to be achieved to effectively remove low volatility DMSO and NMP solvents from the polymer prior to thermal imidization. The onset of a mass loss and a corresponding endotherm associated with solvent expulsion are observed in the

thermal analysis curve of both PAA and PAA/Carbon. The mass loss is recorded at 124.5°C and 144°C for PAA and PAA/carbon respectively. [8] The higher temperature needed to expel solvent from the PAA/Carbon as compared to PAA can be explained by the presence of carbon which can trap the solvent in its porous structure making it harder to remove the solvent from the composite. A 46% and 22% mass loss is observed for PAA and PAA/Carbon respectively. The DSC endotherm associated with the removal of solvent is observed at 124.6°C for PAA which matches the onset of the mass loss. However, the onset temperature for PAA/Carbon could not be determined accurately due to the small size of the endotherm.

The decomposition of pure SC-conductex carbon black proceeds from 572°F (300°C) which is much lower than the temperature observed for PI/carbon.[14] No decomposition endotherm or mass loss is recorded at this temperature. The fact that the decomposition of carbon is not observed at its decomposition temperature suggests that PI binds carbon into its matrix which increases its thermal stability.

5.2.4 Electrochemical Deposition of Platinum

Deposition on freestanding PI/carbon working electrode is achieved using potential cycles that encompass the reduction of $PtCl_4^{2-}$ ion to Pt metal. The reduction reaction and potential for $PtCl_4^{2-}$ are given as follows:

$$PtCl_4^{2-} + 2e^- \longrightarrow Pt(0) + 4Cl^- \qquad E = 0.520V \text{ versus Ag/AgCl [15]}$$

Platinum is electrochemically deposited on the surface of the PI/carbon composite using cyclic voltammetry. The cyclic voltammogram for deposition of platinum on the film is compared and referenced to that of a planar platinum electrode.

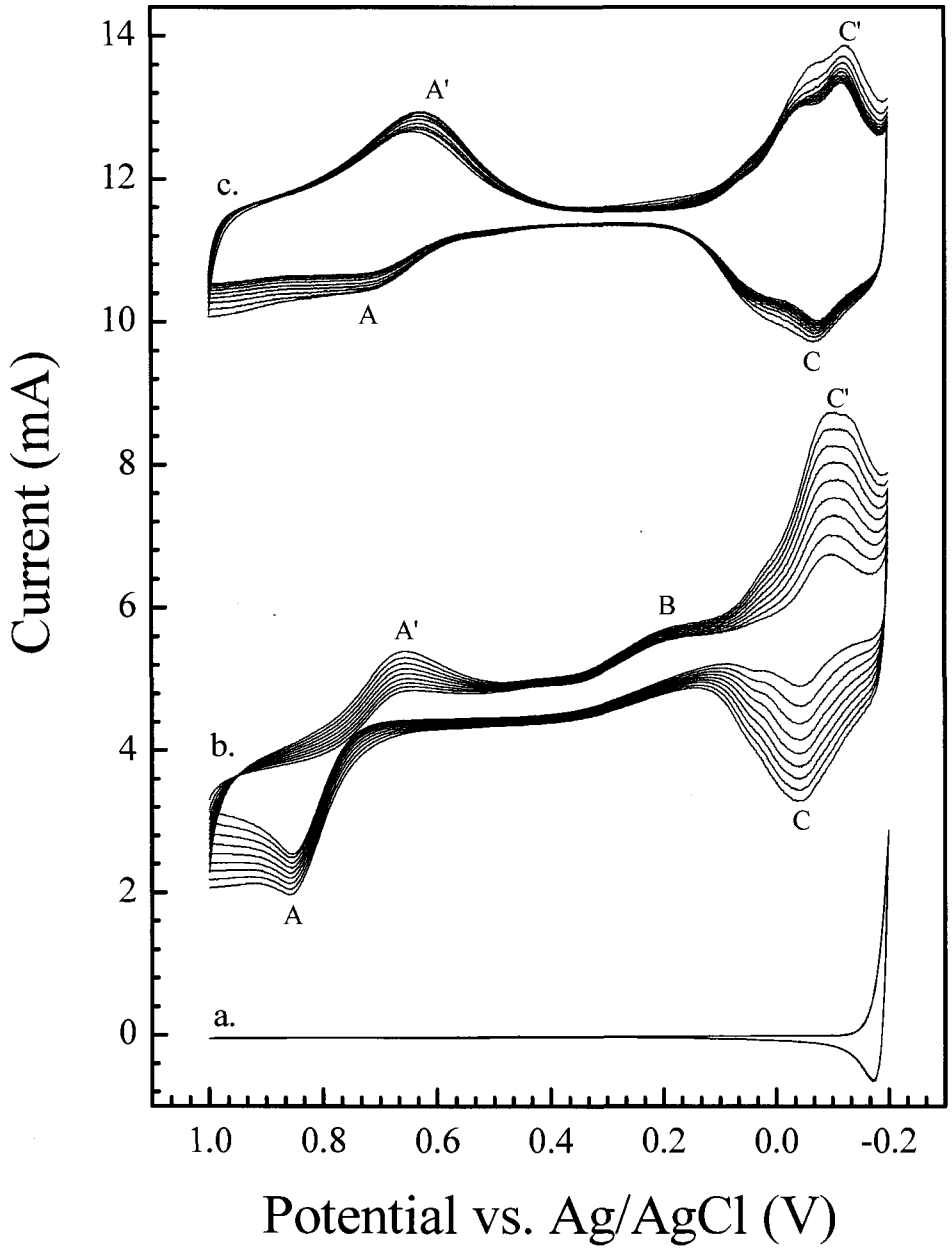

Figure 5.6: Cyclic voltammograms at planar Pt sheet electrode of (a) 1M $HClO_4$ prior to deposition (b) Pt deposition using $2.0x10^{-2}M$ $PtCl_4^{2-}$ in 1M $HClO_4$ (c) 1M $HClO_4$ after deposition. Scan rate: 0.01 V/s

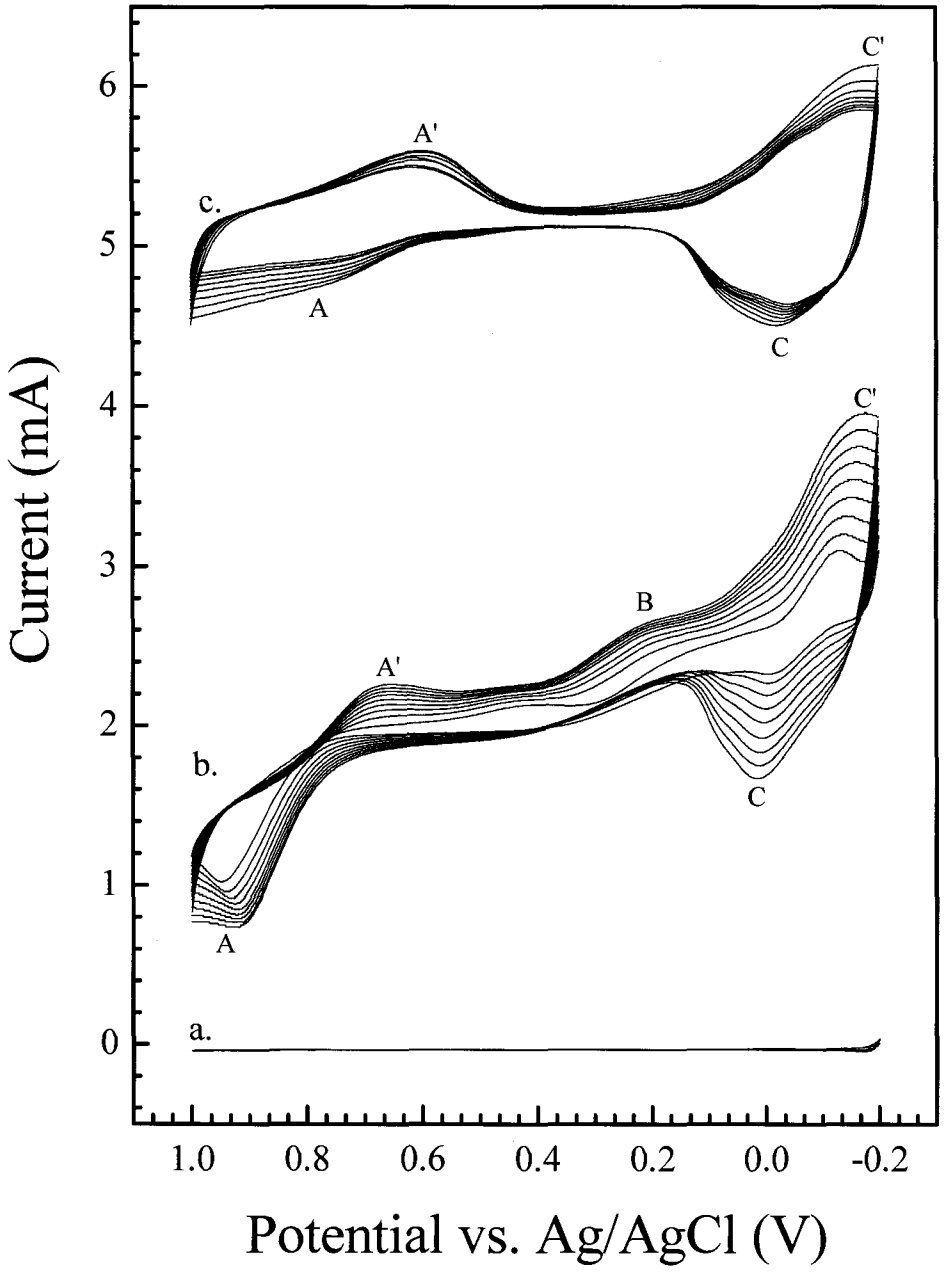

Figure 5.7: Cyclic voltammograms at a PI/carbon electrode of (a) 1M $HClO_4$ prior to deposition (b) Pt deposition using $2.0x10^{-2}M$ $PtCl_4^{2-}$ in 1M $HClO_4$ (c) 1M $HClO_4$ after deposition. Scan rate: 0.01 V/s

Specifically, voltammetric waves related to the deposition of platinum and the ensuing chemistry at the surface of the deposited platinum layer are evaluated for both electrodes.

Figure 5.6a represents the background voltammogram of a bare Pt sheet electrode in 1M $HClO_4$ supporting electrolyte while the deposition of platinum using $2.0x10^{-2}M$ $PtCl_4^{2-}$ in 1M $HClO_4$ on the same electrode is presented in figure 5.6b. Figure 5.6c shows the voltammogram of the electrode immersed in 1M $HClO_4$ following Pt deposition. Figure 5.7a represents the background voltammogram of a PI/carbon in 1M $HClO_4$ supporting electrolyte while the deposition of platinum on the electrode is presented in figure 5.7b. Figure 5.7c shows the voltammogram of the electrode immersed in 1M $HClO_4$ following Pt deposition.

While no voltammetric waves are observed for both electrodes when immersed in supporting $HClO_4$ solution (Figure 5.6a) prior to Pt deposition, significant changes can be seen following the deposition of Pt. New waves associated with the deposition of platinum emerge and are labeled for clarity on the voltammetric wave representing electrode immersed in $PtCl_4^{2-}$ for both the Pt sheet (figure 5.6b) and PI/carbon (figure 5.7b). In addition, waves resulting from competing processes occurring at the surface of the newly deposited platinum are also recorded. Specifically, in acidic medium, the adsorption/desorption of hydrogen following proton reduction and formation and reduction of PtO can occur and inhibit electron transfer at the surface of the electrode.

The small wave centered at 0.201V (wave B) in the Pt sheet voltammogram is assigned to the reduction on $PtCl_4^{2-}$ to Pt metal. This wave is also observed for Pt deposition at carbon/PI as shown in Figure 5.7b and is located at 0.215V. However, it is absent when both electrodes are immersed in $HClO_4$ prior and after metal deposition

suggesting that the wave is related to the reduction of the $PtCl_4^{2-}$ ion. The assignment of the $PtCl_4^{2-}$ reduction wave is made difficult by the small size of wave B. However, the presence of other waves in the deposition voltammogram resulting from surface processes occurring at newly deposited platinum sites can be used to confirm that metal deposition occurs.

For example, the presence of proton adsorption/desorption waves provides further evidence that Pt deposition occurs at the surface of both the Pt sheet and PI/carbon. Wave C' located at -0.107 V is assigned to the adsorption of H atoms produced from the reduction of protons on the newly deposited platinum and is outlined as follows:

$$H^+ + e^- \rightarrow H \rightarrow H_{ads}$$

The location of this wave is consistent with reported values of below 0 V vs. Ag/AgCl for the process. [15-18] Proton adsorption at a polycrystalline platinum electrode is a two step process representing weak adsorption followed by strong adsorption of hydrogen atoms to the surface of the electrode.[17] However, this process is highly dependent on the crystal surface structure of the electrode with the number of peaks observed being determined by the number of crystal planes of the electrodes surfaces that are exposed.[16, 19] The presence of defects and impurities can lead to disorder in the crystal structure of the electrode becoming hard to observe distinct adsorption waves from the different crystal planes. At negative potentials beyond proton adsorption, hydrogen evolution occurs as follows:

$$2H_{ads} \rightarrow H_{2ads} \rightarrow H_2(g) \quad E = -0.197V \text{ vs Ag/AgCl [15]}$$

In the case of the pt sheet electrode and the PI/carbon electrodes, a single peak with a small shoulder is observed. With potential cycling, the area of proton

adsorption/desorption peaks increases because every deposition cycle provides additional sites for the process to occur. As cycling proceeds, proton desorption from the Pt sheet electrode surface is observed at -0.0397V (wave C). A similar trend is observed for Pt deposition at PI/carbon (Figure 5.7b). However, proton adsorption and desorption are observed at slightly more negative potentials of -0.123 V and -0.0660 V respectively as compared to the Pt sheet.

In addition to proton adsorption during Pt deposition, passivation of the Pt surface through the formation of a PtO monolayer (wave A) is observed for both the platinum sheet and PI/carbon.[18] PtO formation is observed at anodic potentials of 0.857V for Pt sheet and 0.915V for carbon/PI. A corresponding wave (wave A') related to the reduction of PtO layer is observed at 0.654V and 0.622 for the pt sheet electrode and carbon PI respectively. PtO reduction is presented as follows [20]:

$$PtO(s) + 2e^- + 2H^+ \rightleftharpoons Pt(s) + H_2O \quad E = 0.78 \text{ V vs. Ag/AgCl}$$

Similar to proton adsorption and desorption waves, an increase in the area of PtO peaks as cycling proceeds is observed as the number of platinum sites increases with every successive metal deposition cycle.

Both proton adsorption/desorption processes and the formation and reduction of PtO can be observed when the Pt sheet and PI/carbon are immersed in $HClO_4$ following Pt deposition as shown in Figure 5.6c and 5.7c respectively. These processes are not observed when the electrodes are immersed in the same solution prior to metal deposition. The occurrence of these processes in the $HClO_4$ electrolyte solution provides further evidence that $PtCl_4^{2-}$ is reduced to Pt metal at the surface of the electrode.

However, some differences can be observed between the deposition voltammograms

of the Pt sheet and PI/carbon electrodes. One difference is the separation of hydrogen/desorption waves and PtO formation/reduction waves is larger for carbon/PI as compared to the Pt sheet suggesting slower electron transfer at PI/carbon. The slower electron transfer could be attributed to the lower electrical conductivity of PI/carbon as compared to the Pt sheet electrode.

5.2.5 Scanning Electron Microscopy and X-Ray Photoelectron Spectroscopy

Scanning electron microscopy (SEM) is used to investigate the morphology of the PI/carbon/platinum composite and particle distribution of deposited platinum on the surface of the PI/carbon platform as shown in Figures 5.8a and 5.8b which represents films with a Pt loading of 6% and 30% respectively. During Pt deposition, the films are divided into two sections with platinum deposited in one partition and no platinum deposited on the other partition. At low Pt loading, the metal appears as evenly spaced, discrete clusters of Pt (~400 nm diameter) in PI/carbon/Pt composites. In contrast, the Pt deposited in the PI/carbon/Pt composites with high loading show a coalesced deposit of metal with no discernible clusters. The morphology of the carbon/PI suggests that good carbon dispersion in PI is achieved with the acetone/DMSO solvent system. Carbon aggregation at the PI surface is not discernable even at a high magnification of 8000 (Figure 5.8c).

Lin et al. observe large surface defects appearing as lumps approximately 60μm in size on the surface PI/carbon films prepared from SC conductex carbon black. The authors attribute these defects to formation of pockets by trapped water vapor produced during imidization. [8]

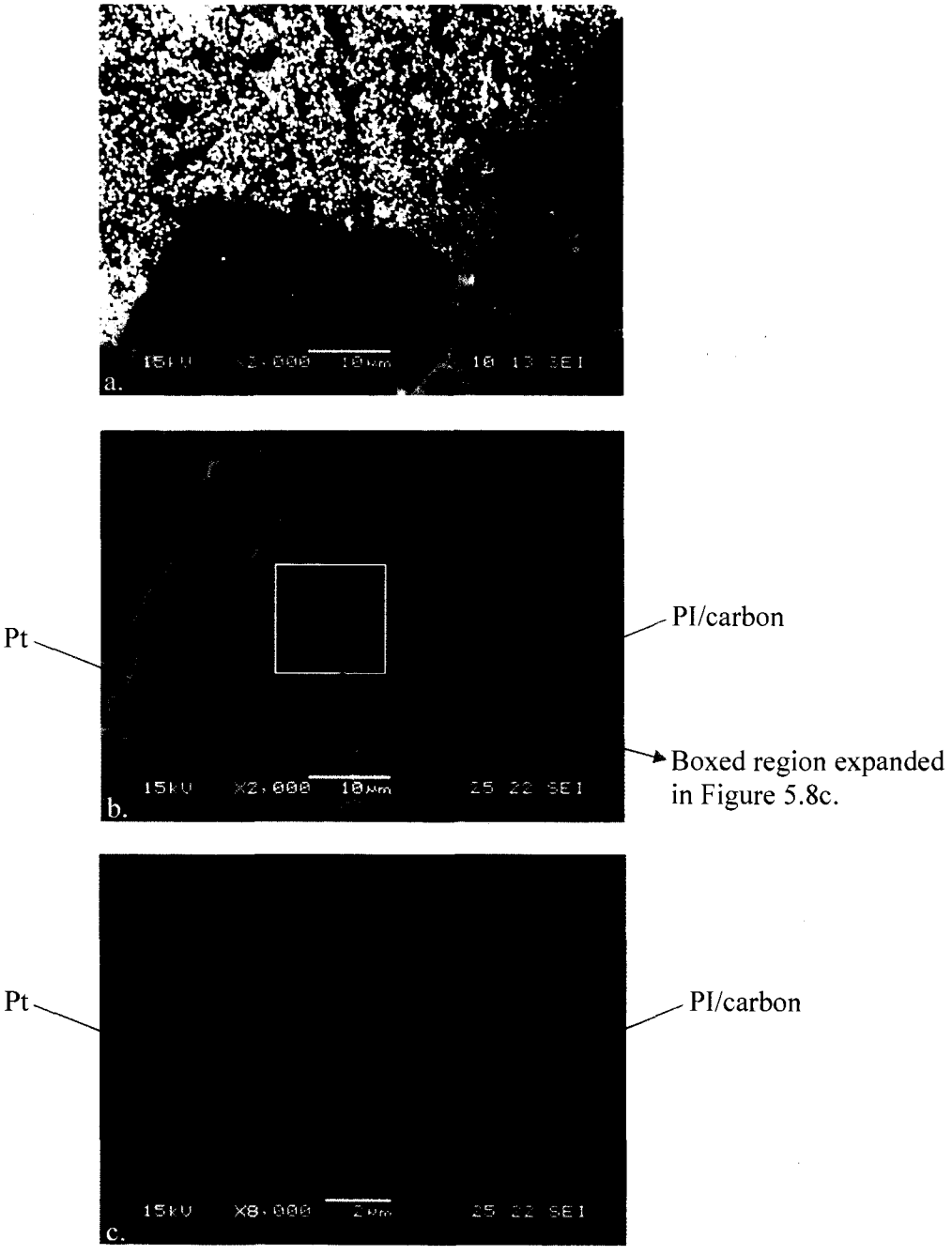

Figure 5.8: SEM images of a. PI/Carbon/Pt composite Low Pt loading (6%). b. PI/Carbon/Pt composite High Pt loading (31%) x2000 magnification c. PI/Carbon/Pt composite High Pt loading (31%) x5000 magnification

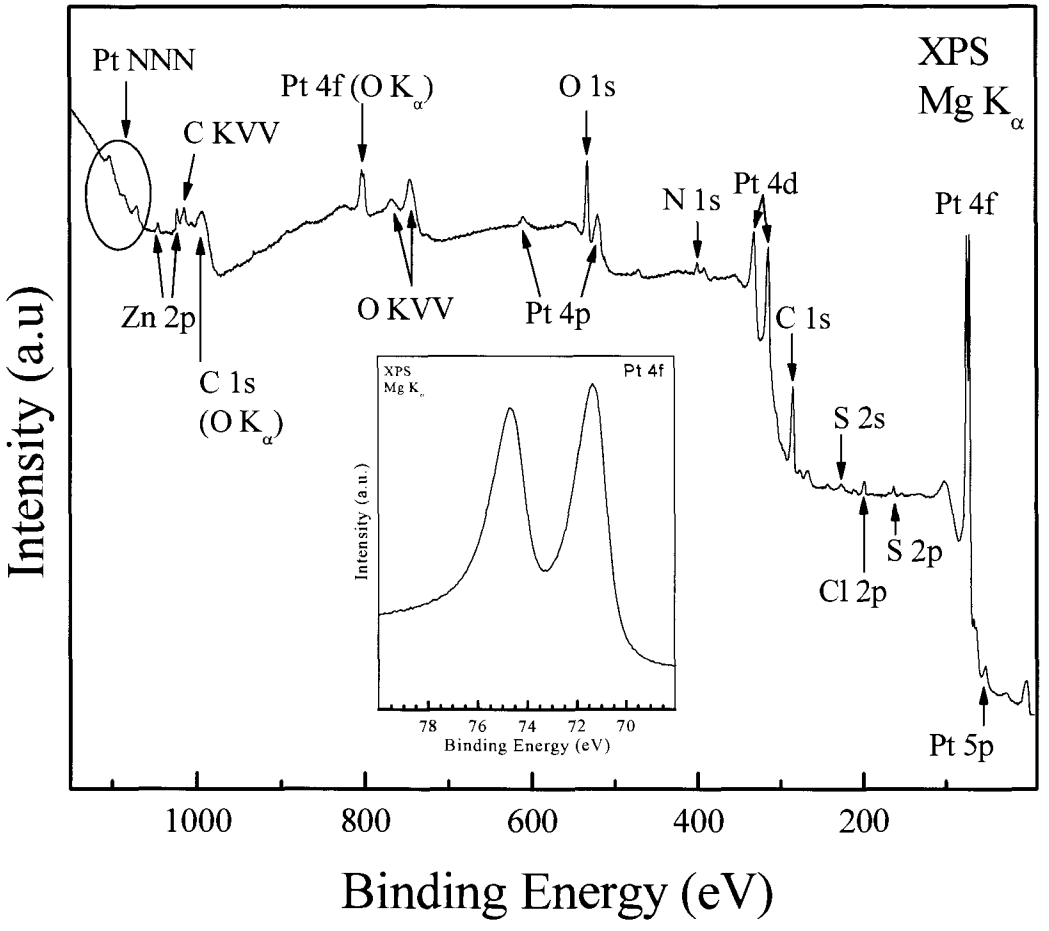

Figure 5.9: XPS survey of PI/carbon/Pt composite

However, the defects are not present in PI/carbon/Pt images presented in Figure 5.8a-b suggesting that the stepwise temperature program used for the imidization process was effective in expelling water vapor without causing any significant surface defects.

X-ray photoelectron spectroscopy (XPS) is used to examine the oxidation state of the Pt metal deposited on PI. The XPS survey spectrum of a representative PI/carbon/Pt film confirms that the surface deposit is Pt metal as presented in Figure 5.9. Specifically, the binding energies for the Pt 4f doublet appear at 71.4ev and 74.7ev which is consistent with the presence of Pt in its zero valent state as shown in the more resolved spectrum presented in Figure 5.9 inset. [21]

5.2.6 Thermal Analysis of Carbon/PI/Pt films

Figure 5.10a-b presents the DSC curves of PI/carbon and PI/carbon/Pt (6% Pt loading) respectively while Figure 5.11a-b shows the TGA curves of PI/carbon and PI/carbon/Pt with a 6 % (w/w) Pt loading respectively. Thermal stability of PI/carbon is maintained following metal deposition. The decomposition onset temperatures obtained from DSC and TGA data for PI/carbon/Pt are in good agreement but slightly lower than those of PI/carbon by 7°C for DSC and 11°C for TGA as seen in Table 5.3.

	DSC decomposition onset temperature (°C)	TGA decomposition onset temperature (°C)
PI/carbon	568	570
PI/Carbon/Pt	561	559

Table 5.3: Decomposition temperatures based on DSC and TGA

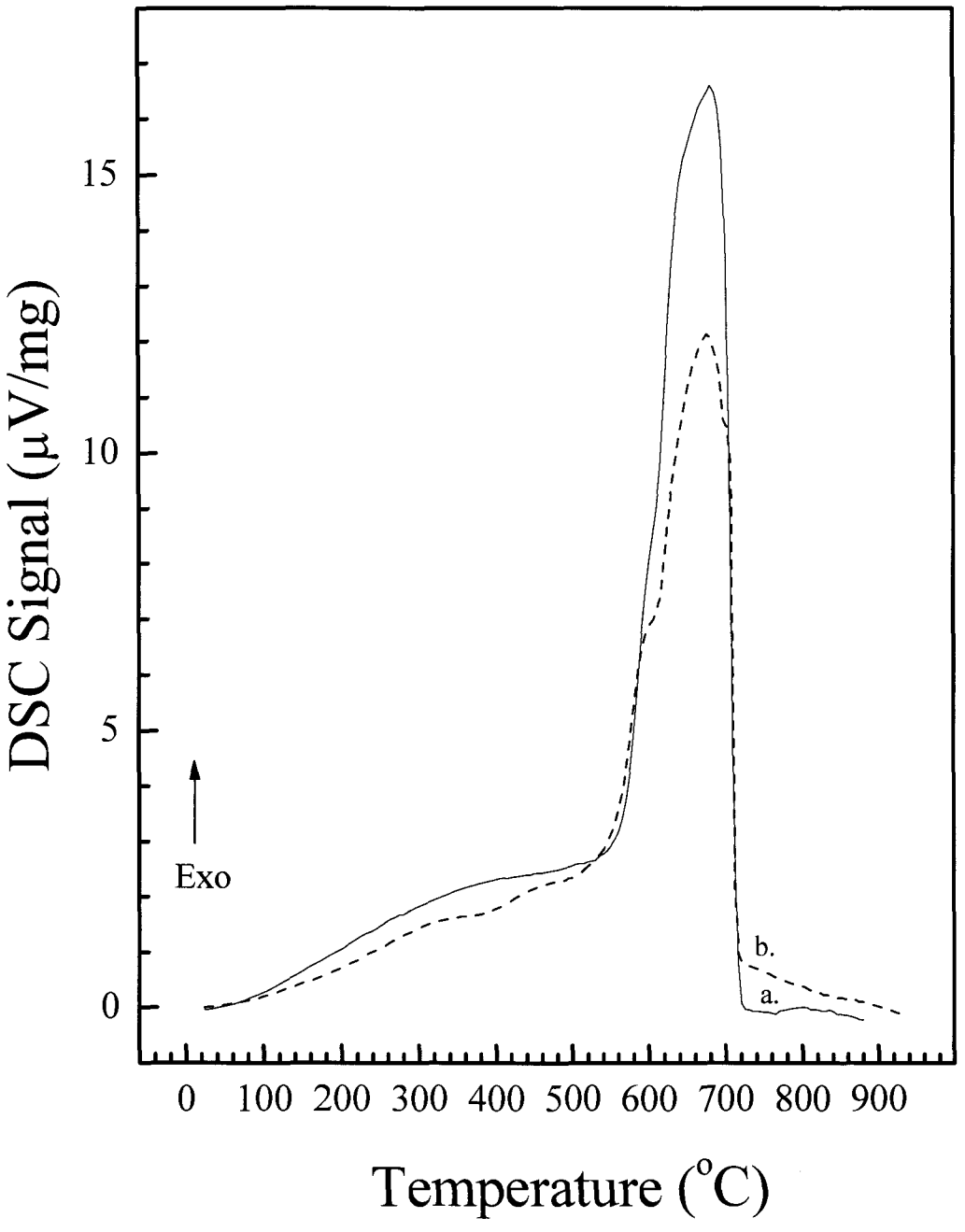

Figure 5.10: DSC curves of a.) PI/carbon b.) PI/carbon/Pt (6% Pt loading) Heating rate: 10K/min

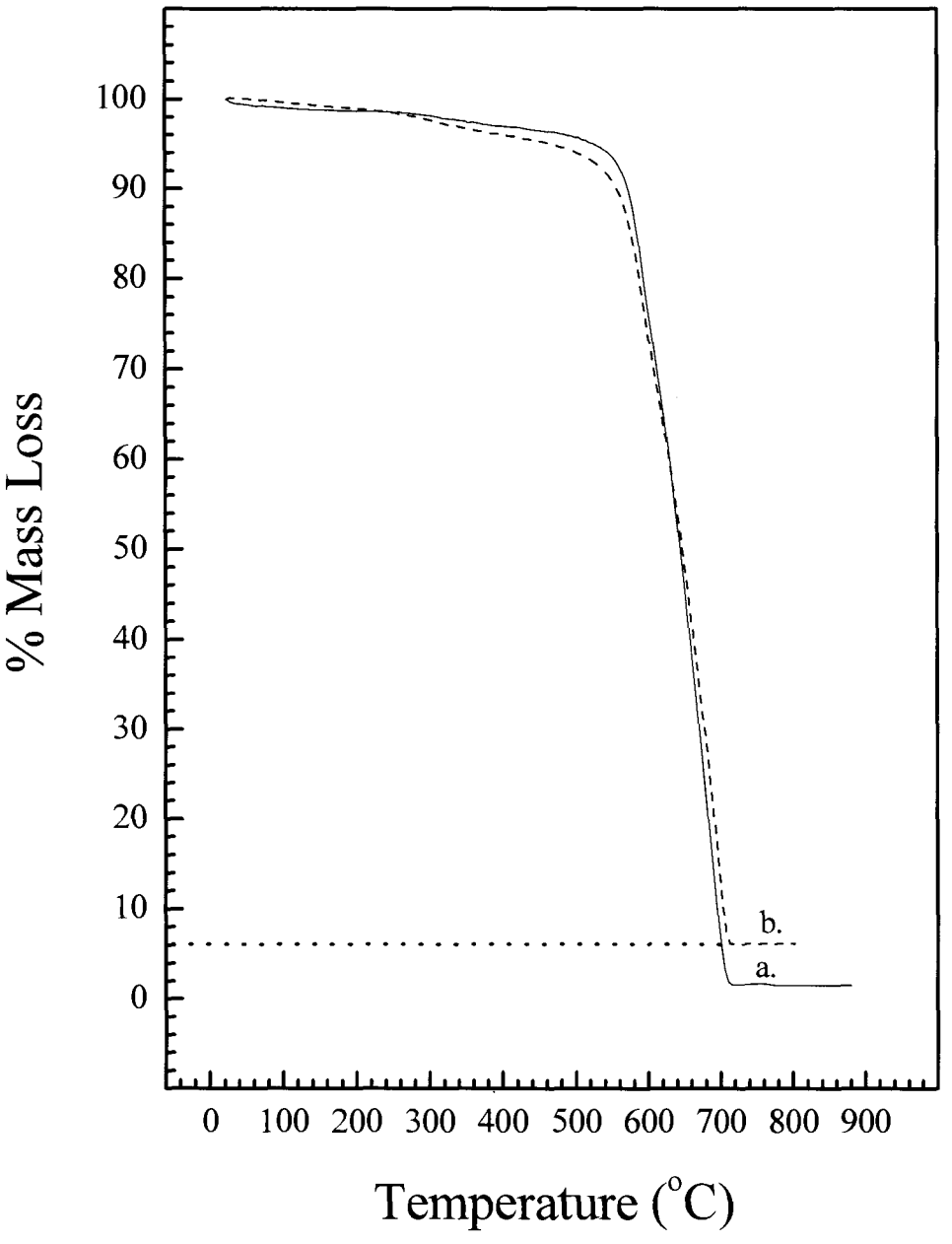

Figure 5.11: TGA curves of curves of a.) PI/carbon b.) PI/carbon/Pt (6% Pt loading)

Heating rate: 10K/min

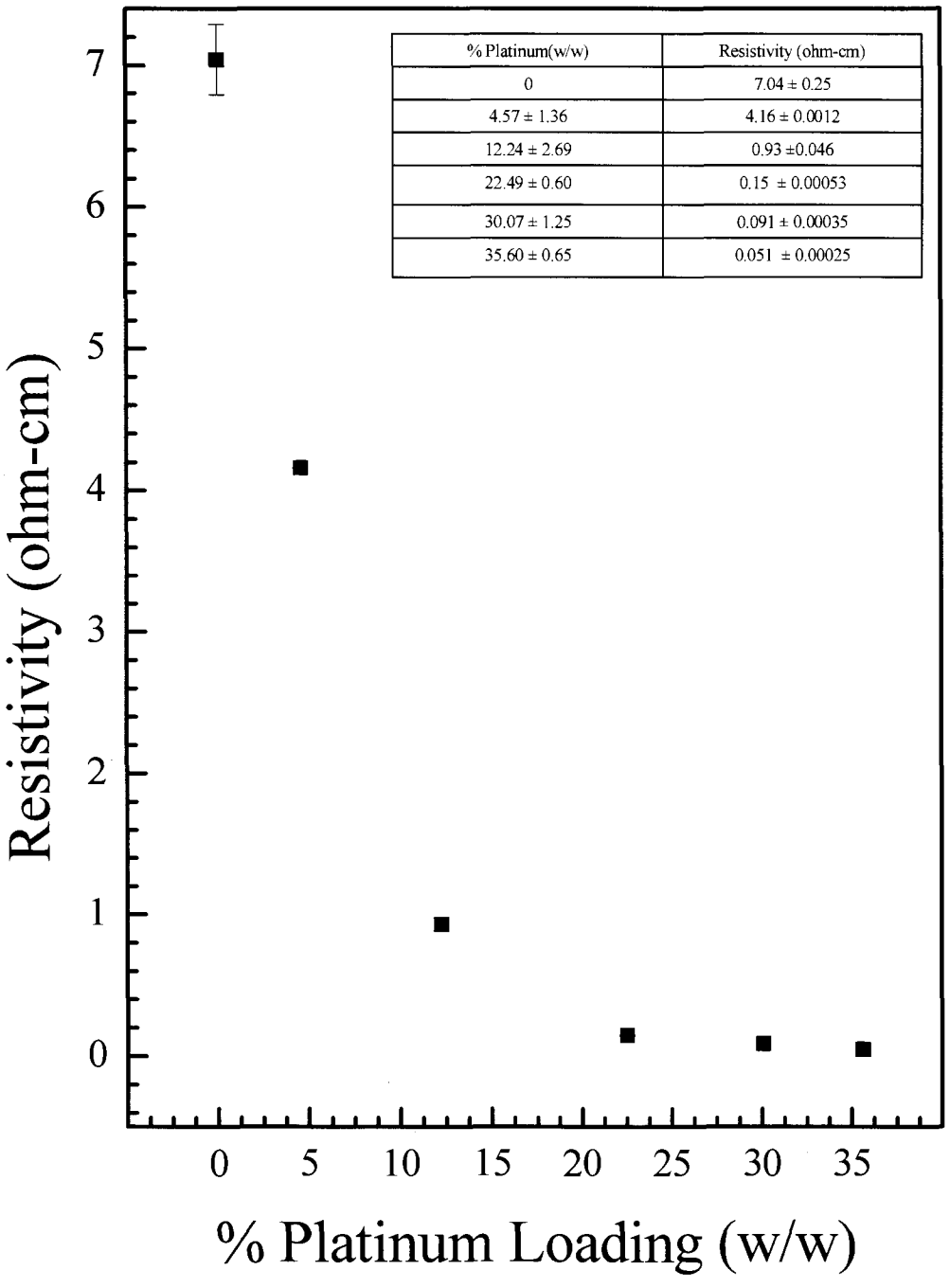

Figure 5.12: Conductivity of PI/carbon/Platinum composite as a function of Pt loading

5.2.7 Estimation of Percent Platinum Content and its Effect on Electrical Conductivity

Platinum loading in the PI/carbon/Pt composites with a uniform carbon loading of 10% is estimated using TGA. The composite is heated to a temperature of about 900°C at which all the PI/carbon organic component of the composite is decomposed. All mass loss is assigned to the decomposition of the organic component, which is complete at about 800°C. The remaining mass in the test crucible at the end of the experiment is then used to estimate the metal content for the composite material. Figure 5.12 represents the electrical conductivity of the PI/carbon/Pt composites as a function of platinum loading. As expected, the electrical conductivity of the composite is enhanced as the amount of platinum deposited on the composite surface is increased relative to PI/carbon. A resistivity of 7.04 ohm-cm is observed for PI/carbon. This value is higher than 1.42 ohm-cm observed for a carbon/PI film in Figure 5.3 suggesting that batch-to-batch conductivity variations might exist. A steady decrease in resistivity is recorded as Pt loading until a 22% loading is achieved. After this loading, there is minimal improvement in the conductivity of the PI/carbon/Pt film. One possible explanation for this plateau is that at higher Pt loading, the Pt layer becomes the main contributor to the recorded resistivity of the film because the contacts of the four point probe are preset to contact and not penetrate the film.

5.2.8 Cyclic Voltammetry of PI/carbon/Gold in the Ferricyanide Redox Couple

As a preliminary test for the electroactivity, freestanding PI/carbon/Au composites are used to probe the simple electrochemical redox reaction involving the ferricyanide redox couple. The Ferricyanide redox couple is as follows:

$$Fe(CN)_6^{3-} + e^- \Leftrightarrow Fe(CN)_6^{4-} \quad E^o = 0.161V \text{ vs. Ag/AgCl [22]}$$

Figure 5.13a shows a cyclic voltammogram of a PI/carbon film in 0.01M $K_2Fe(CN)_6$ in 1M KNO_3. While the PI/carbon film shows minimal electroactivity in ferricyanide, depositing a 100Å layer of gold on the film surface by chemical vapor deposition (PI/carbon/Au_{CVD}) leads to enhanced sensitivity in the same solution as shown in Figure 5.13b. Enhanced sensitivity is also observed for PI/carbon film with gold electrodeposited on its surfaces by cyclic voltammetry (PI/carbon/Au_{ECHEM}) for 5cycles at 0.1V/s Figure 5.13c. For comparison and reference, a planar electrode fabricated from gold coated mica was also used to probe the same ferricyanide solution and is presented in Figure 5.13d.

The anodic and cathodic peaks are well defined and appear in equal magnitudes for all the electrodes, showing that both the forward and reverse reactions of the couple occur at the surface of the electrode. However, differences can be observed for gold deposited PI/carbon films as compared to gold planar electrode. Specifically, shifts in peak cathodic potentials (E_{pc}) and peak anodic potentials (E_{pa}) can are recorded for PI/carbon films relative to the gold planar electrode. The Ep_c and E_{pa} values for both PI/carbon film in the ferricyanide couple are presented in Table 5.4 in addition to those of a gold planar electrode used as a reference. For the (PI/carbon/Au_{CVD}), the Ep_c and E_{pa} are close to values recorded for the gold planar electrode.

The separation between E_{pa} and E_{pc} is denoted as ΔEp and is an indicator for electron transfer on the surface of the electrode. Theoretically for a totally reversible nernstian process, under fast kinetics, ΔEp is equal to 59.1 mV/n where n is the number of electrons involved in the redox reaction.

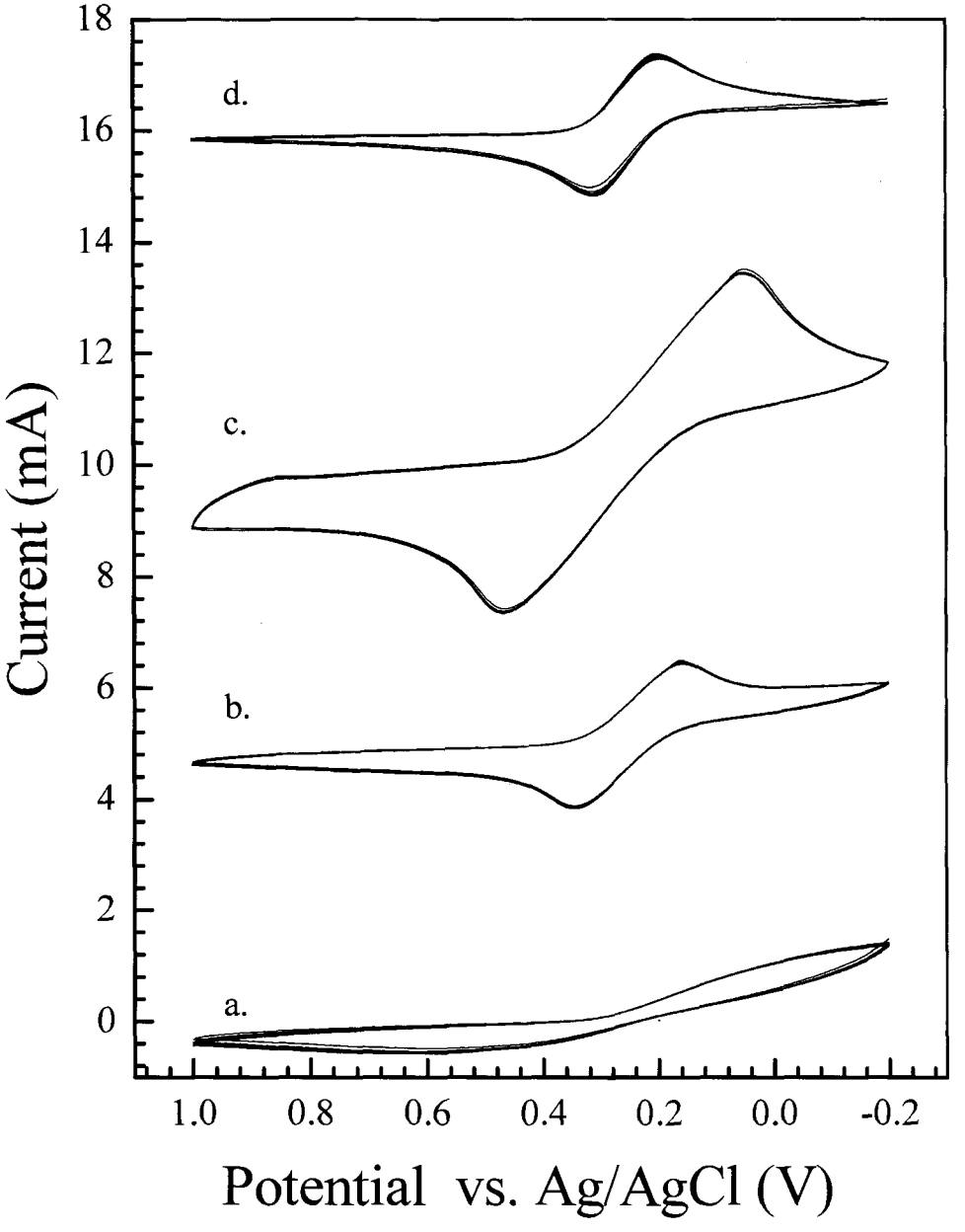

Figure 5.13: Cyclic voltammograms at 0.1V/s of (a) PI/carbon (b) PI/carbon/Au_{CVD} (c) PI/carbon/Au_{ECHEM} (5 deposit segments at a scan rate of 0.1V/s) (d) Gold planar electrode in 0.01M $K_2Fe(CN)_6$ in 1M KNO_3 at 0.1V/s

	E_{pa} vs Ag/AgCl (mV)	E_{pc} vs Ag/AgCl (mV)	ΔP vs Ag/AgCl (mV)	n=59.1mV/ΔE_p
PI/carbon	-	-	-	
PI/Carbon/Au_{CVD}	347	161	186	0.317
PI/Carbon/Au_{ECHEM}	467	48.1	418	0.141
Au planar electrode	316	202	114	0.518

Table 5.4 Redox potentials for $Fe(CN)_6^{4+}$, $Fe(CN)_6^{3+}$ redox couple on PI/carbon deposited electrochemically, or by chemical vapor deposition (CVD). A bare Gold coated mica electrode is used as a reference for potentials for the redox couple

In the case of the ferricyanide couple n=1 and therefore the theoretical ΔEp is equal 59.1mV. However, under experimental conditions, the ΔE_p for the ferricyanide couple is found to be greater than 57mV due to factors such as solution resistance, surface inhomogeneity such as defects on the electrode surface and non linear diffusion.[23] Consequently, ΔE_p can be used as an indicator of reaction kinetics with larger ΔE_p signifying slower electron transfer at the electrode surface. In addition, the experimental value of n can be calculated as follows:

$$n = \frac{59.1}{\Delta E_p}$$

ΔE_p calculations presented in Table 5.4 show that both PI/carbon/Au_{ECHEM} and PI/carbon/Au_{CVD} exhibit slow electron transfer relative to the gold planar electrode. The slowest electron transfer is observed for PI/carbon/Au_{ECHEM} with an n value of 0.141

while a value of 0.317 is obtained for PI/carbon/Au_{CVD}.

5.3 References

1. Ghosh M.K. and Mittal K.L., eds. *Polyimides*. 1996, Marcel Dekker: New York.

2. Silverstein, R.M. and Webster, F.X., *Spectrometric identification of organic compounds*. 1998, New York: John Wiley & Sons.

3. Bart, J.C.J., *Plastics Additives: Advanced Industrial Analysis*. 2006, Amsterdam IOS Press.

4. Kim, G.-H., Dong, W., Yoon, C.S., and Kim, Y.-H., *Synthesis of duplex nanoparticles in polyimide by the reaction of polyamic acid with Cu-Zn alloy films.* Colloids and Surfaces A: Physicochemical and Engineering Aspects, 2008. **321**(1-3): p. 292-296.

5. Zhai, Y., Yang, Q., Zhu, R.Q., and Gu, Y., *The study on imidization degree of polyamic acid in solution and ordering degree of its polyimide film.* Journal of Materials Science, 2008. **43**(1): p. 338-344.

6. Thomas, R.R., Buchwalter, S.L., Buchwalter, L.P., and Chao, T.H., *Organic-Chemistry on a Polyimide Surface.* Macromolecules, 1992. **25**(18): p. 4559-4568.

7. Imai Y., Fueki T., Inoue T., and M-A., K., *A New Direct Preparation of Electroconductive Polyimide/Carbon Composite Via Polycondensation of Nylon-Salt Type Monomer/Carbon Black Mixture* Journal of Polymer Science: Part A:Polymer Chemistry, 1998. **36**: p. 1031-1034.

8. Lin J-S. and Chiu H-T., *Preparation and Properties of Conductive Polyimide films.* Journal of Polymer Research, 2002. **9**: p. 189-194.

9. Narkis, M. and Vaxman, A., *Resistivity Behavior Of Filled Electrically Conductive Crosslinked Polyethylene.* Journal of Applied Polymer Science, 1984. **29**(5): p. 1639-1652.

10. Ghofraniha, M. and Salovey, R., *Electrical Conductivity Of Polymers Containing Carbon-black.* Polymer Engineering and Science, 1988. **28**(1): p. 58-63.

11. Zhang W., Dehghani-Sanij, A.A., and Blackburn R.S., *Carbon based conductive polymer composites.* Journal of Materials Science, 2007. **42**: p. 3408-3418.

12. Pantea, D., Darmstadt, H., Kaliaguine, S., and Roy, C., *Electrical conductivity of conductive carbon blacks: influence of surface chemistry and topology.* Applied Surface Science, 2003. **217**(1-4): p. 181-193.

13. Murugaraj, P., Mora-Huertas, N., Mainwaring, D.E., Ding, Y., and Agrawal, S., *Influence of thermal stresses on electron transport in carbon-polymer nanocomposite films.* Composites Part A: Applied Science and Manufacturing, 2008. **39**(2): p. 308-313.

14. *Material Safety Data Sheet - Carbon Black - Columbian Chemicals Company.* 2007 [cited; Available from: http://www.columbianchemicals.com/Portals/0/Columbian_Ind_Carbon_English_2007-07-03.pdf.

15. Kinyanjui, J.M., Wijeratne, N.R., Hanks, J., and Hatchett, D.W., *Chemical and electrochemical synthesis of polyaniline/platinum composites.* Electrochimica Acta, 2006. **51**(14): p. 2825-2835.

16. Bard, A.J. and Faulkner, L.R., *Electrochemical Methods.* 1980, Hoboken, NJ.: John Wiley & Sons Inc.

17. Rodriguez, J.M.D., Melian, J.A.H., and Pena, J.P., *Determination of the real surface area of Pt electrodes by hydrogen adsorption using cyclic voltammetry.* Journal of Chemical Education, 2000. **77**(9): p. 1195-1197.

18. Aschauer, E., Fasching, R., Urban, G., Nicolussi, G., and Husinsky, W., *Surface characterization of thin-film platinum electrodes for biosensors by means of cyclic voltammetry and laser SNMS.* Journal of Electroanalytical Chemistry, 1995. **381**(1-2): p. 143-150.

19. Bockris, J.O.M., Conway, B.E., and White, R.E., eds. *Modern Aspects of Electrochemistry.* Vol. 22. 1992, Springer: New York.

20. Bard, A.J., Parsons, R., and Jordan, J., *Standard Potentials in Aqueous Solution.* 1985, New York: Marcel Dekker.

21. Liu, Z., Lee, J.Y., Han, M., Chen, W., and Gan, L.M., *Synthesis and Characterization of PtRu/C Catalysts from Microemulsions and Emulsions.* J. Mater. Chem., 2002. **12**: p. 2453-2458.

22. Lide, D.R., ed. *Handbook of Chemistry & Physics* 89 ed. 2008, CRC Press: Boca Raton, FL.

23. Ji, X., Banks, C.E., Crossley, A., and Compton, R.G., *Oxygenated Edge Plane Sites Slow the Electron Transfer of the Ferro-/Ferricyanide Redox Couple at Graphite Electrodes13.* ChemPhysChem, 2006. 7(6): p. 1337-1344.

CHAPTER 6

CONCLUSIONS & FUTURE WORK

A series of analytical tools were developed and used to systematically investigate and interrelate chemical, physical and mechanical properties of complex functionalized or modified polymeric systems. Because of their complex chemistry resulting from modification, complementary techniques and methods were designed to study and confirm changes in these materials as compared to their parent analogs. A requirement for the modification is to introduce new functionalities to the parent polymer without compromising other properties that suit it for the envisioned application. The analytical tools were geared towards providing information specific to possible changes in these inherent properties in addition to new properties that result from modification. Based on the information obtained, applications can be narrowed only to those compatible with the properties of the modified materials. Furthermore, these applications require to be tailored in light of the interdependence between the chemical, physical and mechanical properties in determining the overall properties of the modified material, as evidenced in this study and in previous work in our laboratory.

Specifically, FTIR analysis of PU foam at the center and side of a mold was provided for processing temperatures of 25, 45, 65, and 85°C. The FTIR data suggest that there are two factors that influence the chemical composition of the molded PU foam. First, thermal gradients in the mold arise as the foam expands in the mold with

thermally isolated regions present in the radial direction. These gradients can play a role in the chemical composition with reactions at the center thermally activated relative to the side. Degradation of uretoneimine, emergence of carbodiimide, and the degree of unreacted isocyanate groups as a function of radial position in the mold and thermal processing temperatures produces morphologically and chemically distinct material within the same mold. In spite of the uniform and simple geometry of the mold used in these studies, homogeneity was not achieved at any processing temperature. The side of the mold was shown to minimize the thermal degradation of uretoneimine, emergence of carbodiimide, and reaction of isocyanate due to thermal isolation from the center. The data suggest that thermal gradients in the PU foam mold can influence the chemical and morphological homogeneity of the PU foam. Specifically, PU foams containing thermally degradable chemical structures may not be suitable if homogeneity is required in the final material.

Thermally treated epoxy foams were found to undergo both chemical and structural changes associated with the degradation of Diels-Alder bonds and changing structural packing of siloxane units in the adduct. FTIR results show that these changes are not reversible and occur immediately after thermal exposure. The temperature required to see irreversible changes in the foam chemistry are much lower (40 °C) than the temperatures required for degradation of the Diels-Alder bonds (90 °C). Thermal expansion of the foam occurs at temperatures exceeding the degradation of the Diels-Alder bond decreasing the overall density of the foam. The combination of changing chemistry, structure, and thermal expansion lower the overall density of the foam by approximately 41% relative to the pristine foam. The change in density also influences

the modulus of the material which is reduced by 68% after ten thermal cycles. The results indicate that thermal exposure reduces the rigidity of the material through chemical and structural changes that cause the foam to expand, lowering the density and modulus in the process. The changes in density and modulus, even at low temperatures relative to the breaking of Diels-Alder bonds, suggest that removable epoxy foams may not be a good alternative for more common PU foams if high stability and structural rigidity is required.

A composite material was successfully prepared by incorporating carbon black in PI. Platinum metal was successfully deposited on the resulting PI/Carbon film using cyclic voltammetry. Results obtained from four-point probe conductivity measurements show that increased carbon loading or platinum loading enhances the electrical conductivity of the composite. However, beyond 10% carbon loading, the mechanical integrity of the film is compromised. TGA and DSC results show that the thermal stability of PI is maintained with carbon incorporation and platinum deposition. PI/carbon/Pt was found be thermally stable up to 561°C as determined by DSC and 559°C as determined by TGA. SEM imaging suggests that carbon is well dispersed in PI while XPS results show that the platinum deposited Carbon/PI is metallic. The deposition of gold on carbon/PI was found to enhance its sensitivity to the ferricyanide redox couple. However, slower electron transfer is observed at both PI/Carbon/Pt and PI/Carbon/Au films as compared to Pt and Au planar electrodes.

Future work planned in the characterization and envisioned applications of PI/Carbon/Pt (Pd or Au) composites include:

i. Optimizing the PI/carbon film preparation procedures. Methods to produce

films with uniform thickness and reproducible electrical resistivities should be explored.

ii. Tensile strength testing to investigate the effect of introducing carbon into the PI matrix on the tensile strength of PI. For example, introducing Multi walled carbon nanotubes (MWNTS) into the PI matrix has been shown to enhance the tensile strength of PI. [1] The optimum film thickness that leads to the highest tensile strength while maintaining the flexibility of PI/Carbon could also be examined.

iii. Determination of optimum Pt loading leading to the highest level of catalytic activity in PI/carbon/Pt films prior to testing the films in fuel cell applications.

iv. Improving metal adherence onto PI/carbon through surface etching prior to metal deposition. One method that warrants further investigation is KOH etching which has been shown to provide uniform etching in short periods of time. [2-4]

v. Investigating composite stability under repeated testing at typical operating conditions for envisioned device applications. For example, studies on PI/Carbon/Pt chemical stability and metal adherence in acidic conditions over prolonged times periods are required. In addition, the thermal stability of PI/Carbon/Au envisioned for OFET applications at the elevated FET operating temperatures caused by heat emitted by the transistor, should be investigated.

vi. Fabrication of actual devices for applications outlined following the completion of the PI/carbon/metal composite characterization phase.

6.1 References

1. Zhu B-K., Xie S-H., Xu Z-K., and Y-Y, X., *Preparation and Properties of the Polyimide/Multi-Walled Carbon Nanotubes (MWNTs) Nanocomposites.* Composites Science and Technology, 2005. **66** p. 548–554.

2. Ranucci, E., Sandgren, A., Andronova, N., and Albertsson, A.C., *Improved polyimide/metal adhesion by chemical modification approaches.* Journal of Applied Polymer Science, 2001. **82**(8): p. 1971-1985.

3. Lee, K.W., Kowalczyk, S.P., and Shaw, J.M., *Surface Modification Of PMDA-ODA Polyimide - Surface-Structure Adhesion Relationship.* Macromolecules, 1990. **23**(7): p. 2097-2100.

4. Huang, X.D., Bhangale, S.M., Moran, P.M., Yakovlev, N.L., and Pan, J.S. *Surface modification studies of Kapton (R) HN polyimide films.* 2003: John Wiley & Sons Ltd.

APPENDIX A

METHANOL OXIDATION ON PI/CARBON/Pt AND PI/CARBON/Pd

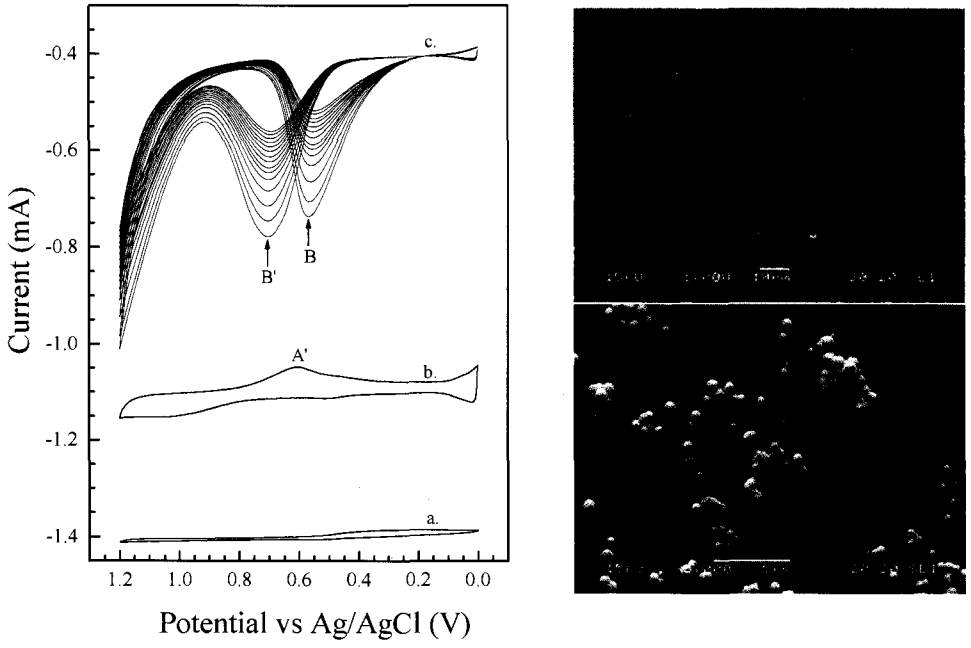

Figure A1: Cyclic Voltammograms at 0.005V/s of a. PI/Carbon in 1M H_2SO_4 b. PI/carbon/Pt in 1M H_2SO_4 (Pt deposited at 0.1 V/s for 5 scans using $2x10^{-2}$M K_2PtCl_4 in 1M $HClO_4$). c. PI/carbon/Pt in 1M Methanol (MeOH) in 1M H_2SO_4

Wave A represents reduction of PtO to Pt. Waves B and B' represent MeOH oxidation at PI/Carbon/Pt during the forward and reverse scans respectively. Arrows point to direction of peak current as cycling proceeds. Images to the right show SEM micrographs of the electrode at x1000 and x5000 magnifications following methanol oxidation.

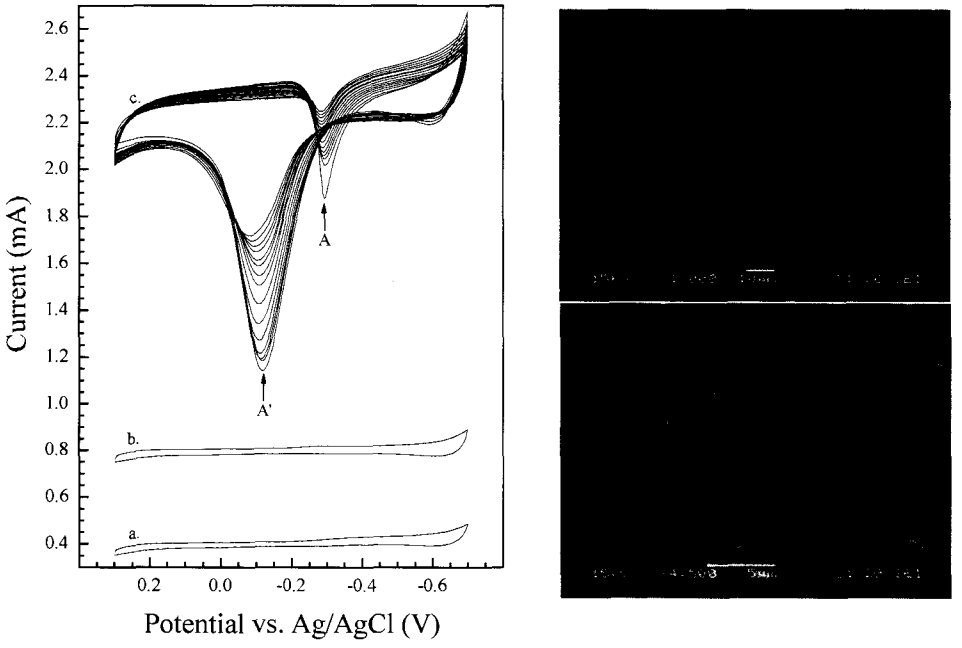

Figure A2: Cyclic Voltammograms at 0.005V/s of a. PI/Carbon in 1M KOH b. PI/carbon/Pd in 1M KOH (Pd deposited at 0.1 V/s for 5 scans using $2x10^{-2}M$ K_2PdCl_4 in 1M $HClO_4$). c. PI/carbon/Pd in 1M Methanol (MeOH) in 1M KOH

Waves A and A' represent MeOH oxidation at PI/Carbon/Pd during the forward and reverse scans respectively. Arrows point to direction of peak current as cycling proceeds. Images to the right show SEM micrographs of the electrode at x1000 and x4500 magnifications following methanol oxidation.

VITA

Graduate College
University of Nevada, Las Vegas

John Macharia Kinyanjui

Local Address:
5223 Caspian Springs Drive #102
Las Vegas, Nevada 89120

Home Address:
P.O. Box 2983
Nakuru, Kenya

Degrees:

Bachelor of Science, Chemical Engineering and Chemistry, 1999
Geneva College, Beaver Falls, Pennsylvania

Master of Science, Chemistry, 2003
University of Nevada, Las Vegas

Special Awards:

Recipient, Nowak-Notre Dame Award to the Most Outstanding Graduate Student for Excellence in Chemistry, Department of Chemistry, University of Nevada, Las Vegas, 2007-2008

Recipient, Merriman Academic Scholarship, Department of Chemistry, Geneva College, 1997-1999.

Publications:

1. Jang, K.; Kinyanjui, J.M.; Hatchett, D.W.; Lee, D-C. *Morphological Control of One-Dimensional Nanostructures of T-Shaped Asymmetric Bisphenazine via Cyanophenyl interactions*. In Press. Chemistry of Materials.
2. Mohan, R.B.; O'Toole B.J.; Malpica, J.; Hatchett D.W.; Kodippili G.; and Kinyanjui J.M. *Effects of Processing Temperature on ReCrete Polyurethane Foam*. Journal of Cellular Plastics 2008; 44: 327-345.
3. Hatchett, DW; Kinyanjui, J. M; Sapochak, L. *FTIR Analysis of Chemical Gradients in Thermally Processed Molded Polyurethane Foam*. Journal of Cellular Plastics 2007; 43, 183-196.
4. Hatchett; Kinyanjui, J. M. *$PtCl_6^{2-}$ and $PtCl_4^{2-}$ Reduction in Polyaniline: Methanol Oxidation at Morphologically Differ*ent Composites. ECS Transactions; 2006; 3 (12), 13-19.
5. Hatchett, D.W; Wijeratne, N. R; Kinyanjui, J. M. *Reduction of $PtCl_6^{2-}$ and $PtCl_4^{2-}$ in Polyaniline: Catalytic Oxidation of Methanol at Morphologically Differ*ent Composites. Journal of Electroanalytical Chemistry; 2006; 593, 203-210.

6. Kinyanjui, J. M.; Wijeratne, N. R; Hatchett, D.W. *Comparison of Chemically and Electrochemically Formed Polyaniline Platinum Composites.* Electrochimica Acta; 2006; 51(14), 2825-2835.
7. Hatchett, DW; Kodippili, G; Kinyanjui, J. M; Benincasa, F.; Sapochak, L. *FTIR Analysis of Thermally Processed PU Foam.* Polymer Degradation and Stability; 2005; 87(3), 555-561.
8. Hatchett, D.W; Kinyanjui, J. M.; Smith, A. J.; Josowicz, M. *Chemical Synthesis of Polyaniline/Gold Composite using Tetrachloroaurate.* Polymer Preprints; 2004; 45(1), 143.
9. Kinyanjui, J. M.; Harris-Burr, R.; Wagner, J. G.; Wijeratne, N. R.; Hatchett, D. W.; *A Hexachloroplatinate-Initiated Synthesis of Polyaniline/Platinum Composite.* Macromolecules; 2004; 37(23); 8745-8753.
10. Kinyanjui, J. M.; Hatchett, D.W; Smith, A. J.; Josowicz, M. *Chemical Synthesis of a Polyaniline/Gold Composite using Tetrachloroaurate.* Chem. Mater; 2004; 16(17), 3390-3398.
11. Kinyanjui, J. M.; Hatchett, D.W.; Hanks, J.; Smith, A. J.; Josowicz, M. *Chemical and Electrochemical Synthesis of Polyaniline/Gold Composites.* J. Electrochem. Soc.; 2004; 151 (12), D113-D120.

Dissertation Title: The Synthesis and Systematic Evaluation of Modified Polymeric Foams and Electrically Conductive Polyimide/Carbon/Metal Films

Dissertation Examination Committee:

Chairperson, Dr. David W. Hatchett, Ph.D.
Committee Member, Dr. Clemens Heske, Ph.D.
Committee Member, Dr. Spencer Steinberg, Ph.D.
Graduate College Representative, Dr. Brendan O'Toole, Ph.D.